CALIFORNIA STATE UNIVERSITY, NORTHRIDGE

AN INVESTIGATION INTO THE EPISODIC BEHAVIOR AND POTENTIAL CAUSES OF JURASSIC MAGMATISM IN THE NORTHERN SIERRA NEVADA, CALIFORNIA

A thesis submitted in partial fulfillment of the requirements

For the degree of Master of Science in Geology

By

Nick Rousseau

May 2016

The thesis of Nick Rousseau is approved:

J. Douglas Yule, Ph.D.	Date
Richard Heermance, Ph.D.	Date
Mary Robinson Cecil, Ph.D., Chair	Date

California State University, Northridge

ACKNOWLEDGMENTS

During my time as a graduate student, I've encountered a wide diversity of individuals who would each place their unique mark on my growth as a developing scientist, an educator, and as a person. It is through these people that I wish to extend my thanks. Without their personal influence on my life, my journey through graduate school would not have been possible.

First and foremost, I deeply thank Marilyn Hanna and the geology faculty at California State University Northridge. It is through the support of the Hanna Fellowship that I was able to financially carry myself through the road towards a Master's degree and expand my level in the sciences. I appreciate her confidence and the confidence of the geology department in my abilities.

I'd like to extend a special thanks to my advisor Dr. Robinson Cecil for her guidance, patience, and willingness to accept me as her first graduate student. Her expertise and passion in the geological sciences was paramount to my education and she has given me a new perspective in the student learning process. I would also like to thank her husband, Dr. Richard Heermance, for his presence during our sample collecting which aided our limited time in the northern Sierra Nevada. His involvement helped ensure our sample collecting successfully. In that regard, I want to extend my appreciation to all of my committee members: Robinson, Dick, and Doug for their efforts in the final stages of my thesis.

I would also like to thank my field assistant, Casey Polon, for her ability to tread the rainfalls with me that have often occurred on field trips that were otherwise predicted to be sunny. Her involvement in my field work was imperative in gathering my samples successfully. Without her, I would not have been so entertained during the long drives, nor would collecting my samples in the rain have been so successful. Casey is an adventurer at heart whom I will always know as my lab buddy.

I thank two very special women in my life, my mother Phyllis Rousseau and my fiancé Jozi Pearson. None of what I was able to accomplish could have been achieved without their support as listeners and supporters. I love you both.

Lastly, I'd like to thank my friends, neighbors, family members as well as colleagues at both the Southern California Earthquake Center and NASA Jet Propulsion Laboratory. It has always been a treat to delve into long conversations about Earthquakes, rocks, minerals and various topics about the dynamic planet Earth. These conversations have always continued to give me the confidence, the inspiration, and the desire to continue to educate others about Earth Science. It is not just my love for rocks and minerals that have brought me to this point in my life. It has also been the ability to spread the interest to others so that they too can share the fascinating world that is geology.

TABLE OF CONTENTS

LIST OF FIGURES

LIST OF TABLES

ABSTRACT

AN INVESTIGATION INTO THE EPISODIC BEHAVIOR AND POTENTIAL CAUSES OF JURASSIC MAGMATISM IN THE NORTHERN SIERRA NEVADA, CALIFORNIA

By

Nick Rousseau

Master of Science in Geology

Jurassic plutons that occupy three metamorphic belts in the northern Sierra Nevada are important for understanding the early development of batholithic rocks in the Mesozoic. These plutons provide a suitable location to study orogenic influences and the spatial and temporal roles of episodic magmatism on early convergent margin batholiths of western North America. New U-Pb zircon geochronology and whole rock major and trace element geochemistry from 7 plutons are presented. New and existing ages, combined with pluton areas estimated from existing mapping, reveal two episodes of increased magma production. The first episode occurs in the Middle Jurassic at ca. 165 – 160 Ma, and the second occurs in the Early Cretaceous at ca. 145 – 140 Ma. Between these two episodes of enhanced magmatism, there is an apparent magmatic lull at ca. 155 – 150 Ma. Pre-Nevadan plutons intruded during the Middle Jurassic episode are calcic to calc-alkalic, metaluminous to weakly peraluminous, and exhibit SiO_2 at 53 – 70%. Trace

element data reveals that these plutons are variable in Sr/Y with values that range from 10 – 75. By comparison, post-Nevadan plutons that intruded during the Late Jurassic-Early Cretaceous episode are also calcic to calc-alkaline, but are more peraluminous and more silicic (60 – 80% SiO_2), with Sr/Y values that range from 2 – 48, with a single pluton as high as 95. Our geochemistry indicates that plutons from the northern Sierra are products of fractional crystallization of mantle-derived magmas from a convergent arc, consistent with previous works. Sr/Y trace element data reveals that there are very little direct correlations between high and low Sr/Y and timing of pluton emplacement, however, it does present an indication that there are significant variations of Sr/Y concentration depending on which metamorphic belt the pluton was emplaced in. While the Western belt primarily contains plutons of low Sr/Y, plutons within the Central and Eastern belts are both significantly higher in Sr/Y concentrations. We propose that these differences suggest a thickening period to the crust during the accretion process of an island arc terrane 155 – 150 Ma. The timing of the lull in magmatism and the change from low to high Sr/Y from west to east offers new constraints on non-steady state magmatism during the Mesozoic. Based on this study, it appears that the timing and volumetric significance of early plutons in the northern Sierra are more complex than previously recognized, and it is likely that two episodes of magmatism are likely due to a crustal thickening period during the Nevadan orogeny, refining the single episode model depicted in previous studies.

1. INTRODUCTION

The Sierra Nevada is one of North America's largest batholiths and is an ideal place to investigate the spatial and temporal magmatic trends that are being increasingly recognized in arcs worldwide. For example, it is now recognized that even though the lower plate is subducted at a steady rate in subduction zones, magmas are not generated at a steady rate. Instead, the growth of batholiths appear to occur episodically (e.g. Ducea and Barton, 2007). This process causes continental arcs to be constructed during short periods of high-flux magmatism (flare-ups) separated by periods of low volume magma additions (lulls). Flare-ups have been recognized in continental arcs around the world, including the modern Andes Mountains (Kay et al., 2005) and the Coast Mountains batholith of British Columbia (Armstrong, 1988; Gehrels et al., 2009). In the Sierra Nevada, there are 2 documented flare-ups that occurred during the Mesozoic. It is estimated that the emplacement of Late Cretaceous plutons in the southern and central Sierran arc occurred during a prominent flare-up, which generated roughly ~78% of the Sierra Nevada batholith (Ducea, 2001). In contrast to the Late Cretaceous flare-up, a relatively small volume (≤ 15%) of batholithic material was intruded during the Jurassic episode. The Late Cretaceous flare-up is generally attributed to an overall heating of the crust over the lifetime of the arc, which weakened it and primed it for a flare-up event (Lackey et al., 2012). This hypothesis, however, cannot be used to explain the Jurassic event because the volcanic arc was presumably cooler then. Much attention has been given to the timing and petrogenesis of plutons in the southern and central Sierra (e.g. Ducea, 2001; Saleeby et al., 2008, Economos et al., 2010; Evernden and Kistler, 1970; Lackey et al., 2005; Bateman, 1992), however, very little attention has been given to the

emplacement history of Jurassic plutons in the northern Sierra which are widely-distributed, variable in their age and composition, and not as well-dated.

This study uses new geochronology and geochemistry from plutons in the northern Sierra Nevada, north of 39°N (Figure 1) in order to: 1) provide better constraints to the timing of flare-up events; and 2) evaluate whether or not the petrogenesis of the plutons are different during these fluxing event. This information is used to refine the spatial and temporal record of Jurassic-to-early Cretaceous magmatism in the northern Sierra and to investigate the conditions under which magmas are generated in an early arc system. Magmatic fluxing episodes have been associated with accretion and orogenic collision (Schweickert et al., 1984; Barth et al., 2011; Ducea, 2001, Lackey et al., 2005; Edleman et al, 1989; Hacker, 1993; Paterson et al., 2011). Petrographic and geochemical study of early arc plutons is used to understand the source of the Jurassic flare-up event(s) and to test the hypothesis that a lull at ca. 155 Ma is the result of subduction cessation during the Nevadan orogeny or alternatively, the influence of crustal thickening generated by post Nevadan deformation during Mesozoic accretion.

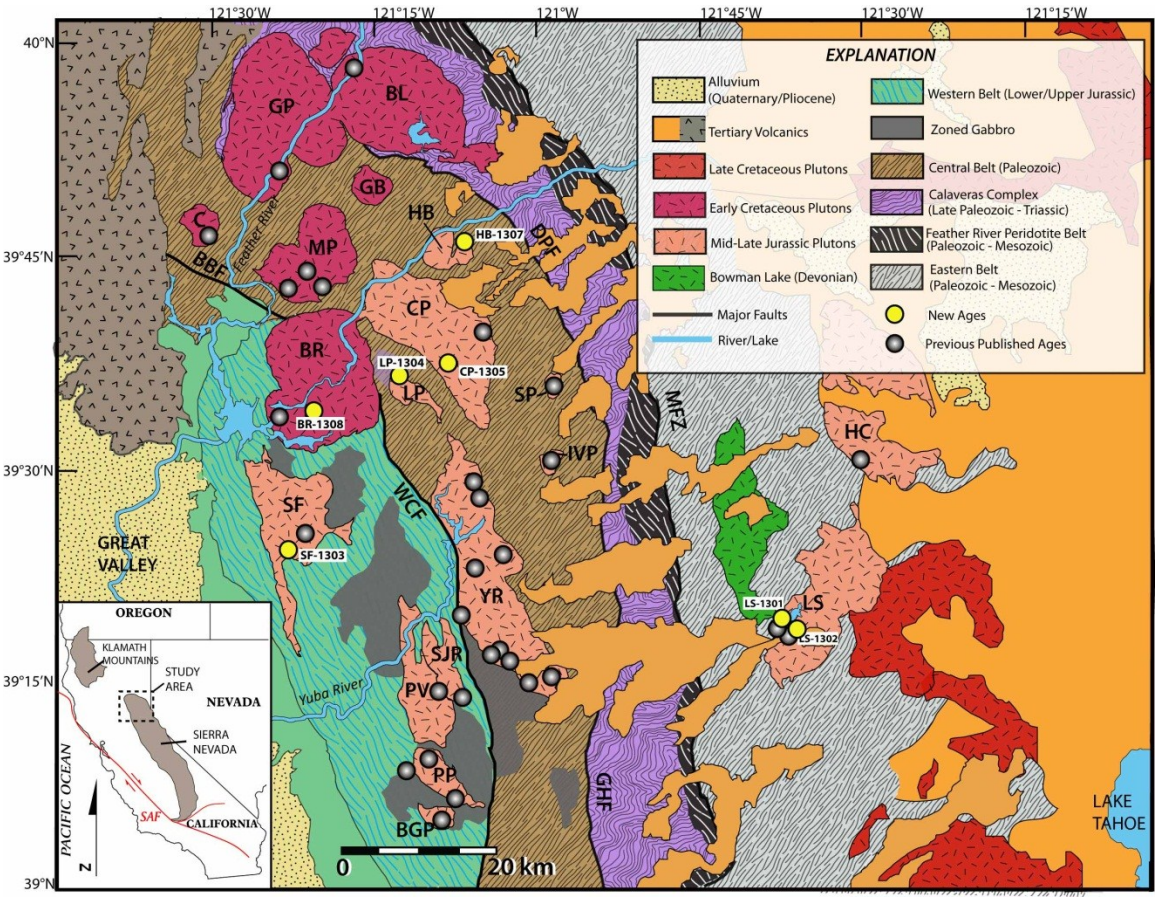

Figure 1. Generalized geologic map of the northern Sierra Nevada, California, modified after Saucedo and Wagner (1992), Irwin and Wooden (2001) and Lackey (2004). The northern Sierra Nevada extends from 39.0°N to ~40°N. Plutonic rock units are indicated by Late Cretaceous (in red), Early Cretaceous (in dark pink), and Mid-Late Jurassic (in light pink) that crosscut five accreted metamorphic belts. Sample locations from previous studies are indicated as gray dots while sample plutons are indicated by yellow dots. Plutons specified on map for this study include Bucks Lake (BL), Bald Rock (BR), Banner Grange pluton (BGP), Concow pluton (C), Granite Basin (GB), Grizzly pluton (GP), Hartman Bar (HB), Haypress Creek (HC), Indian Valley (IVP), Lumpkin pluton (LP), Lake Spaulding (LS), Merrimac pluton (MP), Pilot Peak (PP), San Juan Ridge (SJR), Scales pluton (SP), Swedes Flat (SF), and Pleasant Valley (PV). Other abbreviations: Big Bend fault (BBF), Dogwood Peak fault (DPF), Melones Fault Zone (MFZ), Gillis Hills fault (GHF), Wolf Creek fault (WCF), San Andreas fault (SAF).

This study introduces new U-Pb zircon ages and whole rock geochemical data acquired from 7 plutons in the northern sierra. The U-Pb zircon ages are combined with age data acquired from previous published studies (Cecil et al., 2012; Day et al., 2004; Edleman et al., 1989; Fagan et al., 2001; Girty et al, 1995; Guglielmo et al., 1993; Irwin and Wooden, 2001; and Saleeby et al., 1989 (C)) (Figure 2), and are used to better constrain the timing and aerial extent of episodic magmatism during the Jurassic (Figure 3 and Figure 4). The identification of these episodes provides a framework for which we can portray the timing of flare-up events and introduce an improved understanding of the extent of lulls that might exist between each episode. Furthermore, we make petrological and geochemical comparisons to each flare-up event to draw petrogenetic relationships and to examining the potential role orogeny plays on episodic magmatism. The acquiring of new and pre-existing U-Pb ages and whole rock geochemistry of plutons will provide further insight into the role subduction, accretion and orogeny played on Jurassic magmatism in the northern Sierra. In addition, this study will also provide a further evaluation of the early stages of crustal growth in Mesozoic arc subduction in the North American Cordillera.

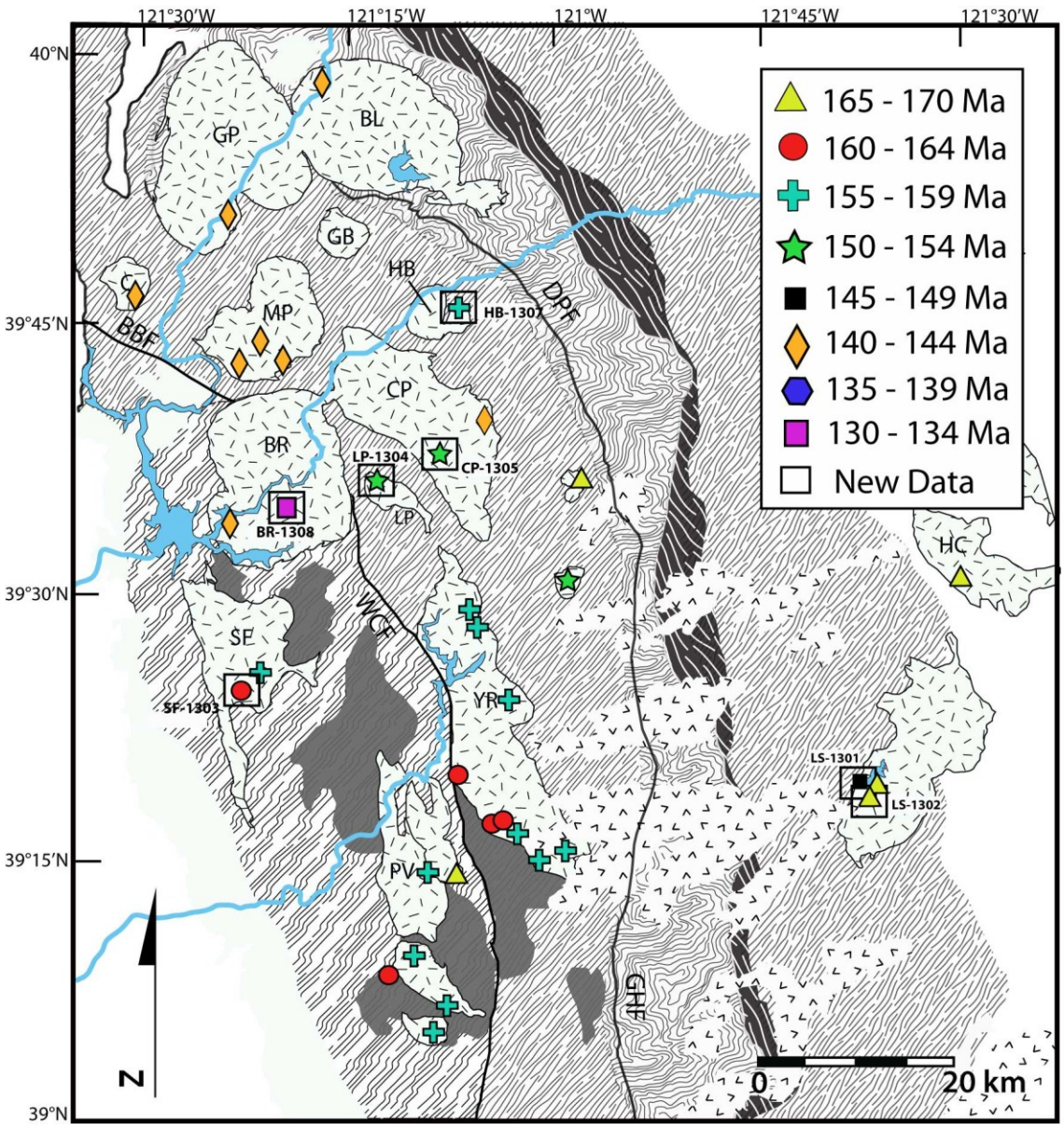

Figure 2. U-Pb sample locations from this study and previous works using 5 m.y. increments. New U-Pb zircon data are combined with age data from Cecil et al., 2012; Day et al., 2004; Edleman et al., 1989; Fagan et al., 2001; Girty et al, 1995; Guglielmo et al., 1993; Irwin and Wooden, 2001; and Saleeby et al., 1989 (C). Geologic units are the same as in figure 1.

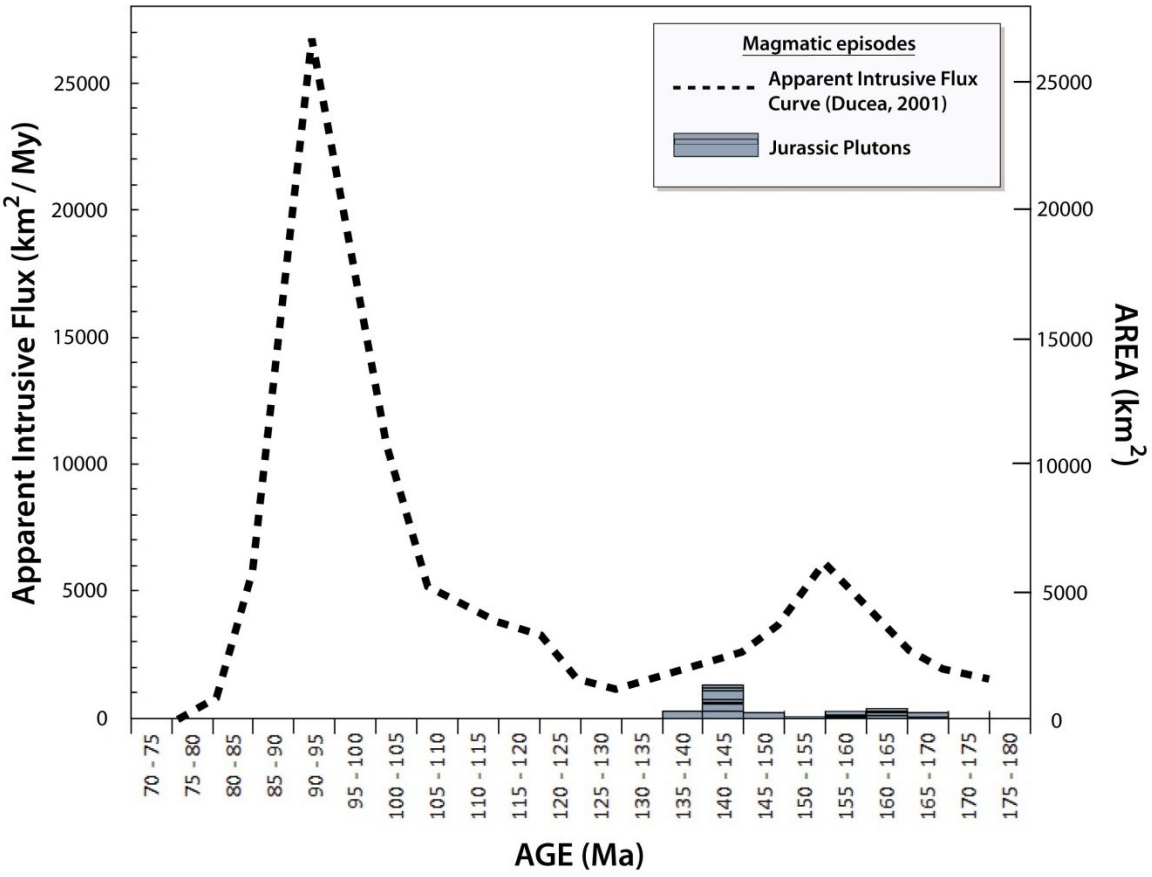

Figure 3. A contrast between a histogram of increased magma production using Area (km^2) vs. Age for plutons in the northern Sierra, and a curve representing apparent intrusive flux by Ducea (2001) for the Sierra Nevada. The histogram on the lower right depicts two episodic events between 170 and 135 Ma. Gray bars represent Middle Jurassic to Early Cretaceous plutons in relation to Area (km^2) in the northern Sierra. On the left Y-Axis, the dashed apparent intrusive flux curve depicts two peaks of magmatic flux in the Jurassic and Late Cretaceous batholith. Aerial estimates for the histogram were gathered through spatial software while ages from this study and published studies were combined in 5 m.y. increments to emphasize changes in magma production through time. The two grayish peaks show that magmatism in the Jurassic was not a single event, as indicated in the apparent intrusive flux curve. The U-Pb zircon ages are combined with age data acquired from previous published studies (Cecil et al., 2012; Day et al., 2004; Edleman et al., 1989; Fagan et al., 2001; Girty et al, 1995; Guglielmo et al., 1993; Irwin and Wooden, 2001; and Saleeby et al., 1989.

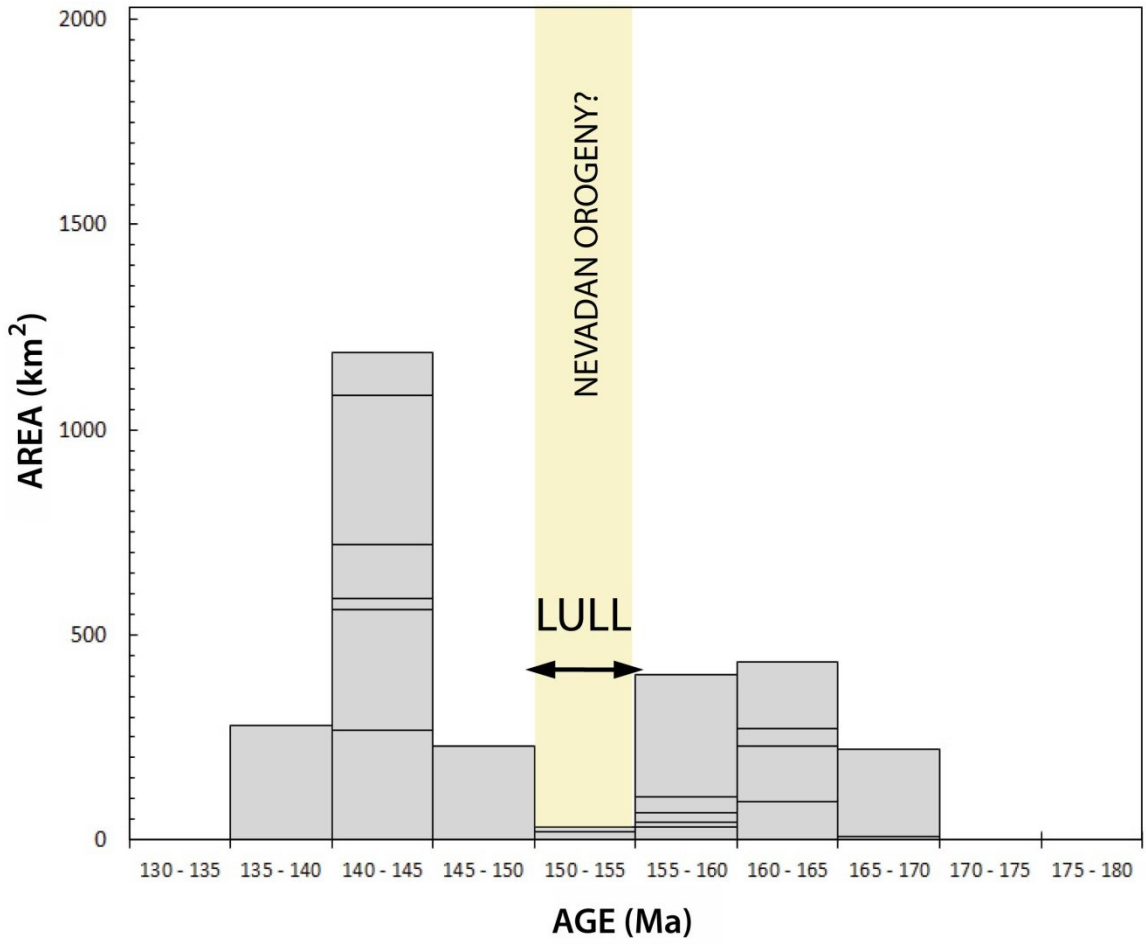

Figure 4. Dated plutons of the Jurassic are binned in 5 m.y. increments and stacked, such that each box represents the calculated aerial extent of a given pluton. The age-area distribution of plutons shown here indicates two magmatic episodes with peaks at ca. 165 - 160 and 145 – 140 Ma. An apparent lull in magmatism is highlighted at 155 – 150 Ma. The U-Pb zircon ages are combined with age data acquired from previous published studies (Cecil et al., 2012; Day et al., 2004; Edleman et al., 1989; Fagan et al., 2001; Girty et al, 1995; Guglielmo et al., 1993; Irwin and Wooden, 2001; and Saleeby et al., 1989.

2. GEOLOGIC BACKGROUND

2.1 Regional Setting

The Sierra Nevada batholith is an 80-100 km wide mountain range that is oriented NNW, and runs the length of approximately 600 km along the eastern half of California (Figure.1). Considered to be one of the largest batholiths in North America, the Sierra Nevada constitutes a rigid block, bounded by the Coast Ranges on the west and the Basin and Range province to the east (Argus and Gordon, 1991). The range, as a whole, exhibits a northeast-southwest topographical asymmetry. This is due to a westward tilt to the block due to an east-dipping fault system that is associated with the eastern margin of the Basin and Range (Bateman, 1992). On the west of the Sierra, the Great Valley forearc basin is located between the Sierra Nevada and the Franciscan subduction complex along central California. The Great Valley is made up of a sequence of sedimentary rocks that reflect the erosional history of the Sierra Nevada. The Great Valley sequence consist of overlain quaternary sedimentation, and a system of complex deposition that ranges from Paleogene and late Jurassic marine and non-marine sediments (Bartow and Nilsen, 1990). Further down section, the base of the sequence meets with Mesozoic intrusive rocks from the Sierra Nevada block that dips beneath the overlain stratigraphy of the Great Valley sequence (Unruh, 1991).

The northern Sierra is defined as being that portion of the arc north of 39°N and is distinguishable from the main body of the Sierra Nevada to the south in the following ways: 1) the northern Sierra has relatively subdued topography, whereas the southern Sierra reaches peak elevations of > 4 km; 2) plutons in the northern Sierra are older assemblages of granodiorites, tonalites and quartz diorites; 3) the smaller volume of

magmatism has permitted a larger exposure of deformed igneous, metamorphic and metasedimentary basement rock contacts than observed in the main batholith, and 4) exposed rocks in the southern and central Sierra have igneous crystallization depths of up to ~30 km (Ague and Brimhall, 1988; Saleeby, 1990) while plutons in the northern Sierra are broadly exposed from less than 4 km (Ague, 1997).

In addition, plutons in the northern Sierra intrude five tectonic, fault-bounded, Paleozoic and Mesozoic metamorphic belts which become progressively older towards the east (Saleeby at al., 1989). From west to east, they include the Western Belt (Smartville complex), the Central Belt, the Calaveras complex, the Feather River Peridotite Belt, and the Eastern Belt (Shoo Fly complex) (Dickinson, 2008; Day and Bickford, 2004; Fagan et al., 2001; Hacker, 1993; Dilek & Moores, 1989; Edelman et al., 1989) (Figure 1). These belts make up most of the metamorphic rocks in the northern Sierra and were tectonically stacked since middle Triassic (Edleman et al., 1989; Dickinson, 2008). The accretion of metamorphic terranes began with the Eastern belt, where today's Basin and Range Province makes up a remnant of the Late Devonian Antler-Sonoma Orogeny. During that time, oceanic miogeoclinal sedimentation was introduced to the edge of western North America, marking the beginning metamorphic complexity of these accreted terranes (Dickinson, 2008). Making up much of the Central belt, the Shoo Fly complex is composed of highly-deformed Ordovician-Silurian sediments overlain by Devonian-Mississippian and Permian-Triassic volcanic arc assemblages (Dilek & Moores, 1989). As convergence progressed, the Feather River peridotite belt, made up of an uplifted portion of accretionary prism sediments and oceanic lithosphere, was formed. The Feather River peridotite follows westward and

marks the edge of the Eastern belt where the Melones fault, an east dipping reverse fault, divides the two terranes and represents the lower portions of ophiolite mélange (Edleman et al., 1989) (Figure 1). The Melones fault is considered to be a former remnant of the plate boundary during early Jurassic subduction and extends the entire length of the western belt. Alongside the Feather River Peridotite belt, the Central belt, which includes Paleozoic metasedimentary rocks and metavolcanic rocks of the Calaveras formation, is divided by the Wolf Creek fault and the Dogwood Peak fault. East of the terrane, the Dogwood peak fault to the north and the Garnet Hills fault, which runs N-S into the central foothills of the Sierra Nevada, suture the Calaveras formation and includes the Slate Creek and Fiddleman Creek Complex (Day and Bickford, 2004). Both of these areas consist of an assortment of Lower Paleozoic metasedimentary rocks with early Paleozoic tectonism (Saleeby, 1989). Lastly, the Western Belt, which includes the Smartville complex, comprises an assemblage of Jurassic ophiolitic, volcanic, and intrusive rocks, remnant of an island arc that is suggested to have collided and amalgamated against the Central belt during the Jurassic (Schweickert et al., 1985).

2.2 Mesozoic arc magmatism

The Sierra Nevada batholith formed as an intrusive underpinning of a continental volcanic arc during subduction of the Farallon plate beneath the western margin of North America between 240 and 80 Ma (e.g. Dickinson, 1981; Ducea, 2001; Saleeby et al., 2008). It is now recognized that the majority of the batholith was formed during two distinct, short-lived magmatic episodes (or flare-up events) in the Mesozoic. The first event occurred around 160 – 150 Ma and was largely constrained to the northern Sierra

(Ducea, 2001). Following this smaller event, the second and more volumetrically significant episode, is predominantly Late Cretaceous in age and occurred at the end of the arcs magmatic life 121 – 85 Ma. This high-volume episode of Cretaceous magmatism formed most of the plutons in the Sierra Nevada (Evernden and Kistler, 1970; Ducea, 2001). Broadly, plutonic rocks on the western front of the Sierra are more mafic in composition (gabbros to tonalites) transitioning to more silicic rocks (granodiorites to granites) to the east (Lackey et al, 2005). In addition to becoming more felsic, plutonic rocks are also younger to the east. Inferred west-to-east migration of magmatism in the Sierra may have been attributed to the flattening of the Farallon slab during subduction in the Cretaceous (Saleeby et al., 2008; Dickinson and Snyder, 1978; Chen and Moore, 1982).

Many previous works discuss the role of tectonic development of volcanic arcs off the coast of western North America during the Jurassic, and two hypothetical models exist regarding the nature of arc-continent collision that formed much of the widespread plutonic and metamorphic rocks of the northern Sierra. One proposed view (Figure 5, model 1) involves magmatism that was initiated by an exotic east-facing arc with a west-facing North American arc. This scenarios is speculated to have caused the formation of both an outboard intraoceanic island arc in the west and an inboard continental arc in the east during the Permian to Late Triassic (Godfrey et al., 1997, Dilek and Moores, 1989; Godfrey and Dilek, 2000). Contrary to model 1, model 2 argues that a single, east-dipping wide arc was responsible for the magmatism, accretion, and tectonic collision of an island arc terrane against a continental arc (Godfrey et al., 1997, Saleeby, 1990) (Figure 5, model 2). The opposing models cannot truly be discriminated in this study,

however, what is known is that magmatism from a west-dipping subduction zone formed the Jurassic continental-margin arc and brought the outboard island arc terrane to become tectonically docked against accreted metamorphic terranes (Day and Bickford, 2004). It is more likely that model 2 provides the ideal setting for middle-to-late Jurassic subduction in the Sierras and is consistent with what is known about the structure style of the arc and geochemistry. The initiation of a new east-dipping subduction zone in the Middle Jurassic (ca. 170 Ma) signaled the early consumption of the Farallon plate.

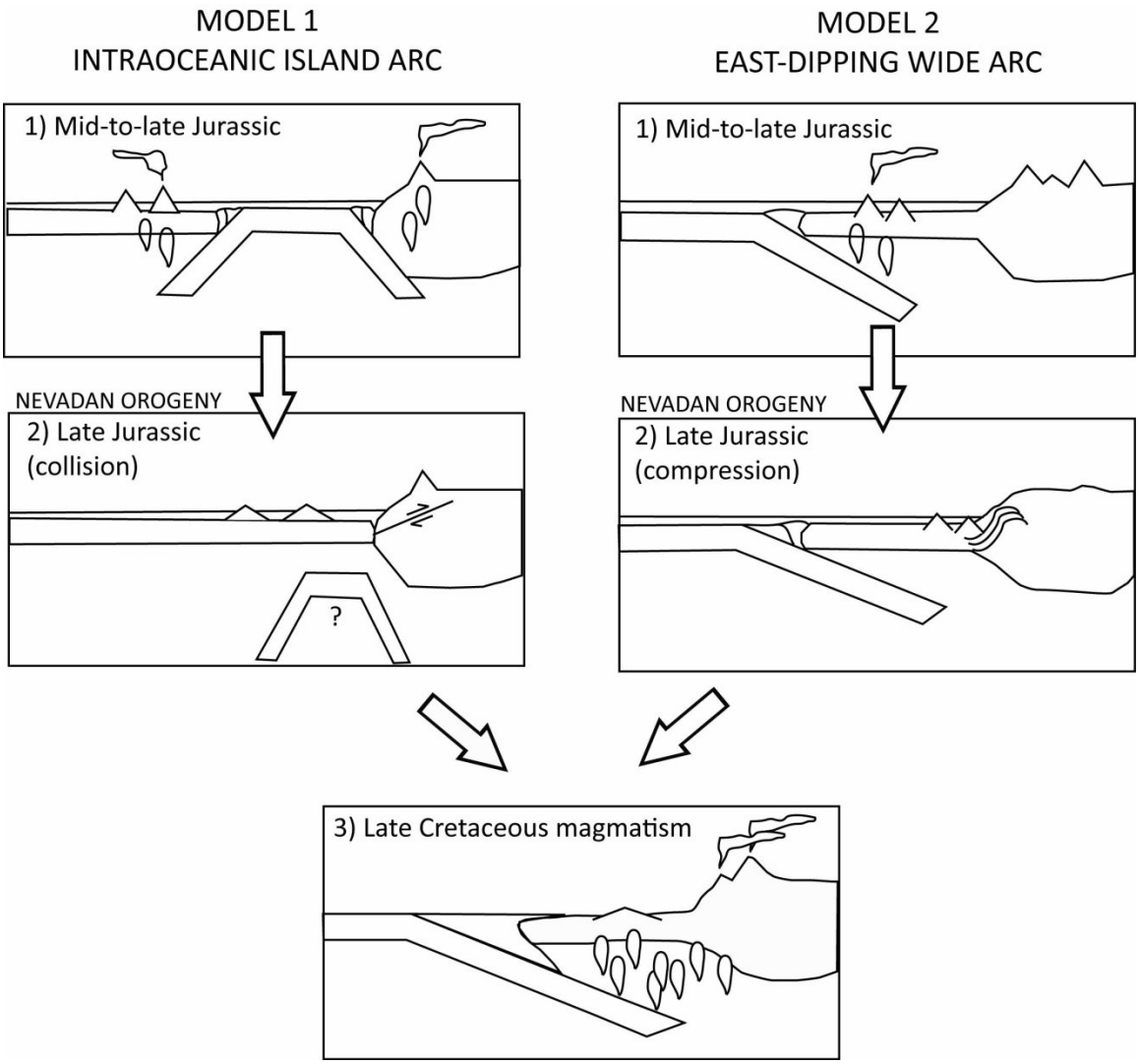

Figure 5. Diagrams show two schematic scenarios of the tectonic evolution of the Sierra Nevada during the Mesozoic. Model 1 present an exotic interpretation, however, model 2 is more likely to depict an accurate setting for the development of the Sierra Nevada. Modified after Godfrey (1997), Day and Bickford (2004), Dilek and Moores (1989), Godfrey and Dilek (2000), Saleeby (1990), Schweickert (1975). Map not to scale.

2.3 Nevadan Orogeny, the Sierra Nevada, and the Klamath Mountains

Jurassic magmatism and orogenic deformation have been well studied in the Klamath Mountains of northern California and southern Oregon (Barnes et al., 2006; Edleman et al., 1989; Ernst et al., 2008; Godfrey et al., 1997; Harper et al., 1994; Hacker et al., 1995; Lamphere et al., 1968; Schweickert et al., 1975 and 1984; wright et al., 1988; Snoke and Barnes, 2006). These studies have led to the distinction that the presence of low-grade metamorphism, reverse faulting, and magmatism was the result of a short-lived deformational event that affected western North America during continental arc convergence termed the "Nevadan orogeny."

Much controversy exists about the timing, spatial extent, and magmatism of the Late Jurassic Nevadan orogeny. In the Klamath Mountains north of 41°N, the Nevadan Orogeny is suggested to have formed due to westward movement of the North American plate. A reorganization of plate motion caused an oceanic island arc to accrete onto the western edge of North America during the Jurassic, now geologically known as the Western Belt. The Nevadan orogeny was, at first, known to be a collisional event suggested to have affected the western coast of North America as far south as the northern Sierra (Hacker et al., 1995). However, previous studies have invalidated this idea due to the prominent, steeply-dipping beds, metamorphism and magmatism that affected the region of the Klamath Mountains (Bateman, 1992). Rather, it was recognized to be a combination of alternating periods of extension and compression that had bridged the unclear distinctions between regional and thermal metamorphism that have been observed in the Klamaths (Wright and Fahan, 1988. Despite the uncertainty over the extent the orogenic event had on the Sierra Nevada during the Jurassic, Harper

(1994) had assigned an age of 151 ± 1 Ma to the timing of the Nevadan orogeny and divided the emplacement of plutonic rocks in the Klamath Mountains into post-Nevadan and pre-Nevadan, a parameter that has been incorporated into this study to differentiate older plutons from younger plutons in the northern Sierra. In the northern Sierra, the timing constraints depict the Nevadan orogeny to have occurred ~155 ± 3 Ma based on Nevadan-style structures observed throughout the Western belt and Central belt. These structures include reverse faults, steep foliations and upright folds which are remnant to the underthrusting of an island arc terrane that was docked against the Central belt prior to the emplacement of Late Jurassic to Early Cretaceous plutons (Schweickert et al., 1984). Further studies have assigned a time span of 155-145 Ma for the beginning and termination of the Nevadan orogeny in the northern Sierra (Harper et al., 1994; Dickinson, 2008) to which may have extended longer than a 10 m.y. span (Saleeby at el., 1989b; Tobisch et al., 1989).

The tectonic, evolutionary similarities such as the coeval development of accreted terranes, composition of plutons, and range of volcanic and deformational history, coincide with the northern Sierra (Hacker et al., 1995; Snoke and Barnes, 2006; Barnes et al., 2006; Hotz, 1971). They argue that the Nevadan orogeny was not restricted to the Klamaths but, rather also affected the Sierra Nevada. Dilek and Moores (1992) describe a similar Mesozoic tectonic history that occurred in the Klamath Mountains and correlate the metamorphic belts of oceanic and island-arc affinities and subsequent plutons to be synchronous with accretion and magmatism in the northern Sierra. The correlation between the Melones fault (or more so the Feather River terrane) of the Northern Sierra and the Trinity thrust in the Klamath Mountains, for example, are two boundaries that

divide the central belts of both regions from their eastern Paleozoic terranes (Hacker and Peacock, 1990) (Figure 6). An apparent structural discontinuity separates the Klamaths and the Northern Sierra, but is today covered by Cenozoic volcanics. This discontinuity is suggested to be a product of sinistral shearing, although the mechanism of this shearing remains unresolved (Ernst et al., 2008; Dickinson et al., 2008; Snoke and Barnes, 2008).

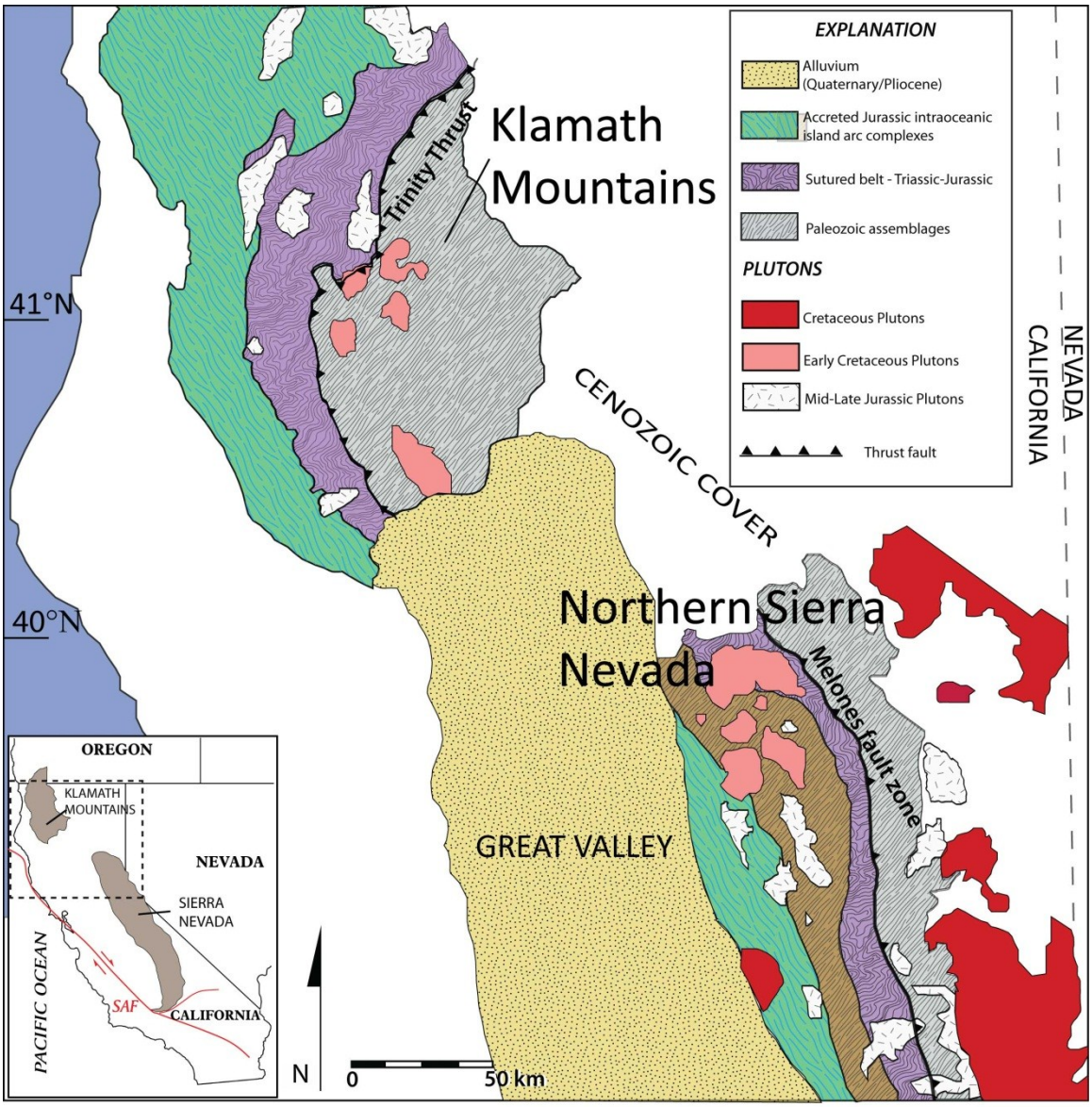

Figure 6. Map displaying similar accretionary and plutonic trends of the Klamath Mountains of the northwest and the Sierra Nevada on the southeast. Each region is separated by a discontinuity and covered by Cenozoic sediments of the Great Valley. After Dickinson, 2008, Lackey et al., 2005, and Snoke and Barnes, 2004.

3. SELECTED SAMPLES

3.1 Sample Strategy and Petrographic Descriptions

Samples chosen for this study were from plutons for which there were few, poor or no existing ages. The sample locations include Lake Spaulding pluton (LS1301, LS1302), Swedes Flat Pluton (SF1303), Lumpkin Pluton (LP1304), Cascade Pluton (CP1305), Hartman Bar Pluton (HB1307), and Bald Rock Pluton (BR1308) (Figure 1). Heavily-weathered samples were avoided and any unavoidable rinds, lichen and weathered surfaces were removed by a rock saw in the lab. Extra cobble-sized samples were also taken from each outcrop to be cut into 4x2 cm billets at CSUN and made into standard thin sections for optical petrography analysis. Sample information, including location, rock type, and U-Pb age data are summarized in Table 1.

6/24/2013 - 6/26/2013 SAMPLE INFORMATION, NORTHERN SIERRA NEVADA, CA

Table 1. Sample Information

SAMPLE	LATITUDE	LONGITUDE	ROCK TYPE	PLUTON/LOCATION	$^{206}Pb/^{238}U$ age	(±2σ)	MSWD
LS1301	39.1931	-121.387	Quartz Monzodiorite	Lake Spaulding	n.d	n.d.	n.d.
LS1302	39.3232	-120.632	Granodiorite	Lake Spaulding	165.7	6.0	6.0
SF1303	39.4069	-120.3925	Quartz Diorite	Swedes Flat Pluton	164.6	4.0	0.43
LP1304	39.6106	-120.2192	Diorite	Lumpkin Pluton	150.8	4.7	4.3
CP1305	39.6253	-121.1425	Biotite Tonalite	Cascade Pluton	151.5	5.9	11.4
HB1307	39.7411	-121.1664	Granodiorite	Hartman Bar Pluton	155.8	3.0	1.5
BR1308	39.5669	-121.3378	Hornblende Biotite Tonalite	Bald Rock Pluton	133.4	3.3	1.5

MSDW - mean standard of weighted deviates. N.d. - not determined.

3.1.2 Lake Spaulding

LS1301 and LS1302 were collected at Lake Spaulding off of CA-20 (Figure 7-A). Both outcrops are homogenous, intermediate rocks that present noticeable fractures and scattered 1-2 cm thick leucocratic veins that are subparallel to noticeable fabrics. Both LS1301 and LS1302 also contain sub-angular-to-angular mafic enclaves, some of which have sharp contacts. Major constituent minerals include predominate plagioclase and

hornblende with minor quartz and potassium feldspar. Sample LS1301 (Figure 8-A) is a quartz monzodiorite collected from the north side of Lake Spaulding. Sample LS1302 (Figure 8-B) is a granodiorite collected from the south side of Lake Spaulding. Under thin section, LS1301is an intermediate, coarse-grained phaneritic rock with mineral grains that include plagioclase, and biotite along with accessory epidote, rutile, zircon, and magnetite. These minerals present a weakly-oriented fabric that is more noticeable with mafic grains. Thin sections reveal a distinguished division between inequigranular-to-equigranular, hypidiomorphic grains. Plagioclase laths depict heavy inclusions and sericite alterations that are observed to be present in most grains (see Appendix A, Sample: LS-1301). Rare merymikites have vermicular wormy structures of quartz replacement with association to plagioclase and possibly potassium feldspar. Quartz grains present very strong undulose extinction and are subhedral to anhedral. Grain boundaries around quartz contain sutured, lobate edges. Resorbed and poikiloblastic hornblende grains have incorporated magnetite replacement as well as chlorite. Chloritization associated with hornblende have also worked into quartz grains as "hair-like" inclusions.

Under thin section, the LS1302 granodiorite is a felsic, course-grained phaneritic rock with mineral grains that include predominant plagioclase, quartz, biotite, hornblende and minor potassium feldspar. Accessory minerals include chlorite, zircon and opaques. The presence of enclaves in hand sample portrays sharp contacts as well as a significant difference between angular and sub-angular grains. No definite fabric is noticeable in sample LS1302, although thin section reveals a course-grained, inequigranular,

hypidiomorphic texture that shows definite crystal alignment with the abundance of tabular plagioclase laths oriented in proximity to quartz grains. Very strong undulose

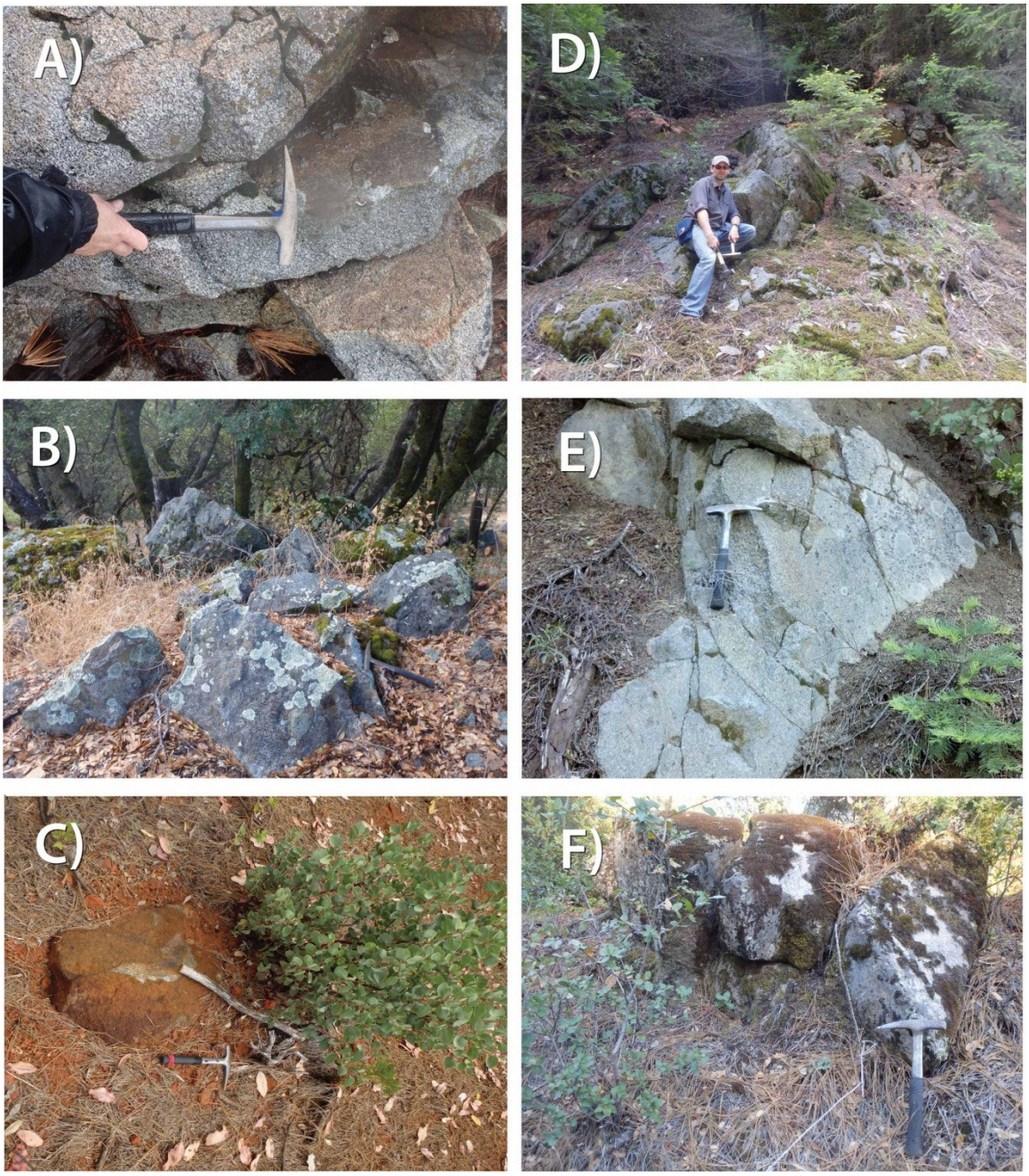

Figure 7. A) Image of a homogenous granodiorite outcrop (LS1302) at lake Spaulding. Rock hammer used for scale. B) Image of a homogenous outcrop of quartz diorite (SF1303) off of La Porte Rd 2.5 km east of Bangor, California. Quartz diorite is part of the Swedes Flat pluton. Outcrops are generally smaller and weathered with lichen. Rock hammer is used for scale. C) Image of a homogenous, heavily weathered diorite outcrop (LP1304) along Lumpkin Road. Outcrop is covered by an orange rind, although freshly broken samples present an intermediate, phaneritic texture. Rock hammer for scale. D) Image of homogenous biotite tonalite outcrop (CP1305) off of Lumpkin Road near Golden Trout Campsite. Tonalite

is part of Cascade pluton. Geology graduate student is used for scale. E) Image of a homogenous granodiorite outcrop (HB1307) along the Hartman Bar truck route above Hartman Bar Ridge. Rock hammer for scale. F) Image of a homogenous lichen-coated biotite tonalite collected on an easterly transect along Lumpkin Road (BR1308). Rock hammer and poison oak for scale.


A
LS 1301
Quartz
Monzodiorite

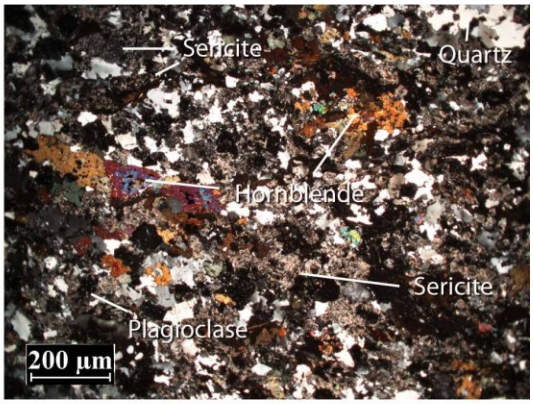
Sericite
Quartz
Hornblende
Sericite
Plagioclase
200 µm

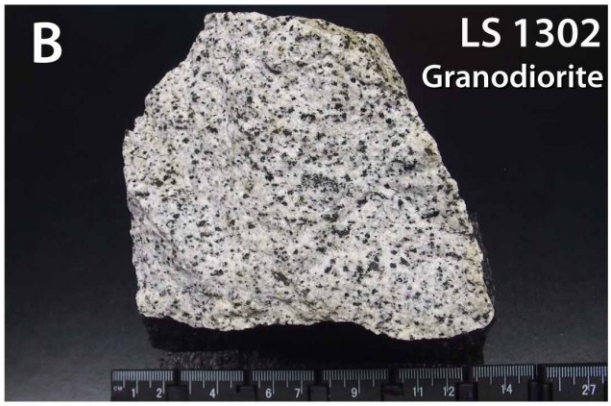
B
LS 1302
Granodiorite

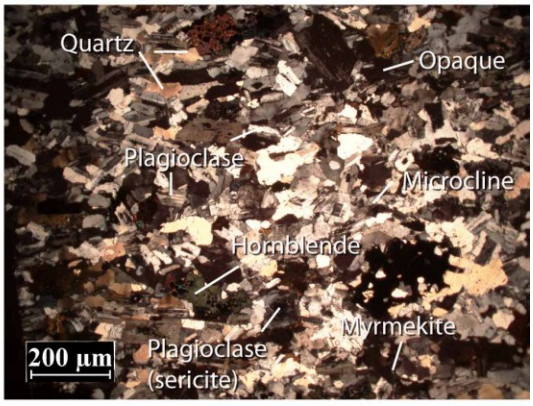
Quartz
Opaque
Plagioclase
Microcline
Hornblende
Myrmekite
Plagioclase
(sericite)
200 µm


C
SF 1303
Quartz Diorite

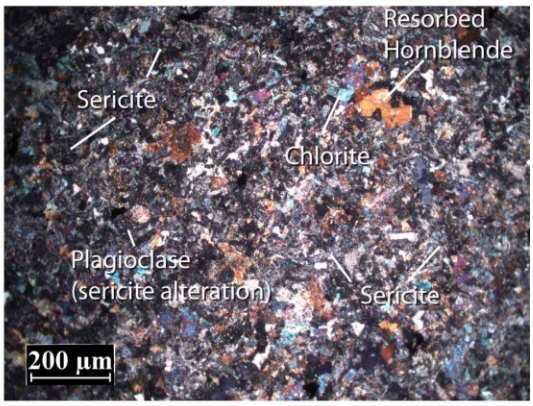
Resorbed
Hornblende
Sericite
Chlorite
Plagioclase
(sericite alteration)
Sericite
200 µm


D
LP 1304
Diorite

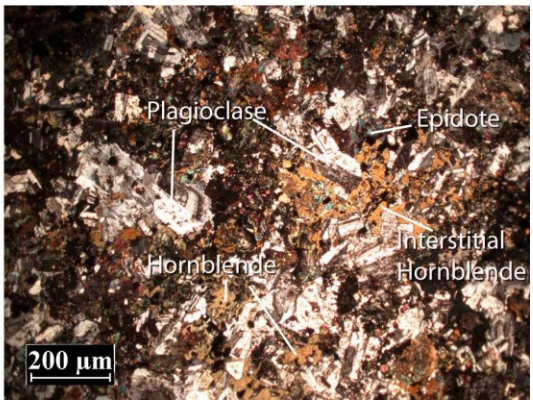
Plagioclase
Epidote
Interstitial
Hornblende
Hornblende
200 µm

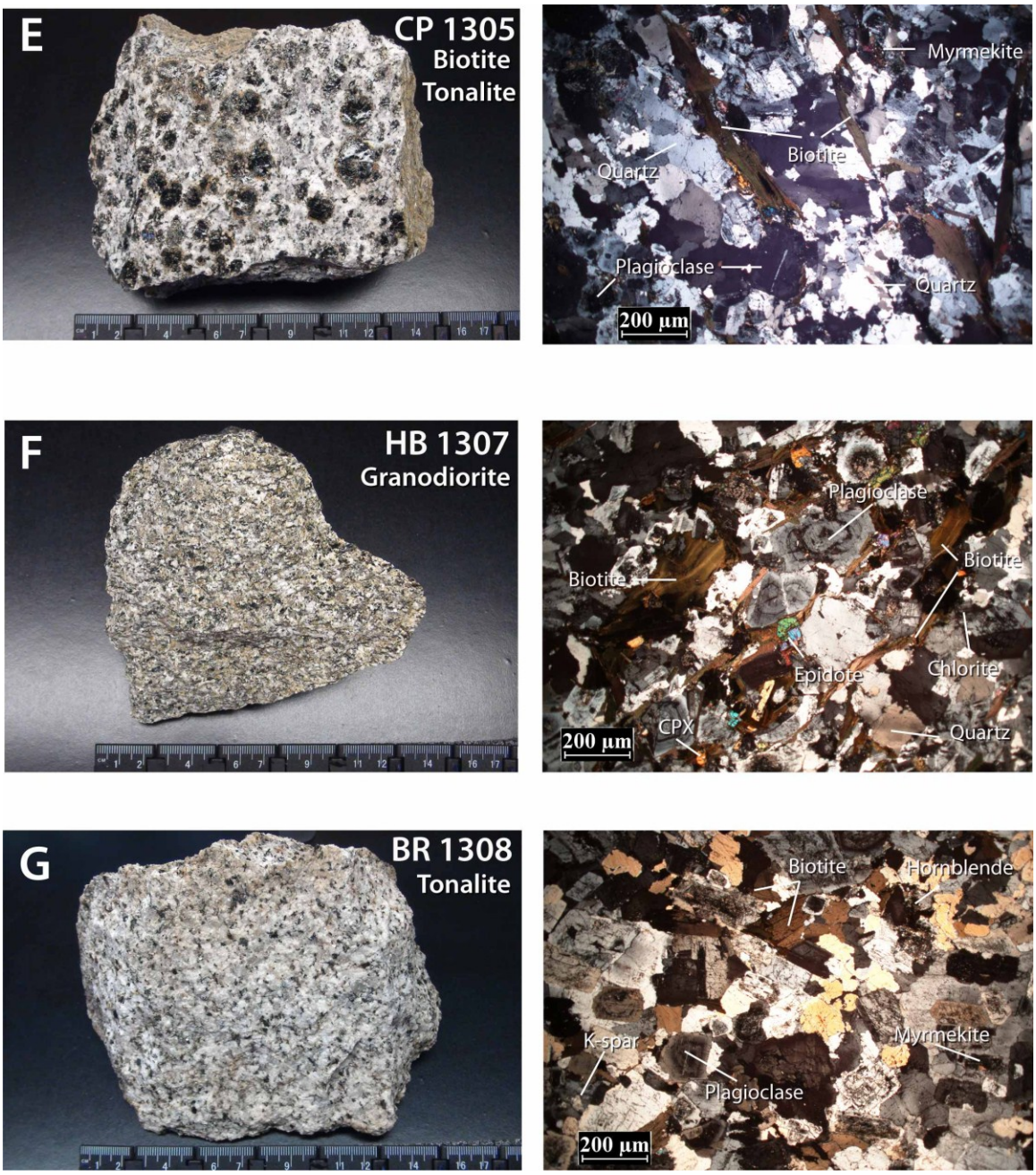

Figure 8 (A-G). Hand samples and adjacent photomicrographs taken in crossed-polarized light. With exception to Lake Spaulding (LS1302) and Swedes Flat pluton (SF1303), all other samples present weakly-to-moderate fabric within texture. All photomicrographs are in 200 µm. For additional material, see appendices.

extinction exists with most quartz grains and they are most likely a secondary texture intermingling with potassium feldspar. The presence of magnetite can be found in association with resorbed and anhedral hornblende grains. Poikilitic hornblende contains epidote crystals that are observed to be interstitial with plagioclase. The enclave contains subhedral-to-anhedral grains of predominant hornblende, moderate chlorite, moderate plagioclase, and trace epidote. The trend of resorption tends to be associated with biotite and hornblende grains into sieve textures. Chloritization is due to the alteration of hornblende while rare myrmekite intergrowth textures show the interaction of hornblende and quartz. Plagioclase within the encalve itself shows heavy sericitization with exception to the host rock where the alignment of euhedral plagioclase laths are predominate.

3.1.3 Swedes Flat pluton

Sample SF1303 is a hornblende quartz diorite collected off of La Porte Rd 2.5 km east of Bangor, California (Figure 7-B). This intermediate, homogenous outcrop is particularly weathered and presents a greenish tinge on freshly broken samples. The minerals present a phaneritic texture with major constituent minerals that include quartz, plagioclase and hornblende. Under thin section, sample SF1303 (Figure 8-C) contains mineral grains that include greenish-tinged plagioclase, quartz, hornblende, and minor potassium feldspar with accessory rutile, epidote, zircon and magnetite. Quartz and plagioclase are equigranular from .5 to 2 mm, along with inequigranular minerals. Thin section reveals a seriate porphyritic, inequigranular, hypidiomorphic texture and heavily-weathered features. Plagioclase laths are almost completely altered to sericite and present

ophitic growths over quartz. Chloritization is associated with the alteration of hornblende where many crystals are partially resorbed. Opaque minerals are mostly pyrite and magnetite.

3.1.4 Lumpkin pluton

Samples LP1304 is a quartz diorite collected along Lumpkin road near a heavily weathered, clay-rich road-cut (Figure 7-C). Weathered outcrop is covered by an orange rind, although freshly broken samples present an intermediate, phaneritic texture. Mafic grains (~ 1 mm) appear to be much smaller than felsic grains (~ 3mm). Major constituent minerals include plagioclase while minor constituents include quartz, hornblende, pyroxene and trace pyrite. Under thin section, sample LP1304 (Figure 8-D) is an intermediate, phaneritic rock with mineral grains that include hornblende, plagioclase, minor potassium feldspar and quartz with trace amounts of pyrite due to weathering. Accessory minerals include epidote, rutile and zircon. Mafic minerals tend to be more fine-grained than felsic grains. A strongly oxidized outer rind with a 2-3 cm thickness exists at the exposed edges of rock sample yet does not penetrate the inner minerals. Thin section reveals a hypidiomorphic, seriate porphyritic texture with inequigranular grains. Plagioclase crystals present a fabric of oriented laths and are euhedral-to-subhedral with ~15% alteration into sericite. Sparse normal ocsillatory zoning can be identified in plagioclase and relict polysynthetic twinning is visible with many altered grains. Mineral replacement is presented in both epidote replacement and seritization (sericite replacement) and crystals tend to have interstitial overgrowths over hornblende. Resorbed and embayed hornblende crystals are anhedral and contain chloritization at most rims.

3.1.5 Cascade pluton

CP1305 is a biotite tonalite also collected along Lumpkin road toward Golden Trout Campsite (Figure 7-D), located at the southern lobe of cascade pluton. These homogenous, lichen-covered outcrops present a primarily grayish rind. Fresh samples, however, are very coarse-grained, phanertic texture with felsic crystals that range from 3-8 mm. Large biotite crystals (1-2 cm) encompass 20% of rock sample and make up much of the fabric observed. Major constituent minerals include quartz, plagioclase, and biotite while minor constituents include k-spar, hornblende and accessory epidote. Under thin section, sample CP1305 (Figure 8-E) is a felsic, course-grained, phaneritic rock with minerals grains that include predominant quartz, plagioclase, large biotite crystals (3 mm to 10 mm), hornblende and minor potassium feldspar with accessory minerals include rutile, zircon and opaque. A stong fabric is exhibited through the orientation and alignment of large biotite crystals alongside the flattening of quartz grains, subparallel to foliation. Thin section reveals inequigranular-to-equigranular, hypidiomorphic grains. Heavily-included and corroded plagioclase laths depict alteration to sericite within the entirety of most grains. Rare merymikites have vermicular wormy structures of quartz replacement with association to plagioclase and possibly potassium feldspar. Quartz grains present very strong undulose extinction and are subhedral to anhedral. Grain boundaries around quartz contain sutured, lobate edges. Resorbed and poikiloblastic hornblende grains have incorporated magnetite replacement as well as chlorite. Chloritization associated with hornblende have also worked into quartz grains as “hair-like” inclusions.

3.1.6 Hartman Bar pluton

HB1307 is a hornblende biotite tonalite collected along the Hartman Bar truck route above Hartman Bar Ridge on the eastern lobe of the pluton (Figure 7-E). Felsic, homogenous outcrops have a surface exposure of ~ 9-12 m with weathered features that are mild-to-weak. Minerals are phaneritic and consist of quartz, plagioclase and biotite. Visible reaction rims are present near biotite grains which also present a weak fabric. Accessory minerals include epidote, perhaps due to the alteration of biotite. Plagioclase grains measure from 2-12 mm. Under thin section, sample HB1307 (Figure 8-F) is an intermediate, finer-grained, phaneritic rock with minerals that include predominant plagioclase, abundant quartz, biotite, clinopyroxenee, hornblende, potassium feldspar with accessory minerals that include epidote, rutile, zircon and opaque. Sample presents a weakly-foliated fabric. Felsic grains appear to be flattened along fabric and range from 2-6 mm in size while mafic grains appear to range from 3-8 mm. Quartz exhibits grayish to weakly-brown appearance and exhibits more equigranular structures than other felsic minerals. Thin section reveals a seriate porphyritic texture with a division of inequigranular-to-equigranular, hypidiomorphic grains. Plagioclase crystals are lath-shaped and present normal-to-patchy oscillatory zoning and resorption within their structure. The alteration of plagioclase into sericite is observed at their cores and along the axis of twinning. Crystals of brownish biotite presents an aligned fabric in thin section, and many grains contain zircons with halo rims. Rare myrmekite is associated with perthitic potassium feldspar and plagioclase. Anhedral quartz crystals appear sutured and heavily-fractured.

3.1.7 Bald Rock pluton

BR1308 is a granodiorite collected on an easterly transect along Lumpkin Road (Figure 7-F). The outcrop was mostly covered in lichen and poison oak. A freshly broken sample exposed weathered surfaces that occur 1 cm deep into fresh material. Rock sample has a phaneritic texture that is predominantly plagioclase. Other minerals include quartz, biotite, hornblende, and biotite. The biotite is euhedral and presents mild alteration with little-to-no apparent fabric. Under thin section, sample BR1308 (Figure 8-G) is a felsic, course-grained, phaneritic rock with mineral grains that include quartz, potassium feldspar, plagioclase, biotite, and hornblende with accessory minerals that include epidote, rutile, zircon and opaque. Equigranular felsic grains range from 2 – 7 mm along with inequigranular mafic grains that range from 3 – 5 mm. No apparent fabric is observed. Thin section reveals a course-grained, hypidiomorphic texture with subhedral grains. Predominant plagioclase crystals are subhedral and exhibits normal oscillatory zoning with mild alteration at their cores and along zoning rings. Moderate myrmekite textures are associated with the intergrowth of many of these plagioclase crystals and they are most likely due to the presence of perthitic potassium feldspar.

4. METHODS

4.1 U-Pb Zircon Geochronology

In order to extract zircon crystals for U-Pb geochronology, rock samples were crushed into large grain-sized gravels through a rock crusher and processed in a disc mill into fine-grained sand. These sands were sieved through a 300 μm mesh screen; sub-300 um grains were passed across a Wilfley water table and the densest grains were retained for further processing. Small aliquots of each sample were collected and set aside for geochemical analysis. All heavies retrieved from the Wilfley underwent Frantz magnetic separation. After a final separation with a hand magnet, each sample underwent heavy liquid separation using Methylene Iodide (MI). Zircons were then hand-picked under a stereo zoom microscope and mounted in a 2 cm epoxy puck. Peixi, Plesovice, Temora-2, NIST 610, NIST 612 and SL standards were mounted with unknown zircons. Grain mounts were polished and imaged using an FEI Quanta 500 Scanning Electron Microscope (SEM) for Cathodoluminescence Imaging (CL) at CSUN in order to identify distinguishable crystallization characteristics such as rim and core domains, inherited components, and deformation history which could be targeted for U-Pb age-dating. Zircons were dated by laser ablation inductively-coupled plasma mass spectrometry (LA-ICPMS) using a ThermoScientific Element2 single collector mass spectrometer with a New Wave Research193 nm Ar-F excimer laser at CSUN. Each spot analysis was ablated for 30 seconds creating pits ~35 μm in diameter and ~15 μm deep. Prior to each analysis, a 30 second gas blank was collected with the plasma which remains active but without laser firing. Details of analytical protocols can be found in Chang et al. (2006).

The isotopes measured for analysis include ^{202}Hg, ^{204}(Pb+Hg), ^{206}Pb, ^{207}Pb, ^{208}Pb, ^{232}Th, ^{235}U, and ^{238}U. NIST 612 standards were used to tune the Element2 before each analytical session in order to maximize intensity of the signal. Peixi and Plesovice standards were used before the start of a session to stabilize fractionation with measured ^{206}Pb/^{238}U and ^{207}Pb/^{206}Pb ratios near to 1% (1 σ standard deviation). Our standard bracketing approach used Peixi and Temora-2 as our primary standards and Plesovice as secondary, followed by two NIST glass analyses at the beginning and end of each session to calibrate U and Th concentrations. The errors that are presented incorporate both analytical error and systematic error resulting from the performance of the standards and uncertainty associated with U decay rates.

Following laser ablation, raw U and Pb isotope ratios were corrected for downhole fractionation effects. Ages were normalized using fractionation factors determined from the Plesovice, Peixi, and Temora standards. These corrected ages were evaluated in Isoplot 4 (Ludwig, 2008), an add-on program that runs under Excel, where the determinations of the mean squared weighted deviation (MSWD) and the construction of concordia diagrams with magmatic age were made. Before assigning a magmatic age, an additional standard systematic error of 2% was added quadratically within each population (Figure 17 A-F).

4.2. Whole Rock Geochemical Analysis

In addition to U-Pb geochronology, whole rock major element geochemistry was measured at Pomona College using the X-Ray Fluorescence (XRF) on each sample (n= 7) in order to interpret their geochemical histories and correlate them with previous

Jurassic pluton data of the northern Sierra. Excess aliquots of rock powder sieved at 300 μm for U-Pb analysis was grounded in the disc mill and stored in individual plastic containers. After each sample was further grounded into rock powder in the shatter box for 5 minutes, 3.5000 g (± 0.0004g) of each sample powder was weighed out and combined with 7.0000g (±0.0004g) pure dilithium tetraborate flux ($Li_2B_4O_7$). The mixed samples were then poured into 33 mm diameter graphite crucibles for fusion melting in a KSL-1700X High Temperature Muffle Furnace at 1000°C for 10 min. Following the first fusion, all glass beads were cooled and re-crushed in the shatter box and returned to the crucibles for a second fusion in the muffle furnace. Each fused bead was polished using 800 grit and sent to Pomona College for XRF analysis using a 3.0 kW Panalytical Axios wavelength-dispersive XRF spectrometer to measure the abundances of 11 major element oxides SiO_2, TiO_2, Al_2O_3, Fe_2O_3, MgO, MnO, CaO, K_2O, Na_2O, P_2O_5, SO_3 and 27 trace elements (> 1 ppm) Zr, Zn, Y, V, U, Th, Ta, Sr, Sm, Sc, Rb, Pr, Pb, Ni, Nd, Nb, Mo, La, Hf, Ga, Cu, Cs, Cr, Co, Ce, Ba, and As (Table 2). Whole-Rock data from this study was then combined with previous published northern Sierra geochemical data. Additionally, data from the rest of the Cretaceous Sierran batholith (130 – 90 Ma), was compiled from the North American Volcanic and Intrusive Rock Database (NAVDAT; http;//www.navdat.org) to compare and contrast age ranges.

TABLE 2. Major and Trace Element Geochemistry

SAMPLE	LS-1301	LS-1302	SF-1303	LP-1304	CP-1305	HB-1307	BR-1308
AGE (Ma)	**n.d.**	**165.7**	**164.6**	**150.8**	**151.8**	**155.8**	**133.4**
SiO2	62.12	61.52	49.55	52.09	66.82	66.06	71.7
TiO2	0.45	0.33	1.07	0.56	0.3	0.32	0.2
Al2O3	15.8	13.65	18.06	15.05	16.37	17.24	14.82
Fe2O3	10.01	13.02	14.62	10.73	6.63	5.89	4.38
MgO	3.03	2.8	4.93	7.3	1.23	1.33	0.57
MnO	0.13	0.17	0.22	0.15	0.08	0.12	0.07
CaO	5.22	5.67	10.48	11.29	4.23	4.85	2.58
K2O	2.69	1.84	0.28	1.53	1.56	1.35	1.89
Na2O	2.7	3.44	2.03	1.96	3.98	3.6	4.41
P2O5	0.16	0.17	0.19	0.06	0.11	0.13	0.09
TOTAL	102.3	102.6	101.4	100.7	101.3	100.9	100.7
S	0.02	0.02	0.02	0.01	0.02	0.02	0.01
Zr	103.2	127.9	38	55.7	84.4	94.3	91.6
Zn	104.5	86.5	168.2	35.4	48.9	76.6	71.8
Y	12.2	16.7	21	16.9	7.3	9.7	12.5
V	122.3	194.8	323.9	201.2	50.2	62.7	29.7
U	2.2	2.4	-0.1	0.3	-0.2	1.4	-1
Th	5.3	6.1	0.5	0.5	-2	-0.2	0.6
Ta	-1.3	-0.5	-3.7	0.5	2.3	-0.2	-1.7
Sr	523.3	573.2	232.2	166.7	696.7	559.7	394.7
Sm	0.2	6	0	5.1	2.7	3.2	5.3
Sc	15	16.7	42.6	39.5	10.9	10.3	4.6
Rb	78.7	35.8	5.9	40.3	32.4	35.3	40.1
Pr	0.4	7.3	1.1	3.7	1.6	6.2	5.7
Pb	9.1	8.7	1.7	0.1	5	6.9	9.6
Ni	39.6	34.2	27.4	80.6	23.3	5.6	10.1
Nd	11.9	44.6	10.2	15.1	1.8	6.3	8.1
Nb	7.3	7	2.7	2.2	5.2	4.3	5.2
Mo	7.3	9.4	7.7	5.5	8	3	5.3
La	22	39.9	4.3	13.8	11.5	14.6	18.2
Hf	2.5	3.4	0.9	1	1.5	1.8	2.6
Ga	17	16.8	19.3	12.1	18	18.6	18.4
Cu	234.3	57.5	246.7	216.9	60	55.2	92.1
Cs	4.5	4.2	6.3	6	4	1	2
Cr	414.1	515.5	310.3	424.4	399.1	219.4	276.2
Co	55.8	76.5	106.6	80.2	26.6	17.3	5.2
Ce	37.9	69.7	4.3	15.2	19.5	34.2	30.8
Ba	725.5	604.8	84.8	348	749.9	597	660.5
As	-8.4	-9.7	-12.8	-14.3	0	-4.4	1.5
Sr/Y	42.89	34.32	11.06	9.86	95.44	57.70	31.58

SUPPLEMENTAL DATA

SAMPLE	G01	G02	G03	G04	G05	G06	G09	G10
AGE (Ma)	162.2	162.0	166.5	145.3	n.d.	109.0	116.4	111.6
SiO2	67.82	69.66	65.73	60.02	78.95	66.55	67.87	63.21
TiO2	0.28	0.53	0.4	0.93	0.06	0.51	0.44	0.68
Al2O3	16.63	15.06	16.55	19.43	12.09	16.28	15.86	16.87
Fe2O3	3.48	3.86	4.24	4.16	0.5	4.05	3.65	5.4
MgO	1.26	1.23	2.03	1.33	0.07	1.7	1.51	2.63
MnO	0.09	0.09	0.09	0.09	0.04	0.08	0.08	0.1
CaO	4.12	4.11	4.73	2.81	0.43	4.2	3.61	5.22
K2O	2.16	1.35	2.53	5.58	4.55	2.73	3.25	2.43
Na2O	4.17	3.98	3.57	5.28	3.3	3.75	3.57	3.43
P2O5	0.09	0.13	0.15	0.26	0.01	0.12	0.12	0.16
TOTAL	100.1	100	100.1	#REF!	#REF!	#REF!	#REF!	#REF!
S	n.d	n.d	n.d.	n.d.	n.d.	n.d.	n.d.	n.d.
Zr	84.5	162.3	108.3	867.9	60.48	106.1	143.9	112.6
Zn	n.d.	n.d	n.d.	n.d.	n.d.	n.d.	n.d.	n.d.
Y	9.5	18.87	9.3	13.33	14.44	13.75	14.58	16.17
V	n.d.	n.d	n.d.	n.d.	n.d.	n.d.	n.d.	n.d.
U	1.0	0.77	1.2	0.74	2.8	2.46	4.04	2.78
Th	2.7	2.33	4.4	1.98	20.91	12.41	10.4	8.73
Ta	n.d.	n.d.	n.d.	n.d.	n.d.	n.d.	n.d.	n.d.
Sr	405.2	218.9	691.9	415.8	34.86	43.3	362.2	461.8
Sm	2.0	2.75	2.7	2.02	2	3.36	3.03	3.73
Sc	6.6	12.08	9.3	6.91	1.24	7.89	7.91	12.06
Rb	47.8	35.41	65.7	45.73	244.6	79.27	111.8	86.34
Pr	n.d.	n.d.	n.d.	n.d.	n.d.	n.d.	n.d.	n.d.
Pb	9.2	2.96	11.2	13.75	32.75	10.83	13.1	9.02
Ni	n.d.	n.d.	n.d.	n.d.	n.d.	n.d.	n.d.	n.d.
Nd	9.4	10.62	13.3	4.21	9.14	16.57	14.01	17.86
Nb	4.1	2.67	4.3	8.75	6.58	6.75	7	6.77
Mo	n.d.	n.d.	n.d.	n.d.	n.d.	n.d.	n.d.	n.d.
La	11.5	10.96	15.8	56.02	13.65	17.47	14.53	18.41
Hf	2.4	4.29	3.0	16.28	2.95	3.18	4.27	3.27
Ga	n.d.	n.d.	n.d.	n.d.	n.d.	n.d.	n.d.	n.d.
Cu	n.d.	n.d.	n.d.	n.d.	n.d.	n.d.	n.d.	n.d.
Cs	1.8	0.88	2.1	0.37	7.88	3.91	4.5	3.4
Cr	n.d.	n.d.	n.d.	n.d.	n.d.	n.d.	n.d.	n.d.
Co	n.d.	n.d.	n.d.	n.d.	n.d.	n.d.	n.d.	n.d.
Ce	20.3	20.85	30.0	6.46	24.7	35.95	29.13	37.58
Ba	753.1	472	886.1	1630	97.46	825.9	763.8	829.8
As	n.d.	n.d.	n.d.	n.d.	n.d.	n.d.	n.d.	n.d.
Sr/Y	42.65	11.06	74.4	31.19	n.d.	n.d.	24.84	28.56

* Supplemental data from Cecil et al. (2012).

G11	G12	G14	G16	G17	G18	G19	G20	G21	G22	G23
120.8	**n.d.**	**166.3**	**163.2**	**148.7**	**121.5**	**105.2**	**101.7**	**109.8**	**90.2**	**106.8**
66.13	54.77	63.13	62.38	78.31	76.66	62.35	69.49	66.97	70.42	67.1
0.51	0.68	0.71	0.53	0.12	0.11	0.79	0.43	0.53	0.37	0.52
16.21	16.38	16.63	17.29	11.53	13.03	16.92	15.33	15.78	15.46	16.69
4.23	8.57	6.01	5.96	1.75	1.05	5.61	3.28	4.27	2.48	3.65
2.01	6	2	1.98	0.01	0.12	2.68	0.12	1.67	0.83	1.08
0.09	0.16	0.12	0.11	0.02	0.06	0.1	0.07	0.07	0.05	0.11
4.54	9.03	4.43	4.79	0.07	0.6	5.57	3.21	4.02	2.69	3.1
2.45	1.49	4.19	3.88	4.33	4.51	2.47	3.38	2.99	3.53	2.41
3.66	2.73	2.51	2.84	3.84	3.74	3.38	3.47	3.45	4.05	5.17
0.14	0.18	0.28	0.24	0.01	0.03	0.15	0.12	0.14	0.11	0.17
0.0	0.0	0.0	0.0	0.0	0.0	0.0	0.0	0.0	0.0	0.0
n.d.	n.d.	n.d.	n.d.	n.d.	n.d.	n.d.	n.d.	n.d.	n.d.	n.d.
128.8	33.66	276.5	181.2	595.7	105.4	180	121.6	138.4	109.3	209.6
n.d.	n.d.	n.d.	n.d.	n.d.	n.d.	n.d.	n.d.	n.d.	n.d.	n.d.
13.36	11.83	26.77	16.13	70.54	18.79	12.19	12.89	10.89	6.5	21.71
n.d.	n.d.	n.d.	n.d.	n.d.	n.d.	n.d.	n.d.	n.d.	n.d.	n.d.
3	0.63	3.65	3.53	3.59	5.05	3.25	4.84	3.5	3.83	2.24
7.48	1.97	14.67	14.13	17.34	20.33	12.7	17.7	13.85	15.39	6.58
n.d.	n.d.	n.d.	n.d.	n.d.	n.d.	n.d.	n.d.	n.d.	n.d.	n.d.
444.5	601.5	560.7	699.2	7.54	49.55	414.3	337.1	453.3	432.6	315.1
3.19	2.56	6.95	5.11	11.17	4.21	3.17	3.2	3.36	2.45	4.65
9.45	30.17	13.55	10.73	1.67	2.43	15.78	6.02	8.28	3.58	7.52
83.32	33.41	165.9	135.7	156.7	168.7	78.91	121.2	85.94	110.5	80.84
n.d.	n.d.	n.d.	n.d.	n.d.	n.d.	n.d.	n.d.	n.d.	n.d.	n.d.
12.25	5.58	13.47	13.24	18.99	21.88	9.98	17.23	11.15	18.58	11.72
n.d.	n.d.	n.d.	n.d.	n.d.	n.d.	n.d.	n.d.	n.d.	n.d.	n.d.
15.22	10.95	31.78	24.9	51.66	24.2	14.44	18.69	18.18	13.69	21
6.87	2.74	20.68	9.48	24.28	18.87	12.19	12.89	10.98	6.5	21.71
n.d.	n.d.	n.d.	n.d.	n.d.	n.d.	n.d.	n.d.	n.d.	n.d.	n.d.
16.27	10.13	30.2	27.85	55.39	18.65	19.06	27.6	25.63	20.07	21.13
3.75	1.08	6.96	4.74	15.22	3.84	4.72	3.72	3.98	3.45	5.38
n.d.	n.d.	n.d.	n.d.	n.d.	n.d.	n.d.	n.d.	n.d.	n.d.	n.d.
n.d.	n.d.	n.d.	n.d.	n.d.	n.d.	n.d.	n.d.	n.d.	n.d.	n.d.
2.97	1.45	5.95	8.06	0.47	1.53	2.38	4.89	2.57	2.84	3.63
n.d.	n.d.	n.d.	n.d.	n.d.	n.d.	n.d.	n.d.	n.d.	n.d.	n.d.
n.d.	n.d.	n.d.	n.d.	n.d.	n.d.	n.d.	n.d.	n.d.	n.d.	n.d.
32.44	19.85	68.87	56.07	121.2	56.02	34.45	50.85	46.77	35.65	42.34
659.3	476.7	979.5	988.2	17.08	270.2	1187	784.6	831.7	865.8	783.1
n.d.	n.d.	n.d.	n.d.	n.d.	n.d.	n.d.	n.d.	n.d.	n.d.	n.d.
33.27	50.85	20.95	43.35	n.d.	n.d.	33.99	26.15	41.63	66.55	14.51

* Supplemental data from Cecil et al. (2012).

5. MAGMA ADDITION RATES

Calculated volumetric magmatic flux, defined as a volume passing through a designated area in a period of time ($km^3/km^2/m.y.$) can be modeled and used as a tool to estimate the periodicity of volcanic arc systems and evaluate the behavior and incremental growth of magmatic systems (Paterson et al, 2011). For the purpose of this paper, volumetric flux was omitted due to the lack of information of the depth of plutonic rocks in the northern Sierra. Alternatively, apparent aerial intrusive fluxes (or magma addition rates) provide a means of obtaining areal measurements for plutons in order to evaluate their emplacement history to understand how a magmas are derived temporally and spatially (Gehrels et al., 2009). This model provides an alternative method due to the lack of information that we know about the 3-dimensional bodies of plutons. The selection of plutons in our sample strategy was determined based on the available geochronology published in previous works (Figure 2), thus, a geochronologic survey was performed using the spatial aerial extent of all plutons north of 38° using ArcGIS supported software with a georeferenced geologic map of the Chico Quadrangle (Saucedo and Wagner, 1992) for accuracy. This operation was important to understand and build upon a histogram that portrays the pulses of magma production that intruded the northern Sierra over the time-span of the Jurassic, and to see which plutons in this study could fill gaps within the data. After data acquisition of U-Pb ages of 22 identified plutons north of 39°, a preliminary histogram was integrated and then plotted with their calculated area (km^2) with 2σ standard deviation. Each pluton, including their aerial extent, was stacked in accordance to their age-range in order to gather a clearer understanding of the spatial-temporal range of plutons (Figure 3) and to highlight the two

existing flare-up events and subsequent lulls during the Jurassic (Figure 4). This method, allowed us to bracket the age populations into pre-Nevadan and post-Nevadan categories to make observational comparisons geochemically.

6. RESULTS

6.1 U-Pb Zircon Geochronology

6.1.1 Zircon Morphology

Ablated spots were targeted using CL images. Rims and cores were targeted in those samples which appeared to have complex zircons (Figure 9). Generally, most samples exhibit euhedral, prismatic zircons with highly-variable zonation patterns, patchy mosaic textures, twinning features, and heavily-resorbed rims. The most common growth patterns observed under CL is oscillatory zoning. Data from LS1301 was removed from the sample selection and discarded due to unreliability of data extracted during LA-ICPMS analysis.

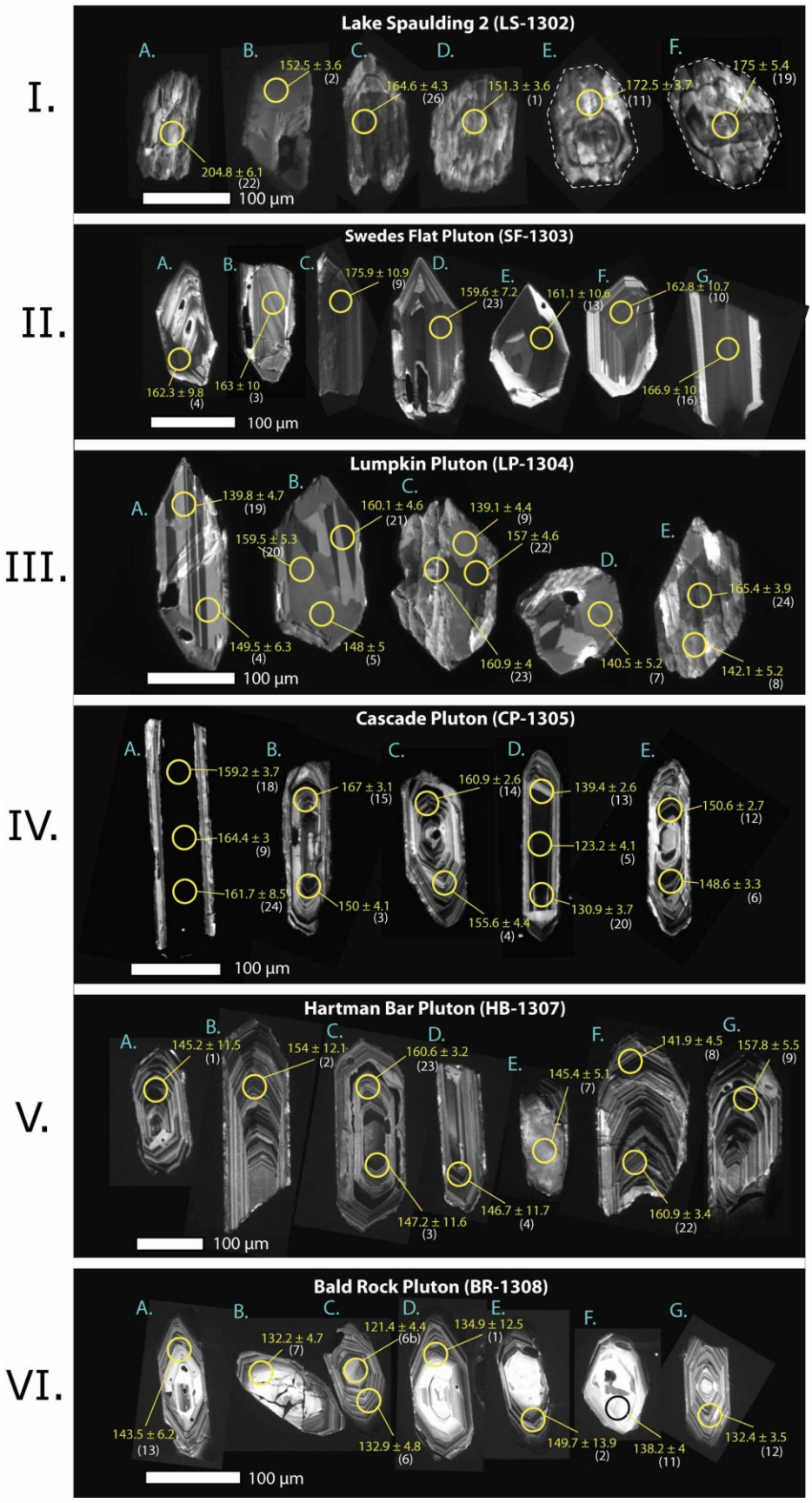
I.
Lake Spaulding 2 (LS-1302)
A.
B.
C.
D.
E.
F.
152.5 ± 3.6 (2)
164.6 ± 4.3 (26)
151.3 ± 3.6 (1)
172.5 ± 3.7 (11)
175 ± 5.4 (19)
204.8 ± 6.1 (22)
100 µm
II.
Swedes Flat Pluton (SF-1303)
A.
B.
C.
D.
E.
F.
G.
175.9 ± 10.9 (9)
159.6 ± 7.2 (23)
161.1 ± 10.6 (13)
162.8 ± 10.7 (10)
162.3 ± 9.8 (4)
163 ± 10 (3)
166.9 ± 10 (16)
100 µm
III.
Lumpkin Pluton (LP-1304)
A.
B.
C.
D.
E.
139.8 ± 4.7 (19)
160.1 ± 4.6 (21)
139.1 ± 4.4 (9)
157 ± 4.6 (22)
159.5 ± 5.3 (20)
165.4 ± 3.9 (24)
149.5 ± 6.3 (4)
148 ± 5 (5)
160.9 ± 4 (23)
140.5 ± 5.2 (7)
142.1 ± 5.2 (8)
100 µm
IV.
Cascade Pluton (CP-1305)
A.
B.
C.
D.
E.
159.2 ± 3.7 (18)
167 ± 3.1 (15)
160.9 ± 2.6 (14)
139.4 ± 2.6 (13)
150.6 ± 2.7 (12)
164.4 ± 3 (9)
123.2 ± 4.1 (5)
161.7 ± 8.5 (24)
150 ± 4.1 (3)
155.6 ± 4.4 (4)
130.9 ± 3.7 (20)
148.6 ± 3.3 (6)
100 µm
V.
Hartman Bar Pluton (HB-1307)
A.
B.
C.
D.
E.
F.
G.
145.2 ± 11.5 (1)
154 ± 12.1 (2)
160.6 ± 3.2 (23)
145.4 ± 5.1 (7)
141.9 ± 4.5 (8)
157.8 ± 5.5 (9)
147.2 ± 11.6 (3)
146.7 ± 11.7 (4)
160.9 ± 3.4 (22)
100 µm
VI.
Bald Rock Pluton (BR-1308)
A.
B.
C.
D.
E.
F.
G.
132.2 ± 4.7 (7)
121.4 ± 4.4 (6b)
134.9 ± 12.5 (1)
143.5 ± 6.2 (13)
132.9 ± 4.8 (6)
149.7 ± 13.9 (2)
138.2 ± 4 (11)
132.4 ± 3.5 (12)
100 µm

Figure 9. Cathodoluminescence images of zircons from plutonic rocks of the northern Sierra Nevada. Blue letters correspond to the sample population. Yellow numbers correspond to the age acquired under LA-ICPMS analyses. White numbers correspond to the order in which analyses was performed on the zircons (see Table 3). The textures shown under CL are varietal and range from weak (LS1302) to strong (HB1307) oscillatory zoning, patchy textures with twinning features (LP1304), and euhedral to heavily-damaged metamict zircons. Dark cores in LS1302, SF1303, and CP1305 contrast brighter cores in BR1308. Scale bars are in 100 microns. For entirety of zircon CL images, see Appendix II.

Zircon samples from the Lake Spaulding quartz monzodiorite (LS1302) exhibit extensive, heavily-damaged crystals under CL. Dark and bright seams are observed in conjunction with inclusions and resorbed rims (Figure 9-I). There are slight differences in contrast between the darker cores versus lighter outer rims yet any noticeable oscillatory zoning can be seen in zircons that also present xenocrystic cores (E and F). Swedes Flat pluton quartz diorite (SF1303) yields zircons that are predominantly euhedral and display irregular, patchy oscillatory zoning with predominantly darker cores and bright rims (Figure 9-II). The sample set produced 10 zircons of which are mostly zoned megacrysts. Zircons from the Lumpkin pluton diorite (LP1304) have few distinguishable CL characteristics (Figure 9-III). Most zircons display no evident concentricity in their growth zoning under CL, but they commonly contain patchy mosaic, sector-zoned textures. Localized bright microfractures are observed such as in zircons C and E, and they are blended with darker fractures within. Irregular patterns of growth-zoning appear to be a common distinction for this rock sample. Zircons from the Cascade pluton tonalite (CP 1305) are characterized by doubly-terminated, prismatic features with internal oscillatory growth zoning under CL (Figure 9-IV). Samples mostly contain dark-to-gray cores with bright rims. Samples A and D, for example, are sector-zoned that display truncated rims that sort of cut off their contiguous heavy, dark cores. There are 3 samples with possible xenocrystic cores that are observed in zircons B, C, and E. Zircons from the

Hartman Bar pluton granodiorite (HB1307) exhibit fairly narrow oscillatory zones under CL (Figure 9-V) with many that are fractured but would otherwise be prismatic and doubly-terminated. Apparent xenocrystic cores are observed in zircons B, C, and G. Cores tend to be lighter in gray, however, there appears to be no differentiation between cores and rims other than those that display xenocrysts. Zircons for the Bald Rock pluton tonalite (BR1308) display characteristics of prismatic, narrow zones of oscillation under CL (Figure 9-VI), similar to Hartman bar pluton (Figure 9-V). Samples A thru G are examples of noticeably bright cores with darker rims while all others are indistinguishable. Inheritance seems more apparent in this rock through xenocrystic cores. These are observed in A, F, G, H, K, L, O, R, and W (see Appendix B, Hartman Bar pluton), many of which have yielded younger Mesozoic ages between 120 Ma and 137 Ma.

6.1.2 U-Pb Zircon Ages

U-Pb zircon ages acquired from sampled plutons in the northern Sierra are presented and U-Pb data results are provided in the Supplementary data table (Table 3). All reported ages for this study are $^{206}Pb/^{238}U$ ages with a 95% confidence level. Best ages, 2σ error, and the mean square of weighted deviates (MSDW) are presented in Table 1. U-Pb concordia diagrams and weighted mean Pb/ U ages for zircons from plutons in the northern Sierra are presented in Figure 10 (A thru F).

TABLE 3. U-Pb Geochronologic Analysis

LS1302	ISOTOPIC RATIOS							APPARENT AGES (Ma)									
	207/235	1 sigma	206/238	1 sigma	RHO	207/206	1 sigma	207/235	1 sigma	206/238	1 sigma	207/206	1 sigma	Th/U	U cps	Real Th/U	U in ppm
	intercept	abs err	intercept	abs err		average	abs err	age	abs err	age	abs err	age	abs err			=AI*razon	=AJ*convfact
LS2_1	0.1670	0.0065	0.0238	0.0006	0.6671	0.0510	0.0015	156.85	5.61	151.3	3.6	241.16	65.27	0.2852	608372.20	0.7524	283.33
LS2_2	0.1676	0.0063	0.0239	0.0006	0.6843	0.0508	0.0014	157.35	5.49	152.5	3.6	230.61	62.50	0.1831	536957.39	0.4830	250.07
LS2_3	0.1979	0.0080	0.0286	0.0006	0.5262	0.0503	0.0017	183.31	6.76	181.5	3.7	206.68	77.84	0.3220	317242.80	0.8495	147.75
LS2_4	0.1896	0.0078	0.0274	0.0007	0.6371	0.0501	0.0016	176.30	6.60	174.4	4.3	201.55	71.67	0.2532	333819.97	0.6680	155.47
LS2_5	0.1928	0.0082	0.0260	0.0007	0.6209	0.0537	0.0018	179.03	6.98	165.7	4.2	358.85	73.83	0.2672	279265.64	0.7049	130.06
LS2_6	0.2070	0.0098	0.0274	0.0008	0.5817	0.0549	0.0021	191.06	8.25	174.0	4.8	407.12	84.30	0.4466	299841.70	1.1782	139.64
LS2_7	0.3044	0.0129	0.0399	0.0009	0.6194	0.0554	0.0019	269.80	10.01	252.1	5.8	426.65	72.92	0.2230	362475.18	0.5882	168.81
LS2_8	0.2062	0.0094	0.0256	0.0007	0.6628	0.0583	0.0020	190.33	7.85	163.2	4.5	542.20	72.84	0.3424	469404.02	0.9034	218.61
LS2_9	0.2207	0.0086	0.0278	0.0006	0.6674	0.0576	0.0017	202.47	7.14	176.6	3.8	515.17	63.19	0.2814	829220.20	0.7424	386.18
LS2_10	0.2900	0.0115	0.0300	0.0006	0.6311	0.0702	0.0022	258.56	9.01	190.3	4.0	934.42	62.25	0.7444	565260.26	1.9639	263.25
LS2_11	0.2000	0.0079	0.0271	0.0006	0.6570	0.0535	0.0016	185.12	6.65	172.5	3.7	348.67	66.38	0.2448	506900.68	0.6458	236.07
LS2_12	2.5790	0.0994	0.1483	0.0041	0.7577	0.1261	0.0032	1294.71	27.82	891.6	23.0	2044.03	43.89	0.3007	772734.56	0.7932	359.88
LS2_13	0.2598	0.0105	0.0329	0.0010	0.7493	0.0573	0.0015	234.47	8.44	208.4	6.0	504.14	58.01	0.3628	453839.02	0.9570	211.36
LS2_14	0.1665	0.0072	0.0240	0.0008	0.8222	0.0503	0.0012	156.40	6.22	152.9	5.1	209.55	55.91	0.2584	596691.03	0.6817	277.89
LS2_15	0.2269	0.0113	0.0249	0.0009	0.7335	0.0662	0.0022	207.61	9.29	158.4	5.7	811.18	69.09	0.2426	430340.54	0.6399	200.42
LS2_16	0.1995	0.0092	0.0266	0.0009	0.7885	0.0545	0.0015	184.68	7.74	168.9	5.9	390.74	62.36	0.3228	485629.34	0.8515	226.17
LS2_17	0.1927	0.0082	0.0254	0.0008	0.6931	0.0551	0.0017	178.91	6.96	161.6	5.0	414.60	67.31	0.3276	436462.63	0.9732	160.51
LS2_18	0.2099	0.0092	0.0269	0.0009	0.6882	0.0565	0.0018	193.43	7.69	171.3	5.4	473.46	68.94	0.2468	265647.47	0.7333	97.69
LS2_19	0.2020	0.0081	0.0275	0.0009	0.7668	0.0533	0.0014	186.82	6.78	175.0	5.4	339.91	56.96	0.2874	447426.43	0.8537	164.55
LS2_20	0.2518	0.0121	0.0318	0.0011	0.6927	0.0574	0.0020	228.06	9.80	202.1	7.1	505.35	74.86	0.4263	297374.59	1.2665	109.36
LS2_21	0.1807	0.0083	0.0228	0.0009	0.8141	0.0576	0.0015	168.67	7.07	145.2	5.4	512.82	57.28	0.2496	331740.54	0.7414	122.00
LS2_22	0.2524	0.0113	0.0323	0.0010	0.6057	0.0567	0.0020	228.56	9.10	204.8	6.1	481.15	76.90	0.3576	570434.82	0.9433	265.66
LS2_23	0.1875	0.0075	0.0232	0.0008	0.7803	0.0585	0.0015	174.47	6.43	148.1	4.7	548.44	54.04	0.3491	403409.16	0.9210	187.88
LS2_25	0.1930	0.0080	0.0263	0.0008	0.6462	0.0532	0.0017	179.20	6.76	167.3	4.8	339.25	70.04	0.2758	338639.79	0.7276	157.71
LS2_26	0.1786	0.0061	0.0259	0.0007	0.7647	0.0501	0.0011	166.90	5.24	164.6	4.3	200.53	50.32	0.3246	649050.16	0.8563	302.28

SF1303	ISOTOPIC RATIOS							APPARENT AGES (Ma)									
	207/235	1 sigma	206/238	1 sigma	RHO	207/206	1 sigma	207/235	1 sigma	206/238	1 sigma	207/206	1 sigma	Th/U	U cps	Real Th/U	U in ppm
	intercept	abs err	intercept	abs err		average	abs err	age	abs err	age	abs err	age	abs err			=AI*razon	=AJ*convfact
SF_1	0.1734	0.0124	0.0254	0.0015	0.9137	0.0494	0.0015	162.34	10.71	161.9	9.6	168.59	67.94	0.2014	676141.79	0.6080	316.34
SF_1b	0.1701	0.0122	0.0250	0.0015	0.9180	0.0494	0.0014	159.53	10.57	158.9	9.5	168.10	66.59	0.2307	786149.34	0.6966	367.80
SF_2	0.1576	0.0120	0.0235	0.0015	0.8895	0.0486	0.0017	148.63	10.48	149.9	9.2	128.45	80.99	0.2272	450013.84	0.6858	210.54
SF_3	0.1963	0.0152	0.0256	0.0016	0.8804	0.0556	0.0021	182.01	12.80	163.0	10.0	436.71	80.57	0.2566	210357.67	0.7746	98.42
SF_4	0.1733	0.0128	0.0255	0.0016	0.9067	0.0493	0.0016	162.28	10.99	162.3	9.8	162.56	72.26	0.2853	639797.52	0.8613	299.33
SF_5_1	0.1843	0.0134	0.0276	0.0017	0.9208	0.0484	0.0014	171.74	11.43	175.4	10.8	119.49	66.98	0.3361	1354243.78	1.0148	633.59
SF_6	0.1907	0.0146	0.0269	0.0017	0.8738	0.0514	0.0019	177.20	12.38	171.1	10.5	258.15	84.01	0.1589	336275.23	0.4796	157.33
SF_7	0.1873	0.0152	0.0262	0.0017	0.8589	0.0518	0.0022	174.32	12.88	166.6	10.7	278.43	92.68	0.1542	206824.90	0.4656	96.76
SF_8	0.1802	0.0135	0.0266	0.0017	0.9140	0.0490	0.0015	168.26	11.51	169.5	10.7	149.00	70.40	0.4256	1095052.48	1.2847	512.33
SF_9	0.1955	0.0147	0.0277	0.0017	0.8963	0.0512	0.0017	181.29	12.44	175.9	10.9	250.89	75.83	0.3021	441566.39	0.9122	206.59
SF_10	0.1634	0.0115	0.0256	0.0017	0.9587	0.0463	0.0009	153.69	9.99	162.8	10.7	13.70	48.86	0.2722	602134.22	0.8219	281.71
SF_11	0.1725	0.0119	0.0251	0.0017	0.9797	0.0498	0.0007	161.61	10.27	159.8	10.5	187.69	31.98	0.3404	1506248.83	1.0278	704.71
SF_12	0.1751	0.0122	0.0253	0.0017	0.9664	0.0502	0.0009	163.84	10.49	161.1	10.5	203.51	41.15	0.2707	708964.53	0.8173	331.69
SF_13	0.1720	0.0118	0.0253	0.0017	0.9854	0.0493	0.0006	161.12	10.21	161.1	10.6	161.21	27.28	0.2927	1758979.67	0.8837	822.95
SF_14	0.1745	0.0127	0.0254	0.0017	0.9416	0.0499	0.0012	163.28	10.93	161.5	10.7	189.08	56.16	0.3174	383597.09	0.9583	179.47
SF_15	0.1661	0.0116	0.0252	0.0015	0.9314	0.0477	0.0012	156.07	10.01	160.7	9.6	85.63	59.84	0.2595	798412.04	0.7833	373.54
SF_16	0.1670	0.0119	0.0262	0.0016	0.9190	0.0461	0.0013	156.78	10.30	166.9	10.0	11.67	60.80	0.3310	632340.28	0.9992	295.84
SF_17	0.1731	0.0120	0.0264	0.0016	0.9490	0.0476	0.0011	162.13	10.32	167.7	10.1	79.83	51.97	0.4118	2219168.90	1.2433	1038.25
SF_18	0.1799	0.0129	0.0252	0.0015	0.9103	0.0517	0.0016	168.00	11.06	160.5	9.6	274.17	67.50	0.3433	767199.90	1.0364	358.94
SF_19	0.1773	0.0125	0.0266	0.0016	0.9366	0.0482	0.0012	165.75	10.72	169.5	10.3	110.64	58.21	0.3516	782854.05	1.0615	366.26
SF_20	0.1720	0.0097	0.0261	0.0011	0.8570	0.0479	0.0014	161.16	8.40	165.8	7.0	92.82	68.73	0.3402	598613.56	1.0271	280.07
SF_21	0.1810	0.0102	0.0278	0.0012	0.8422	0.0472	0.0015	168.90	8.70	176.9	7.2	58.26	71.12	0.1831	551693.49	0.5527	258.11
SF_22	0.2835	0.0180	0.0263	0.0011	0.7548	0.0782	0.0033	253.45	14.11	167.3	7.0	1151.95	81.07	0.2146	285800.36	0.6479	133.71
SF_23	0.1646	0.0102	0.0251	0.0011	0.8207	0.0476	0.0017	154.70	8.88	159.6	7.2	80.09	82.77	0.2678	266917.99	0.8084	124.88
SF_24	0.1725	0.0097	0.0256	0.0011	0.8567	0.0488	0.0014	161.58	8.38	163.1	6.8	139.07	68.09	0.2705	624331.72	0.8165	292.10
SF_25	0.1672	0.0094	0.0255	0.0011	0.8623	0.0475	0.0014	156.99	8.17	162.3	6.9	76.96	67.38	0.2824	1153953.80	0.8525	539.88

LP1304	ISOTOPIC RATIOS							APPARENT AGES (Ma)									
	207/235	1 sigma	206/238	1 sigma	RHO	207/206	1 sigma	207/235	1 sigma	206/238	1 sigma	207/206	1 sigma	Th/U	U cps	Real Th/U	U in ppm
	intercept	abs err	intercept	abs err		average	abs err	age	abs err	age	abs err	age	abs err			=AI*razon	=AJ*convfact
LP_1	0.1625	0.0085	0.0228	0.0010	0.8338	0.0517	0.0015	152.89	7.37	145.2	6.0	273.86	64.67	0.1996	420198.28	0.5729	175.14
LP_2	0.1780	0.0093	0.0233	0.0010	0.8449	0.0555	0.0016	166.32	8.02	148.3	6.3	431.39	61.42	0.1857	399917.23	0.5329	166.69
LP_3	0.1674	0.0092	0.0226	0.0010	0.8376	0.0539	0.0016	157.20	7.95	143.8	6.3	365.21	66.15	0.1006	491007.06	0.2888	204.65
LP_4	0.1691	0.0090	0.0235	0.0010	0.8298	0.0523	0.0016	158.60	7.78	149.5	6.3	297.11	66.39	0.1744	400276.16	0.5006	166.84
LP_5	0.1627	0.0087	0.0232	0.0008	0.6932	0.0509	0.0020	153.05	7.60	147.7	5.0	236.67	87.22	0.1521	211949.48	0.4364	88.34
LP_7	0.1566	0.0087	0.0220	0.0008	0.6752	0.0516	0.0021	147.75	7.61	140.5	4.7	265.52	91.71	0.1316	216923.42	0.3777	90.41
LP_8	0.1744	0.0093	0.0223	0.0008	0.7495	0.0568	0.0020	163.22	7.97	142.1	5.2	481.86	76.00	0.1398	251396.27	0.4012	104.78
LP_9	0.1524	0.0073	0.0218	0.0007	0.7289	0.0507	0.0017	144.04	6.45	139.1	4.4	226.25	74.83	0.1374	278709.79	0.3944	116.17
LP_10	0.1515	0.0076	0.0211	0.0007	0.7436	0.0521	0.0018	143.22	6.68	134.6	4.6	289.37	75.23	0.1796	363056.41	0.5155	151.32
LP_11	0.1969	0.0104	0.0233	0.0008	0.6851	0.0613	0.0024	182.54	8.81	148.4	4.8	651.28	80.99	0.1505	242785.02	0.4320	101.19
LP_12	0.1854	0.0105	0.0219	0.0008	0.6700	0.0613	0.0026	172.70	8.95	140.0	4.8	648.64	88.02	0.1449	194158.47	0.4159	80.93
LP_13	0.2059	0.0099	0.0248	0.0007	0.6633	0.0603	0.0022	190.13	8.32	157.8	4.4	612.93	76.43	0.1630	235890.62	0.4678	98.32
LP_14	0.2103	0.0101	0.0224	0.0007	0.7249	0.0681	0.0023	193.78	8.46	142.7	4.5	872.35	67.56	0.2287	292514.02	0.6562	121.92
LP_15	0.2055	0.0129	0.0188	0.0009	0.8154	0.0792	0.0029	189.80	10.79	120.3	5.8	1175.96	70.29	0.1938	217295.71	0.5562	90.57
LP_16	0.1698	0.0072	0.0259	0.0008	0.6763	0.0475	0.0015	159.22	6.21	165.1	4.9	72.66	72.03	0.1894	388980.49	0.5435	162.13
LP_17	0.1681	0.0074	0.0251	0.0008	0.6524	0.0486	0.0016	157.79	6.42	159.6	4.8	130.42	76.81	0.1950	394800.50	0.5598	164.55
LP_18	0.5429	0.0411	0.0169	0.0010	0.7925	0.2323	0.0107	440.33	26.69	108.3	6.6	3068.09	71.97	0.1296	230551.22	0.3721	96.09
LP_19	0.1731	0.0079	0.0219	0.0007	0.7234	0.0573	0.0018	162.07	6.78	139.8	4.7	501.33	67.65	0.2327	364817.23	0.6678	152.06
LP_20	0.2029	0.0101	0.0251	0.0008	0.6260	0.0587	0.0023	187.60	8.50	159.5	5.3	557.65	82.72	0.1757	248413.42	0.5043	103.54
LP_21	0.1811	0.0070	0.0251	0.0006	0.5729	0.0522	0.0017	168.97	5.98	160.1	3.9	295.79	70.73	0.1719	303474.58	0.4932	126.49
LP_22	0.1721	0.0072	0.0247	0.0007	0.6684	0.0506	0.0016	161.27	6.23	157.0	4.6	224.07	70.59	0.1771	365783.35	0.5082	152.46
LP_23	0.1914	0.0077	0.0253	0.0006	0.5616	0.0549	0.0018	177.85	6.55	160.9	4.0	409.46	73.12	0.1737	274208.66	0.4984	114.29
LP_24	0.1883	0.0071	0.0260	0.0006	0.5731	0.0526	0.0016	175.21	6.03	165.4	3.9	310.69	68.82	0.1836	373880.08	0.5268	155.83
LP_25	0.1995	0.0084	0.0261	0.0007	0.6040	0.0555	0.0019	184.67	7.09	166.0	4.6	430.70	73.37	0.1800	281410.66	0.5165	117.29
LP_26	0.1915	0.0073	0.0237	0.0006	0.6260	0.0585	0.0017	177.89	6.19	151.2	3.8	549.95	63.65	0.1898	320118.01	0.5447	133.43

CP1305	ISOTOPIC RATIOS							APPARENT AGES (Ma)									
	207/235	1 sigma	206/238	1 sigma	RHO	207/206	1 sigma	207/235	1 sigma	206/238	1 sigma	207/206	1 sigma	Th/U	U cps	Real Th/U	U in ppm
	intercept	abs err	intercept	abs err		average	abs err	age	abs err	age	abs err	age	abs err			=AI*razon	=AJ*convfact
CP_1	0.1324	0.0054	0.0187	0.0007	0.9077	0.0513	0.0009	126.28	4.81	119.5	4.2	255.31	38.85	0.0533	2194752.16	0.1572	885.36
CP_2	0.1501	0.0057	0.0221	0.0007	0.8494	0.0493	0.0010	142.01	5.01	140.9	4.3	159.80	46.32	0.1579	1410109.09	0.4652	568.83
CP_3	0.1685	0.0058	0.0235	0.0006	0.8523	0.0519	0.0009	158.11	5.01	150.0	4.1	281.14	40.73	0.0586	1856354.41	0.1726	748.85
CP_4	0.1673	0.0059	0.0244	0.0007	0.8705	0.0497	0.0009	157.11	5.11	155.6	4.4	180.03	40.10	0.1386	1842941.29	0.4083	743.44

CP_5	0.1362	0.0055	0.0193	0.0007	0.8772	0.0512	0.0010	129.67	4.89	123.2	4.1	250.02	44.04	0.0717	1792009.92	0.2112	722.89
CP_6	0.1622	0.0065	0.0233	0.0005	0.7819	0.0504	0.0013	152.63	5.66	148.6	3.3	214.96	60.20	0.1550	2469155.17	0.4568	996.05
CP_7	0.1564	0.0059	0.0224	0.0004	0.7914	0.0507	0.0013	147.54	5.12	142.7	2.7	225.81	57.15	0.0954	2379845.21	0.2812	960.02
CP_8	0.1227	0.0079	0.0172	0.0009	0.8598	0.0516	0.0017	117.50	7.13	110.1	5.6	269.30	74.31	0.0662	1634213.40	0.1952	659.24
CP_9	0.1750	0.0064	0.0258	0.0005	0.8062	0.0492	0.0012	163.77	5.52	164.4	3.0	155.15	55.74	0.3588	5655715.95	1.0574	2281.50
CP_10	0.1875	0.0069	0.0264	0.0005	0.8001	0.0515	0.0013	174.53	5.92	168.0	3.2	264.08	55.56	0.2013	4312918.50	0.5931	1739.82
CP_11	0.1402	0.0045	0.0191	0.0005	0.8435	0.0534	0.0009	133.22	3.97	121.7	3.0	344.42	38.56	0.0432	1524953.80	0.1272	615.16
CP_12	0.1658	0.0046	0.0236	0.0004	0.7594	0.0509	0.0009	155.76	4.00	150.6	2.7	235.38	41.69	0.1708	2646612.84	0.5033	1067.64
CP_13	0.1506	0.0043	0.0219	0.0004	0.7616	0.0500	0.0009	142.47	3.77	139.4	2.6	194.32	42.78	0.0740	1590282.81	0.2180	641.52
CP_14	0.1747	0.0043	0.0253	0.0004	0.7913	0.0501	0.0008	163.45	3.75	160.9	2.6	200.85	35.86	0.2616	4259149.03	0.7708	1718.13
CP_15	0.1853	0.0050	0.0262	0.0005	0.8202	0.0512	0.0008	172.63	4.26	167.0	3.1	250.16	35.65	0.0551	3275808.86	0.1624	1321.45
CP_16	0.1294	0.0064	0.0174	0.0008	0.9070	0.0539	0.0011	123.53	5.76	111.2	4.9	367.12	46.45	0.0987	1441939.18	0.2909	581.67
CP_17	0.1761	0.0051	0.0247	0.0005	0.7755	0.0516	0.0009	164.69	4.41	157.6	3.5	268.13	41.54	0.1301	1142500.79	0.3834	460.88
CP_18	0.1747	0.0048	0.0250	0.0006	0.8759	0.0507	0.0007	163.48	4.15	159.2	3.7	226.31	30.43	0.3172	4805030.51	0.9346	1938.34
CP_19	0.1726	0.0048	0.0244	0.0006	0.8894	0.0512	0.0007	161.66	4.17	155.6	3.7	251.93	29.19	0.1449	2285967.48	0.4271	922.15
CP_20	0.1494	0.0050	0.0205	0.0006	0.8684	0.0528	0.0009	141.34	4.41	130.9	3.7	320.52	37.33	0.0602	1649878.19	0.1775	665.56
CP_21	0.1520	0.0089	0.0220	0.0012	0.9494	0.0500	0.0009	143.66	7.84	140.6	7.5	195.64	42.46	0.2285	1870595.02	0.6732	754.59
CP_22	0.1372	0.0083	0.0197	0.0011	0.9644	0.0505	0.0008	130.56	7.43	125.9	7.1	216.28	36.98	0.0529	2075471.22	0.1558	837.24
CP_23	0.1805	0.0189	0.0237	0.0022	0.9192	0.0552	0.0023	168.47	16.09	151.1	14.1	420.98	89.33	0.0557	1024496.81	0.1642	413.28
CP_24	0.1742	0.0099	0.0254	0.0014	0.9711	0.0497	0.0007	163.07	8.50	161.7	8.5	183.17	31.42	0.4032	5242563.97	1.1880	2114.84
CP_25	0.1688	0.0096	0.0247	0.0013	0.9607	0.0495	0.0008	158.38	8.33	157.5	8.3	172.12	36.68	0.1018	2006994.30	0.2999	809.62

HB1307	ISOTOPIC RATIOS							APPARENT AGES (Ma)									
	207/235	1 sigma	206/238	1 sigma	RHO	207/206	1 sigma	207/235	1 sigma	206/238	1 sigma	207/206	1 sigma	Th/U	U cps	Real Th/U	U in ppm
	intercept	abs err	intercept	abs err		average	abs err	age	abs err	age	abs err	age	abs err			=AI*razon	=AJ*convfact
HB_1	0.1555	0.0137	0.0228	0.0018	0.9714	0.0495	0.0011	146.79	11.99	145.2	11.5	170.11	49.71	0.0946	3176214.40	0.2753	1334.39
HB_2	0.1628	0.0143	0.0242	0.0019	0.9707	0.0488	0.0011	153.18	12.38	154.0	12.1	138.44	50.18	0.1047	2752393.12	0.3048	1156.33
HB_3	0.1572	0.0138	0.0231	0.0018	0.9729	0.0493	0.0010	148.26	12.00	147.2	11.6	163.51	48.17	0.1521	2893529.13	0.4427	1215.63
HB_4	0.1510	0.0134	0.0230	0.0019	0.9689	0.0475	0.0011	142.78	11.73	146.7	11.7	75.88	52.74	0.1271	2316641.00	0.3699	973.27
HB_5	0.1644	0.0146	0.0241	0.0019	0.9670	0.0495	0.0012	154.58	12.69	153.3	12.2	172.74	53.54	0.0894	3708273.62	0.2603	1557.92
HB_6	0.1753	0.0090	0.0250	0.0009	0.8672	0.0508	0.0014	164.04	7.75	159.3	5.4	234.02	62.33	0.1125	3026730.01	0.3276	1271.59
HB_7	0.1578	0.0080	0.0228	0.0008	0.8844	0.0502	0.0013	148.80	7.03	145.4	5.1	204.20	58.68	0.0196	4634318.39	0.0569	1946.97
HB_8	0.1495	0.0072	0.0223	0.0007	0.8841	0.0487	0.0012	141.49	6.37	141.9	4.5	135.25	57.67	0.0191	5607275.38	0.0556	2355.73
HB_9	0.1644	0.0086	0.0248	0.0009	0.8642	0.0482	0.0014	154.59	7.51	157.8	5.5	107.17	65.40	0.2228	4871993.02	0.6484	2046.82
HB_10	0.1649	0.0082	0.0245	0.0008	0.8723	0.0489	0.0013	155.00	7.10	155.9	5.0	141.54	60.89	0.1738	3718971.52	0.5059	1562.41
HB_11	0.1555	0.0060	0.0229	0.0007	0.8739	0.0492	0.0009	146.80	5.29	146.1	4.4	158.03	44.24	0.0648	925536.78	0.1887	388.84
HB_12	0.1628	0.0057	0.0247	0.0007	0.8821	0.0479	0.0008	153.18	4.94	157.0	4.2	95.03	39.29	0.0287	1655130.94	0.0837	695.35
HB_13	0.1609	0.0062	0.0238	0.0007	0.8282	0.0490	0.0011	151.48	5.38	151.8	4.2	146.37	50.27	0.0860	979131.96	0.2504	411.35
HB_14	0.1669	0.0062	0.0244	0.0007	0.8256	0.0497	0.0011	156.74	5.41	155.1	4.2	181.75	49.16	0.1197	824326.60	0.3484	346.32
HB_15	0.1615	0.0056	0.0244	0.0007	0.8782	0.0480	0.0008	151.98	4.90	155.4	4.1	99.26	39.82	0.1415	2234741.46	0.4118	938.86
HB_16	0.1704	0.0066	0.0248	0.0009	0.9736	0.0498	0.0004	159.73	5.70	158.0	5.9	184.94	20.45	0.1176	3589262.03	0.3425	1507.92
HB_17	0.1638	0.0065	0.0241	0.0009	0.9663	0.0493	0.0005	154.01	5.62	153.5	5.8	161.93	23.58	0.0999	3555776.01	0.2907	1493.85
HB_18	0.1722	0.0067	0.0247	0.0009	0.9717	0.0505	0.0005	161.34	5.77	157.4	5.9	219.00	21.08	0.0596	4573880.26	0.1734	1921.58
HB_19	0.1702	0.0067	0.0252	0.0009	0.9568	0.0491	0.0006	159.61	5.79	160.2	5.9	151.25	26.55	0.1555	2423560.58	0.4527	1018.19
HB_20	0.1609	0.0064	0.0238	0.0009	0.9566	0.0491	0.0006	151.45	5.56	151.4	5.7	152.01	26.85	0.1733	2603003.35	0.5045	1093.57
HB_21	0.1658	0.0051	0.0245	0.0005	0.8201	0.0491	0.0009	155.77	4.40	156.0	3.1	152.08	42.00	0.0782	2032395.71	0.2278	853.85
HB_22	0.1726	0.0054	0.0253	0.0005	0.8342	0.0495	0.0009	161.64	4.63	160.9	3.4	173.04	40.91	0.2162	4135961.40	0.6294	1737.60
HB_23	0.1716	0.0053	0.0252	0.0005	0.8216	0.0493	0.0009	160.84	4.54	160.6	3.2	163.99	41.87	0.0773	1888337.25	0.2249	793.33
HB_24	0.1647	0.0048	0.0246	0.0005	0.8317	0.0486	0.0008	154.83	4.15	156.6	2.9	128.14	39.42	0.1312	3528788.63	0.3820	1482.51
HB_25	0.1808	0.0059	0.0259	0.0005	0.7744	0.0507	0.0011	168.74	5.10	164.6	3.4	226.84	48.63	0.0799	1282510.35	0.2326	538.81

BR1308	ISOTOPIC RATIOS							APPARENT AGES (Ma)									
	207/235	1 sigma	206/238	1 sigma	RHO	207/206	1 sigma	207/235	1 sigma	206/238	1 sigma	207/206	1 sigma	Th/U	U cps	Real Th/U	U in ppm
	intercept	abs err	intercept	abs err		average	abs err	age	abs err	age	abs err	age	abs err			=AI*razon	=AJ*convfact
BR_1	0.1402	0.0143	0.0211	0.0020	0.9690	0.0481	0.0012	133.21	12.63	134.9	12.5	101.79	59.43	0.1764	2057654.26	0.5223	1281.96
BR_2	0.1584	0.0161	0.0235	0.0022	0.9700	0.0489	0.0012	149.29	14.03	149.7	13.9	142.32	58.05	0.1155	3027371.84	0.3420	1886.12
BR_3	0.1296	0.0133	0.0202	0.0019	0.9642	0.0465	0.0013	123.76	11.92	129.0	12.0	22.95	65.71	0.1369	1129109.43	0.4054	703.46
BR_3b	0.1384	0.0143	0.0200	0.0019	0.9659	0.0501	0.0014	131.60	12.65	127.9	12.0	198.37	61.83	0.1024	1426556.67	0.3032	888.78
BR_4	0.1437	0.0146	0.0217	0.0020	0.9693	0.0481	0.0012	136.36	12.90	138.3	12.8	101.82	59.14	0.1075	2795418.57	0.3184	1741.61
BR_4b	0.1751	0.0068	0.0240	0.0008	0.9284	0.0529	0.0008	163.85	5.85	153.0	5.2	322.82	32.62	0.2123	2895306.05	0.6285	1803.84
BR_5	0.1589	0.0072	0.0219	0.0008	0.8437	0.0527	0.0013	149.76	6.26	139.4	5.0	316.22	54.25	0.2066	667850.79	0.6118	416.09
BR_6	0.1584	0.0067	0.0208	0.0008	0.9037	0.0551	0.0010	149.34	5.85	132.9	4.8	418.22	40.11	0.1372	3613770.69	0.4063	2251.46
BR_6b	0.2314	0.0137	0.0190	0.0007	0.6497	0.0883	0.0040	211.38	11.27	121.4	4.4	1388.29	84.37	0.1741	1446237.74	0.5154	901.04
BR_7	0.1368	0.0060	0.0207	0.0007	0.8652	0.0479	0.0011	130.22	5.33	132.2	4.7	93.48	51.40	0.1045	960702.39	0.3094	598.54
BR_8	0.1346	0.0046	0.0200	0.0005	0.8331	0.0489	0.0009	128.19	4.10	127.4	3.3	143.11	44.03	0.1002	1288224.06	0.2967	802.59
BR_9	0.1584	0.0051	0.0218	0.0006	0.8656	0.0527	0.0009	149.30	4.49	138.9	3.5	317.32	36.86	0.1257	1897595.55	0.3722	1182.24
BR_10	0.1390	0.0048	0.0201	0.0006	0.8685	0.0502	0.0009	132.17	4.28	128.3	3.5	202.87	39.61	0.1147	2454589.93	0.3397	1529.26
BR_11	0.1528	0.0062	0.0217	0.0006	0.7839	0.0511	0.0013	144.37	5.41	138.2	4.0	246.75	56.90	0.1983	461587.99	0.5871	287.58
BR_12	0.1412	0.0047	0.0207	0.0006	0.8753	0.0494	0.0008	134.16	4.19	132.4	3.5	165.63	37.71	0.1125	1683601.78	0.3330	1048.92
BR_13	0.1499	0.0069	0.0225	0.0010	0.9681	0.0483	0.0006	141.85	6.04	143.5	6.2	114.30	26.82	0.1816	2651244.54	0.5378	1651.78
BR_14	0.1577	0.0074	0.0207	0.0009	0.9660	0.0553	0.0007	148.68	6.49	131.9	5.9	425.22	26.94	0.0901	2425306.70	0.2668	1511.02
BR_15	0.1462	0.0069	0.0219	0.0010	0.9628	0.0485	0.0006	138.55	6.09	139.4	6.2	123.64	29.73	0.1758	2405604.31	0.5205	1498.74
BR_16	0.1470	0.0068	0.0224	0.0010	0.9551	0.0477	0.0007	139.23	6.02	142.5	6.2	83.21	32.36	0.1414	1546213.97	0.4185	963.32
BR_17	0.1400	0.0067	0.0210	0.0009	0.9573	0.0484	0.0007	133.06	5.91	133.9	6.0	117.70	32.09	0.1180	1846763.17	0.3493	1150.57
BR_18	0.1302	0.0074	0.0193	0.0010	0.8858	0.0490	0.0013	124.23	6.62	123.0	6.1	146.87	60.63	0.1658	440760.23	0.4907	274.60
BR_19	0.1430	0.0064	0.0212	0.0009	0.9033	0.0488	0.0009	135.68	5.70	135.4	5.4	139.46	44.73	0.1242	1506731.30	0.3678	938.73
BR_20	0.1244	0.0058	0.0180	0.0008	0.9500	0.0501	0.0007	119.07	5.26	115.1	5.0	199.56	33.71	0.1165	2748434.75	0.3449	1712.33
BR_21	0.1385	0.0064	0.0201	0.0009	0.9408	0.0501	0.0008	131.69	5.68	128.0	5.4	198.00	35.97	0.1289	2168281.30	0.3815	1350.89
BR_22	0.1327	0.0066	0.0190	0.0009	0.9167	0.0505	0.0010	126.52	5.94	121.6	5.5	219.33	45.68	0.1787	663825.23	0.5291	413.58
BR_23	0.1546	0.0065	0.0222	0.0009	0.9352	0.0505	0.0008	145.99	5.69	141.5	5.4	219.69	34.03	0.1416	1792085.11	0.4191	1116.51
BR_24	0.1259	0.0060	0.0192	0.0008	0.8827	0.0475	0.0011	120.45	5.40	122.8	5.1	73.64	52.39	0.1261	740874.47	0.3734	461.58
BR_25	0.1616	0.0066	0.0222	0.0008	0.9383	0.0527	0.0008	152.07	5.79	141.7	5.3	317.21	32.05	0.1010	1919435.06	0.2990	1195.85
BR_25b	0.1524	0.0074	0.0215	0.0009	0.8487	0.0514	0.0013	144.07	6.47	137.2	5.5	258.21	57.71	0.1848	538844.53	0.5472	335.71

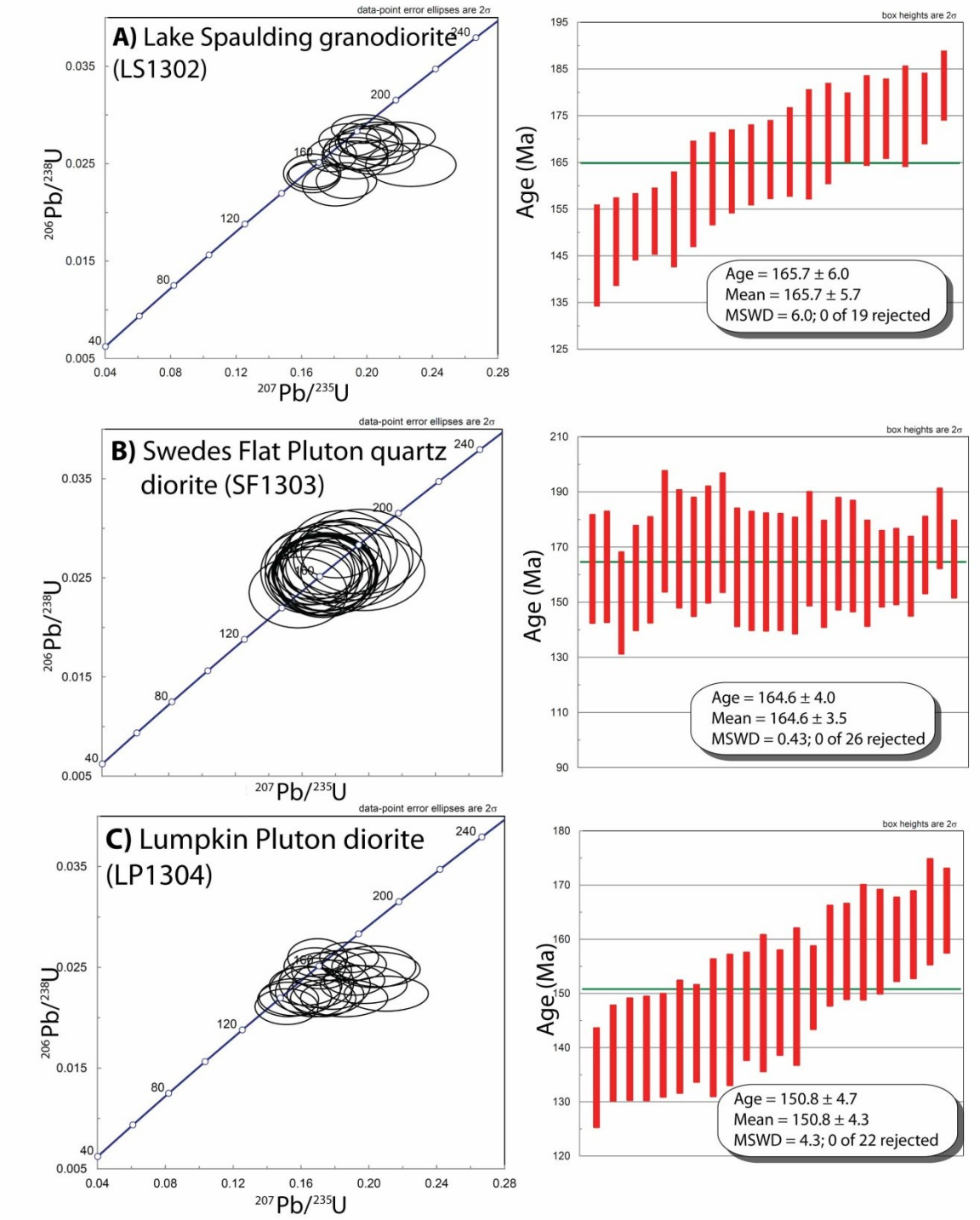
data-point error ellipses are 2σ
A) Lake Spaulding granodiorite (LS1302)
206Pb/238U
207Pb/235U
box heights are 2σ
Age (Ma)
Age = 165.7 ± 6.0
Mean = 165.7 ± 5.7
MSWD = 6.0; 0 of 19 rejected
B) Swedes Flat Pluton quartz diorite (SF1303)
Age = 164.6 ± 4.0
Mean = 164.6 ± 3.5
MSWD = 0.43; 0 of 26 rejected
C) Lumpkin Pluton diorite (LP1304)
Age = 150.8 ± 4.7
Mean = 150.8 ± 4.3
MSWD = 4.3; 0 of 22 rejected

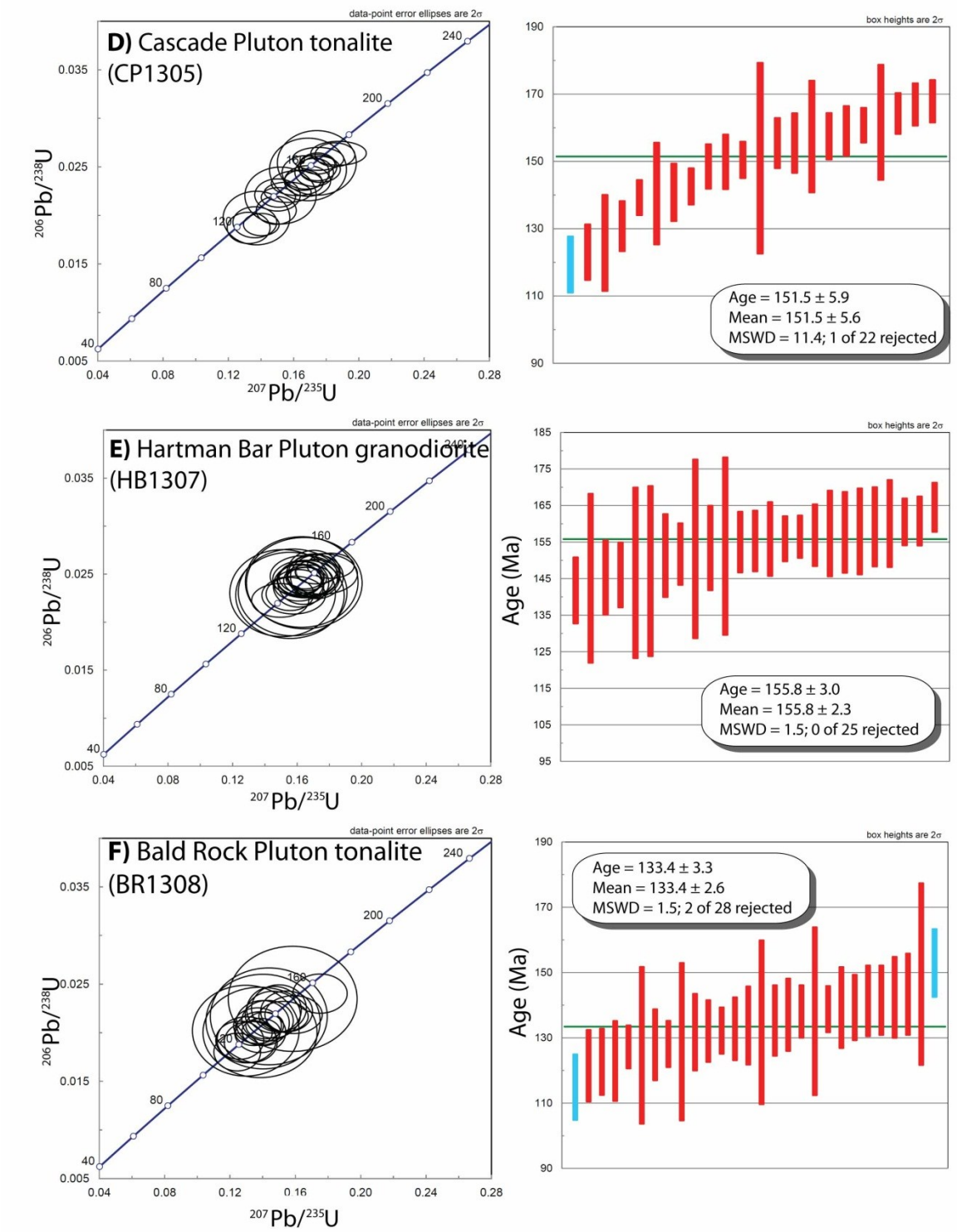

Figure 10 (A thru F). U-Pb concordia diagrams and adjacent weighted mean Pb/ U ages for zircons from plutons in the northern Sierra Nevada. Blue analyses indicate samples zircons that have been statistically excluded from the populations. Error bars are designated at 2σ. MSWD - mean square of the weighted deviates.

Zircons from the Lake Spaulding granodiorite (LS1302) consist of 19 analyses and is the oldest Jurassic age so far reported out of the 6 zircon samples. With common-Pb correction and weighted average, the granodiorite yields a $^{206}Pb/^{238}U$ age of 165.7 ± 6.0 Ma (MSWD = 6.0) (Figure 10-A). The Swedes Flat Pluton quartz diorite (SF1303) yields a $^{206}Pb/^{238}U$ age of 164.6 ± 4.0 Ma (MSWD = 0.43) (Figure 10-B) with no inherited grains. It must be noted that this age is slightly inconsistent with a published age of 159 Ma (Irwin and Wooden, 2001). Despite this offset parameter, it falls within range with the peaks of higher magma addition. The Lumpkin pluton diorite, yields a $^{206}Pb/^{238}U$ age of 150.8 ± 4.7 Ma (MSWD = 4.3) (Figure 10-C). Lumpkin pluton does not have a previous publish age to correlate with.

The Cascade pluton tonalite (CP1305) consists of 22 analyses from 10 zircon samples. Due to many zircons that were lost or damaged during polishing, multiple spot ablations were performed on the same 10 zircons. With common-Pb correction and weighted average, the tonalite yields a $^{206}Pb/^{238}U$ age of 151.5 ± 5.6 Ma (MSWD = 11.4) with 1 out of 22 analyses rejected. The zircon fractions overlap in a linear progression, yet they generate a considerably high MSWD (Figure 10-D). Cascade pluton may have a previously-unrecognized composite make-up (Day and Bickford, 2004). Two distinct morphologies occur, showing older zircons that appear to have common prismatic, oscillatory zoned feature whereas younger zircons tend to have truncated features from overgrowths (Figure 10-IV, A and E) or what appears to be inherited cores. The presence of high discordancy within the sample set may reflect lead loss. We used the 'unmix' algorithm tool (after Sambridge and Compston, 1994) in Isoplot version 4.15 (Ludwig, 2008) for deconvoluting the suite of mixed ages obtained in a zircon sample set and can

be used as a good indicator of the relative significance of individual components. The mixture modeling ages have generated three separate age estimates of 165. 7 ± 3.9 (MSWD = 1.6), 145.0 ± 4.7 (MSDW = 2.0), and 125.1 ± 8.7 (MSDW = 1.5) (Figure 11).

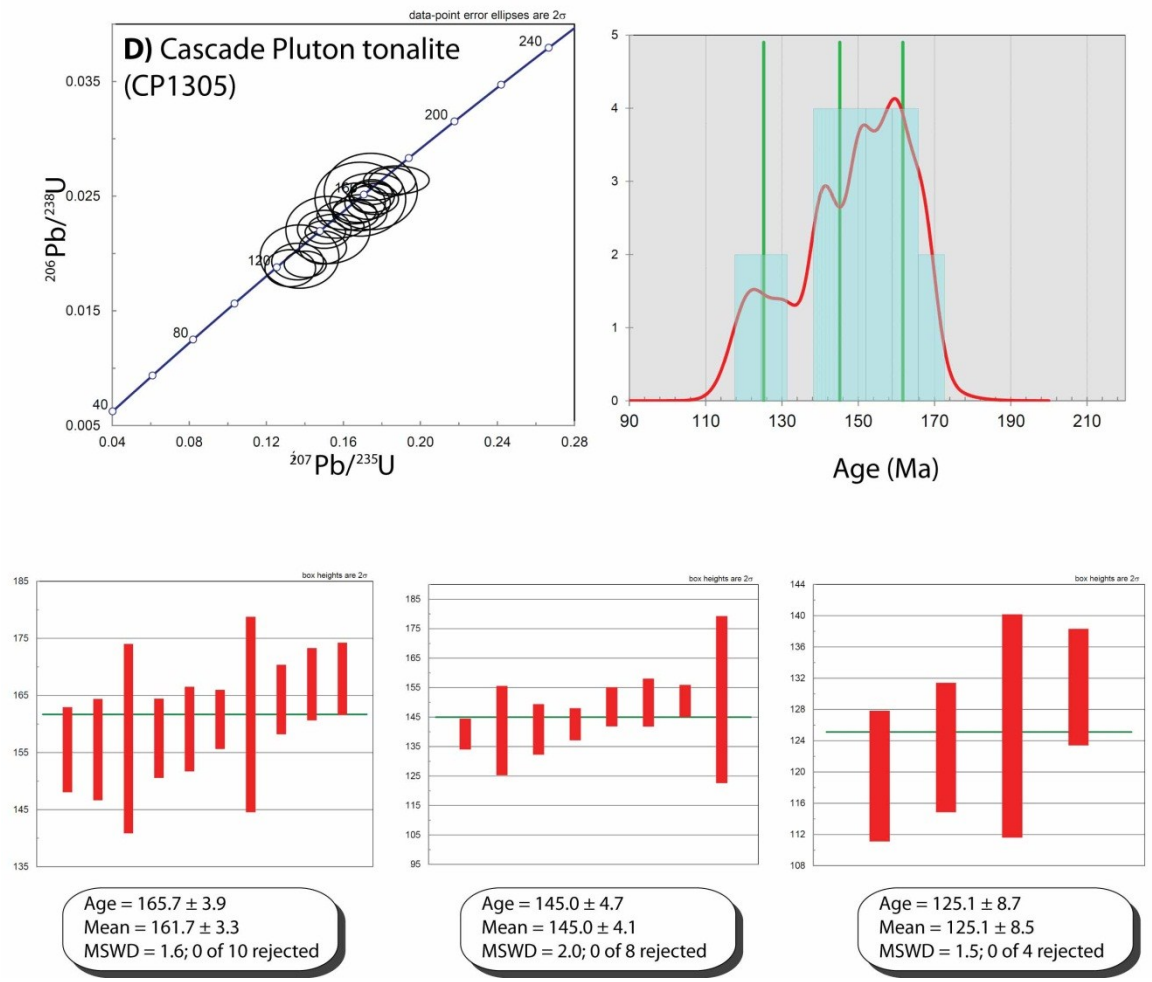

Figure 11. Cascade pluton Concordia diagram brought into deconvolution diagrams by the 'unmix' tool (after Sambridge and Compston, 1994) in Isoplot version 4.15 (Ludwig, 2008). The figure to the right of the Concordia diagram is a histogram with Gaussian distribution. The red curve indicates a population density plot with black lines indicating the mean $^{206}Pb/^{235}U$ ages with 2σ error. This tool is used for deconvoluting a suite of ages obtained in a zircon sample set. The mixture modeling ages have generated three separate age estimates of 165. 7 ± 3.9 (MSWD = 1.6), 145.0 ± 4.7 (MSDW = 2.0), and 125.1 ± 8.7 (MSDW = 1.5).

Because such a high MSDW was calculated, the 'unmix' tool in Isoplot v. 4.15 (Ludwig, 2008) was used to assess a plutonic body that may have incorporated multiple crystallization ages. The unmixing of age data reveals three ages at 165. 7 ± 3.9, 145.0 ± 4.7, and 125.1 ± 8.7. Although inheritance may exist, as seen under CL, 145.0 ± 4.7 is closer to Day and Bickford's granodiorite 143 ± 2 Ma age. Our sample was collected on the rim where it is predominantly tonalite, agreeable to Heitanen (1976) to which the reported Jurassic age can potentially be correlated with 165. 7 ± 3.9.

Lastly, zircons from Hartman Bar pluton granodiorite (HB1307) yields a $^{206}Pb/^{238}U$ age of 155.8 ± 3.0 Ma (MSWD = 1.5) (Figure 10-E) while zircons from the Bald Rock pluton tonalite (BR1308) yields a $^{206}Pb/^{238}U$ age of 133.4 ± 3.3 Ma (MSWD = 1.5) (Figure 10-F), both with no apparent inherited zircons. With subsequent U-Pb ages incorporated into the ages of this study (Cecil et al., 2012; Day et al., 2004; Edleman et al., 1989; Fagan et al., 2001; Girty et al, 1995; Guglielmo et al., 1993; Irwin and Wooden, 2001; and Saleeby et al., 1989 (C)) two peaks at 160 Ma and 142 Ma provide a correlation in apparent magma addition that is depicted in Figure 4.

6.2 Whole Rock Geochemistry

6.2.1 Major Elements

Plutons in the northern Sierra are predominantly are composed of granodiorite, quartz diorite, diorite, and tonalite rocks (Figure 12). For the purpose of emphasizing the timing of the Nevadan orogeny and its influence on magmatism by way of U-Pb age, these samples have been bracketed into pre-Nevadan plutons (166-156 Ma) and post-Nevadan plutons (152-142 Ma). These samples are then compared with the Late

Cretaceous batholithic samples (121-85 Ma) taken from the North American volcanic and intrusive rock database (NAVDAT; www.navdat.org). Hence, pre-Nevadan plutons are plotted primarily as granodiorites and granites. Post-Nevadan plutons are plotted in a range of tonalite, granodiorite, and quartz monzodiorite rocks with some minor plots in the granite range. Samples in this study are categorized as granodiorite and quartz diorite that are pre-Nevadan in age while post-Nevadan samples are predominantly tonalities.

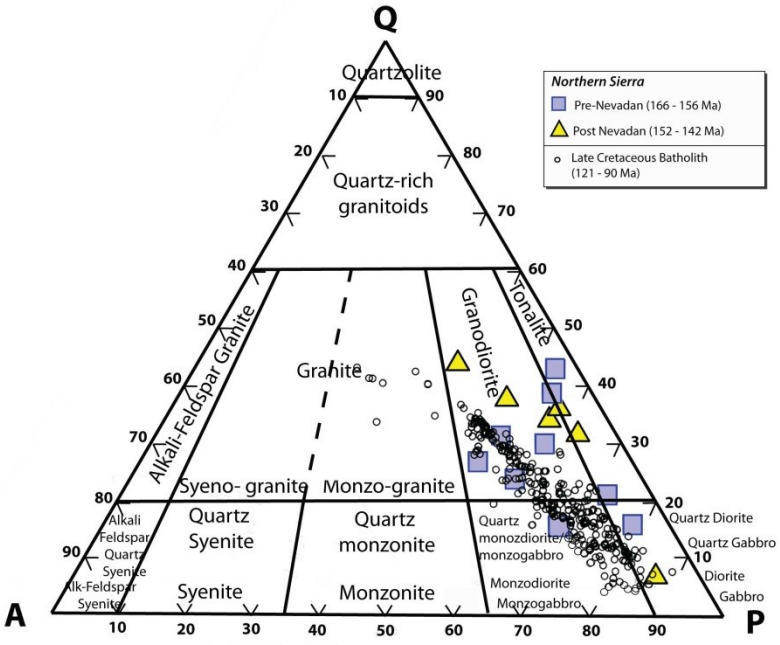

Figure 12. QAP diagram of samples collected in the northern Sierra Nevada. Samples are predominantly granodiorite, quartz diorite, diorite, and tonalitic rocks. Samples are divided into pre-Nevadan Middle Jurassic (blue squares), post-Nevadan Late Jurassic-Early Cretaceous (yellow triangles) and compared with the Late Cretaceous batholithic samples (black dots) taken from the North American volcanic and intrusive rock database (NAVDAT; www.navdat.org). Data are from Kistler and Peterman (1978); Peck and Van Kooten (1983); Bateman et al. (1984) (1988); Ague and Brimhall (1988); Barbarin-Bernard (1990); Hirt (1991); Moore (1991) Clemens-Knott (1993); Sisson (1992); Macias (1996); Hirt (2007). Additional northern Sierra data is from Cecil et al., 2012.

With respect to all samples plotted in the northern Sierra, Harker diagrams (Figure 13) are observed to portray plutons with an overall wt% silica content that ranges from 50 – 80%. Oxides FeO and CaO exhibit negative trends while TiO_2, K_2O, NaO_2, and Al_2O_3 present positive correlations with higher scatter. Plutons that formed prior to the Nevadan orogeny (166 – 156 Ma) have a silica range of 53% - 70%. When comparing these samples with post-Nevadan plutons (152 – 142 Ma), higher values are expressed in FeO, TiO_2, Al_2O_3, and CaO. Pre-Nevadan plutons are also lower in NaO_2, yet they appear blended with K_2O concentrations when compared with pre-Nevadan plutons. It is important to note that plutons in the western belt such as the Swedes Flat quartz diorite contains the lowest concentration of SiO_2 in this study with as low as ~ 50 wt% and is considered to be pre-Nevadan in age. In comparison to pre-Nevadan plutons, post-Nevadan plutons exhibit a higher SiO_2 range of 60 – 80%. They are also expressed in lower FeO, TiO_2, and CaO and higher NaO_2. Above all, the oxide concentrations with respect to SiO_2 present clear differentiations of younger, more-evolved plutons of higher silica verses older lesser-evolved plutons with lower silica.

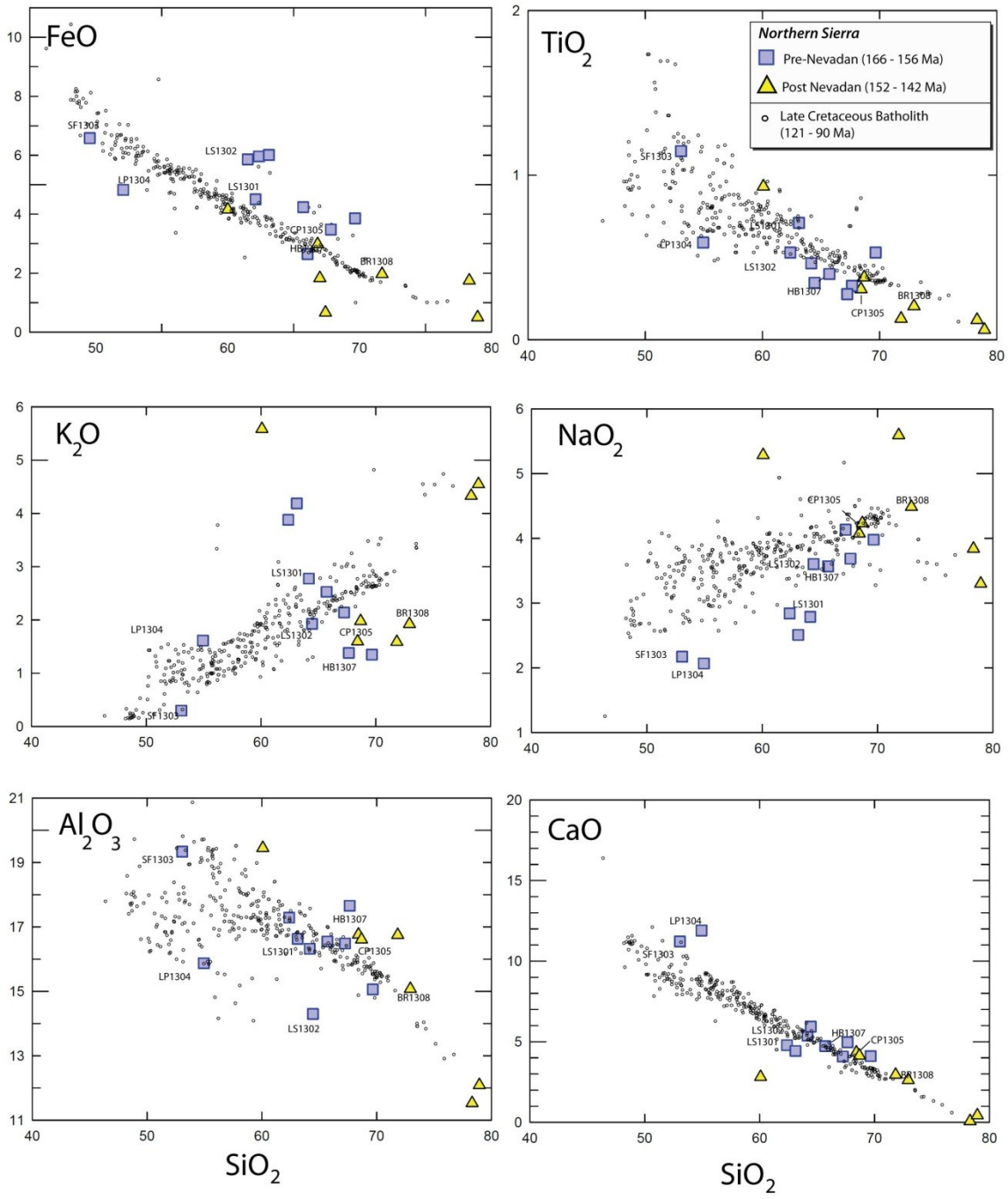

Figure 13. Harker Diagrams displaying major oxides versus SiO_2 geochemical plots in wt%. All geochemical data is divided into pre-Nevadan (blue squares), post-Nevadan (yellow triangles) and compared with the Late Cretaceous batholithic samples (black dots) taken from the North American volcanic and intrusive rock database (NAVDAT; www.navdat.org). Data are from Kistler and Peterman (1978); Peck and Van Kooten (1983); Bateman et al. (1984)(1988); Ague and Brimhall (1988); Barbarin-Bernard (1990); Hirt (1991); Moore (1991) Clemens-Knott (1993); Sisson (1992); Macias (1996); Hirt (2007). Additional northern Sierra data is from Cecil et al., 2012.

Most igneous rocks in the northern Sierra are metaluminous-to-slightly peraluminous when plotted on a Al/(Na+K) vs. Al/Ca+Na+K) diagram (Figure 14). Pre-Nevadan plutons, however, tend to be primarily metaluminous while post-Nevadan plutons are plotted in the peraluminous to weakly metaluminous field. In contrast, pre-Nevadan and post-Nevadan rocks, when plotted on a K_2O+Na_2O-CaO versus SiO_2 diagram (Figure 15) fall on similar calcic to calc-alkalic trends, identical to all data from the northern Sierra (170 – 130 Ma). Samples from this study that include Lake Spaulding (LS1301)/(LS1302), Swedes Flat (SF1303), and Lumpkin pluton (LP1304), for example, are calcic, yet plot in the metaluminous field in Figure 14. Once again, these pre-Nevadan samples are distinguished by their lower silica content than in progressively-younger rocks in the northern Sierra, and this trend is exhibited throughout all geochemical data. Another such trend depicting these evolutionary differences is clearly evident on an AFM (Irvine and Barager, 1971) variation diagram ($Na_2O + K_2O$ vs. $FeO + Fe_2O_3$ vs. MgO) (Figure 16), in which all rocks in the northern Sierra follow the calc-alkaline trend, as would be expected of geochemical signatures common to continental arc magmas. A clear depiction of pre-Nevadan and post-Nevadan separation is exhibited. Post-Nevadan rocks appear to cluster nearest to the alkaline trend (Na_2O+K_2O) with more removal of Mg from parental basaltic lavas and magnetite enrichment. With regard to pre-Nevadan samples, plutons are clustered further away from the path of higher alkalinity.

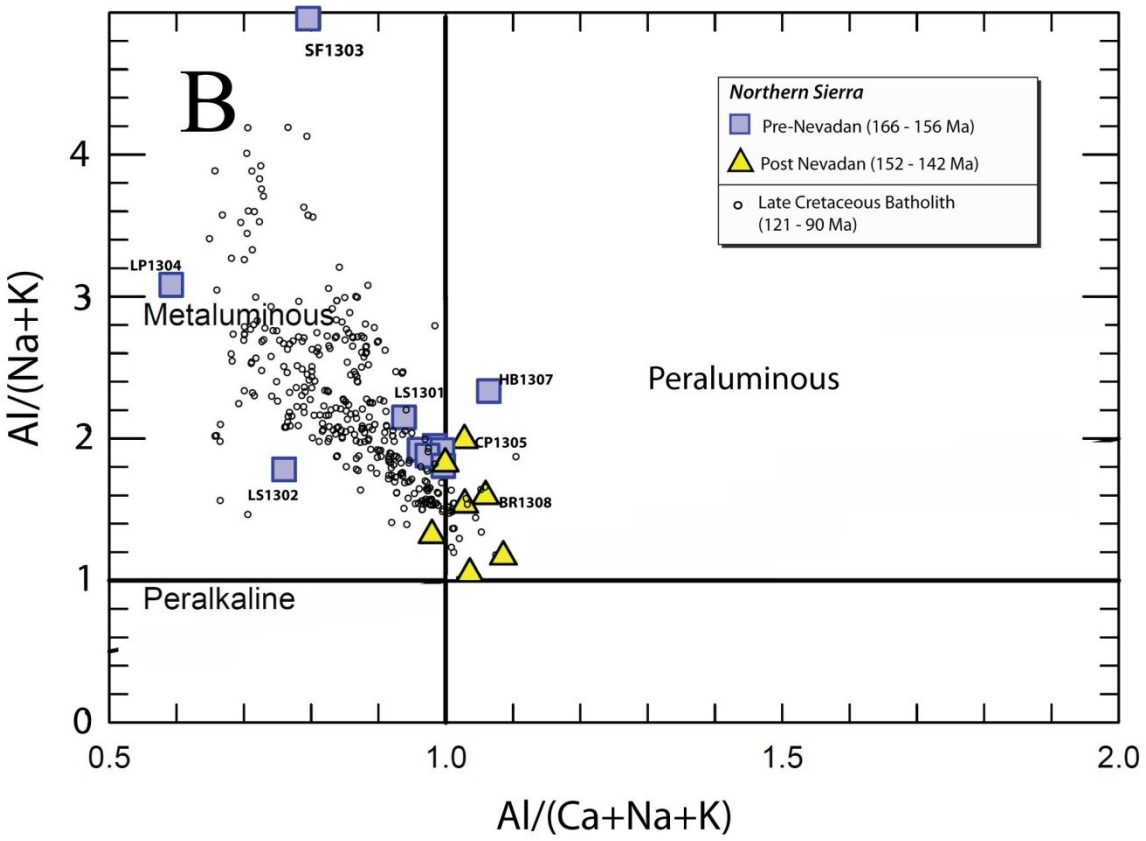

Figure 14. A general classification of sampled plutons from the northern Sierra Nevada. Diagram showing Al_2O_3 /CaO + Na_2O_3 + K_2O) versus Al_2O_3 /Na_2O_3 + K_2O in mol% used to distinguish peralkaline, metaluminous, peraluminous compositions. Middle Jurassic plutons are metaluminous to weakly peraluminous. Late Jurassic plutons are moderately peraluminous to weakly metaluminous. All geochemical data is divided into pre-Nevadan (blue squares), post-Nevadan (yellow triangles) and compared with the Late Cretaceous batholithic samples (black dots) taken from the North American volcanic and intrusive rock database (NAVDAT; www.navdat.org). Data are from Kistler and Peterman (1978); Peck and Van Kooten (1983); Bateman et al. (1984)(1988); Ague and Brimhall (1988); Barbarin-Bernard (1990); Hirt (1991); Moore (1991) Clemens-Knott (1993); Sisson (1992); Macias (1996); Hirt (2007). Additional northern Sierra data is from Cecil et al., 2012.

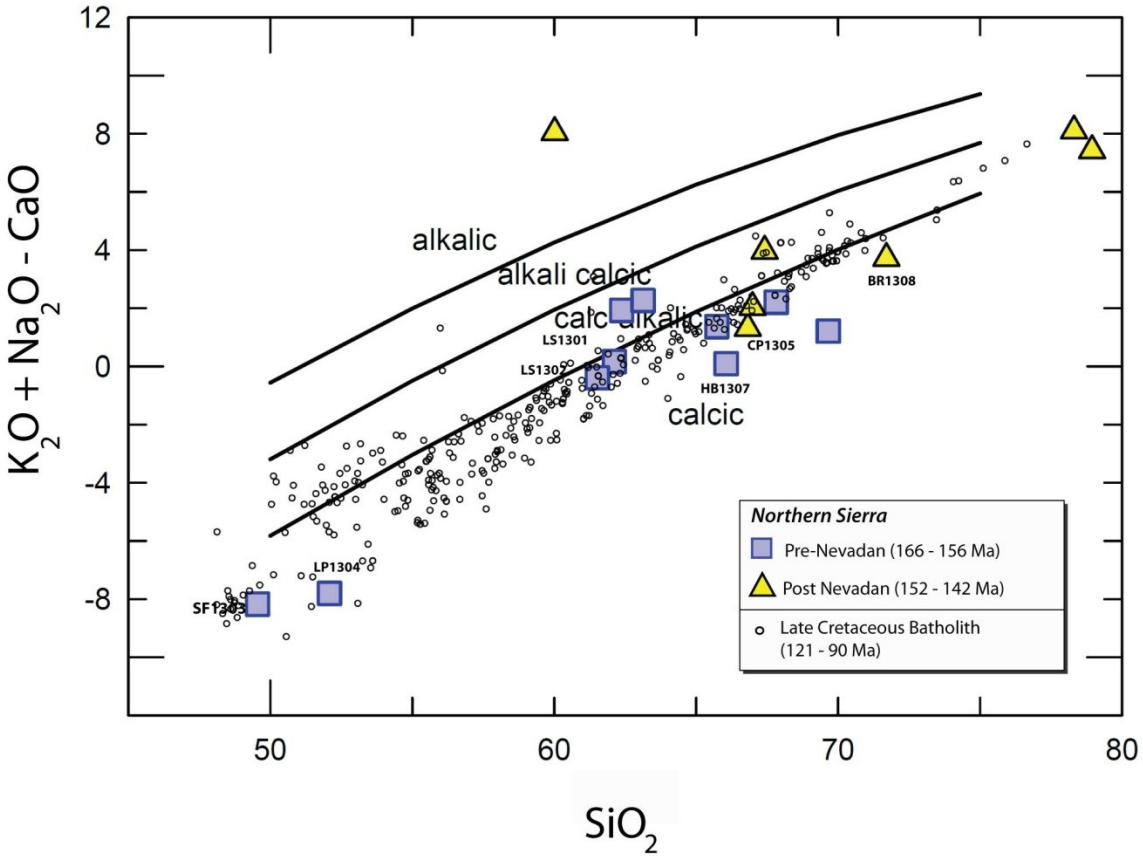

Figure 15. A general classification of sampled plutons from the northern Sierra Nevada. Diagram showing $K_2O + Na_2O$ - CaO versus SiO_2. Most northern Sierra samples plot in the calc-alkalic and calcic field. All geochemical data is divided into pre-Nevadan (blue squares), post-Nevadan (yellow triangles) and compared with the Late Cretaceous batholithic samples (black dots) taken from the North American volcanic and intrusive rock database (NAVDAT; www.navdat.org). Data are from Kistler and Peterman (1978); Peck and Van Kooten (1983); Bateman et al. (1984)(1988); Ague and Brimhall (1988); Barbarin-Bernard (1990); Hirt (1991); Moore (1991) Clemens-Knott (1993); Sisson (1992); Macias (1996); Hirt (2007). Additional northern Sierra data is from Cecil et al., 2012.

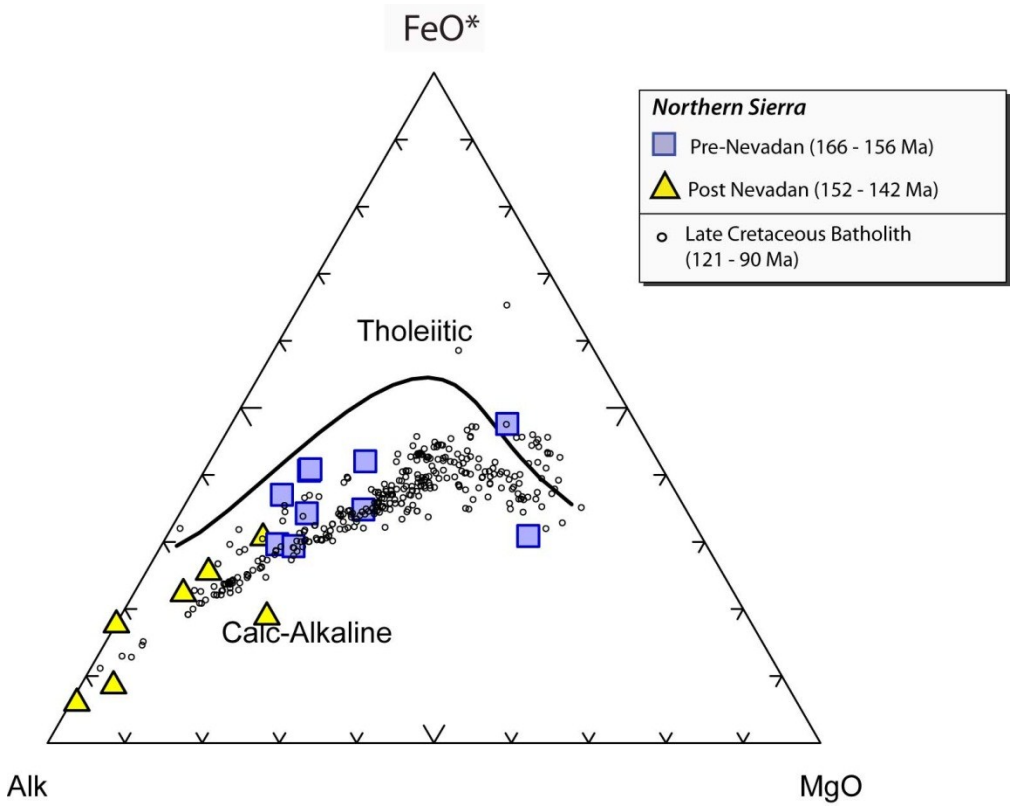

Figure 16. AFM diagram (A:Na_2O + K_2O versus FeO*: FeO + Fe_2O_3 versus MgO) showing the magmatic evolutionary trends of calc-alkaline and tholeiitic granitoid rocks. All geochemical data is divided into pre-Nevadan (blue squares), post-Nevadan (yellow triangles) and compared with the Late Cretaceous batholithic samples (black dots) taken from the North American volcanic and intrusive rock database (NAVDAT; www.navdat.org). Northern Sierra samples yield higher evolved trends that correspond to post-Nevadan samples while older pre-Nevadan samples plot in more primitive zones of the diagram. Data are from Kistler and Peterman (1978); Peck and Van Kooten (1983); Bateman et al. (1984)(1988); Ague and Brimhall (1988); Barbarin-Bernard (1990); Hirt (1991); Moore (1991) Clemens-Knott (1993); Sisson (1992); Macias (1996); Hirt (2007). Additional northern Sierra data is from Cecil et al., 2012.

6.2.2 Trace Elements

Plutonic rocks in the northern Sierra record a variation of high and low Sr/y magmatism. Pre-Nevadan plutons (166 – 156 Ma) portray a wide range of Sr/Y at 9.86 – 75. Similarly, Sr/Y ratios for post-Nevadan plutons (152 – 142 ma) depicts a range of 2 – 48, with a single data point that is plotted up to 95 (Figure 17). It is important to note that, while there contains much variance in Sr/Y between pre and post-Nevadan plutons, a pattern of location within the metamorphic terranes is highlighted. Samples from this study that include Cascade pluton (CP1305), Hartman Bar (HB1307), and Lake Spaulding (LS1301) correlate well with high Sr/Y signatures within the Central and Eastern belts, along with previous works for Cascade Pluton east (Hietanen, 1976) the Yuba River (G01; Cecil et al., 2012) and Lake Spaulding (G03; Cecil et al., 2012). Together, these plutons show high Sr/Y (>40) as a result of high Sr (~ 400 – 600) and low Y (~7 – 12) (Table 2). In that regard, Pleasant Valley pluton (G02; Cecil et al, 2012), Bald rock pluton (BR1308), Lake Spaulding (1302), and Swedes Flat pluton (SF1303), however, lay within areas of the Western belt where they show significantly-lower Sr/Y (< 12) as a result of low Sr (~260) and high Y (17 – 21) (Table 2). Two exceptions include Lumpkin pluton (LP1304) and Merrimac pluton (Heitenan, 1977), both dated post-Nevadan in age and reside within the Central belt where predominantly more plutons contain high Sr/Y. Data from the rest of the Cretaceous batholith is used as a comparison and is seen as black dots that show a trend typical of continental convergence. The linear trends by these data points are most likely due to the data output from NAVDAT.

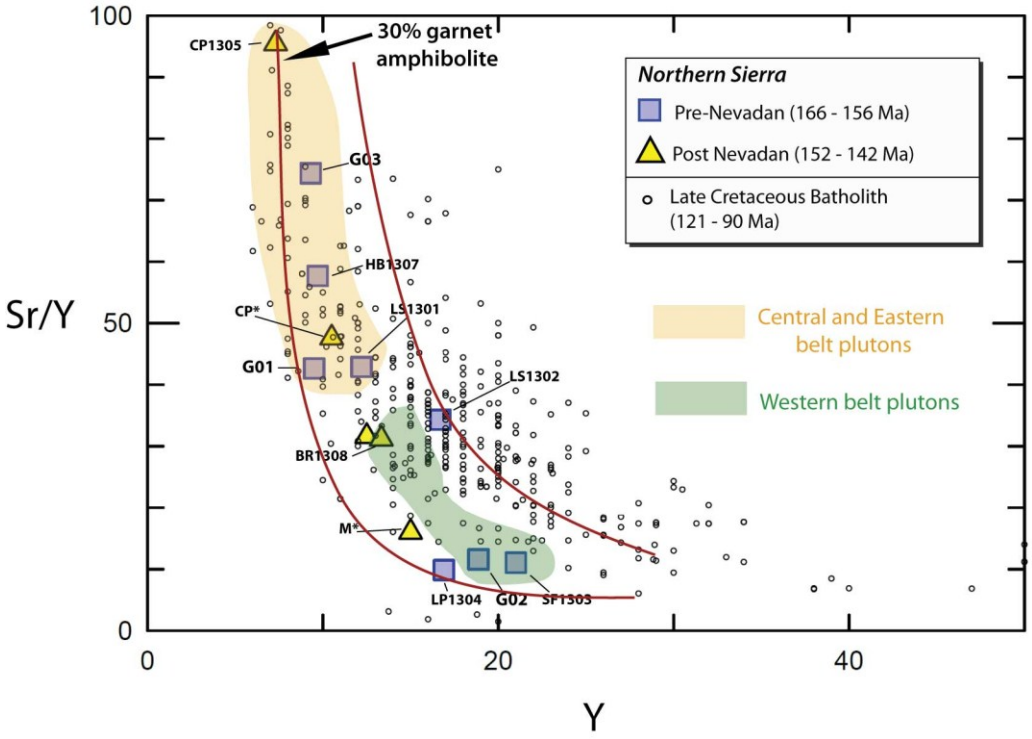

Figure 17. Plot of Sr/Y versus Y for plutons in the northern Sierra Nevada. Sr/Y values from both Middle Jurassic and Late Jurassic rocks tend to be variable. Highlighted areas in orange depict plutons with high Sr/Y that reside in the Central and Eastern belts while highlighted areas in green depict lo Sr/Y plutons that exist within the Western belt. All geochemical data is divided into pre-Nevadan (blue squares), post-Nevadan (yellow triangles) and compared with the Late Cretaceous batholithic samples (black dots) taken from the North American volcanic and intrusive rock database (NAVDAT; www.navdat.org). Data are from Kistler and Peterman (1978); Peck and Van Kooten (1983); Bateman et al. (1984)(1988); Ague and Brimhall (1988); Barbarin-Bernard (1990); Hirt (1991); Moore (1991) Clemens-Knott (1993); Sisson (1992); Macias (1996); Hirt (2007). Additional northern Sierra data is from Cecil et al., 2012.

Spider diagrams consist of normal-mid-ocean-ridge basalt (N-MORB) from Sun and McDonald (1989), Mid-ocean-ridge basalt (MORB) from Pearce (1989), and Rock/chondrite from Sun (1980). Additional northern Sierra data is from Cecil et al., 2012. MORB-normalized spider diagrams show distinguishable characteristics for pre and post-Nevadan plutons (Figure 18, A thru C). Pre-Nevadan plutons yield enrichment in large ion lithophyle elements (LILE) with strong positive K and Rb anomalies. These elements are associated with moderately-negative Sr and Ba anomalies which present a possible role of fractional crystallization. Pre-Nevadan plutons also yield strong negative high field strength elements (HFSE) in Nb and Ti. In comparison, post-Nevadan plutons yield stronger enrichment in LILE with greater positive K and Rb than pre-Nevadan plutons, however, they are strongly negative in Sr and Ba. HFSE in post-Nevadan plutons yield stronger positive Zr, Hf, Th, yet they have a moderate depletion in Th, Ta, Ti, U.

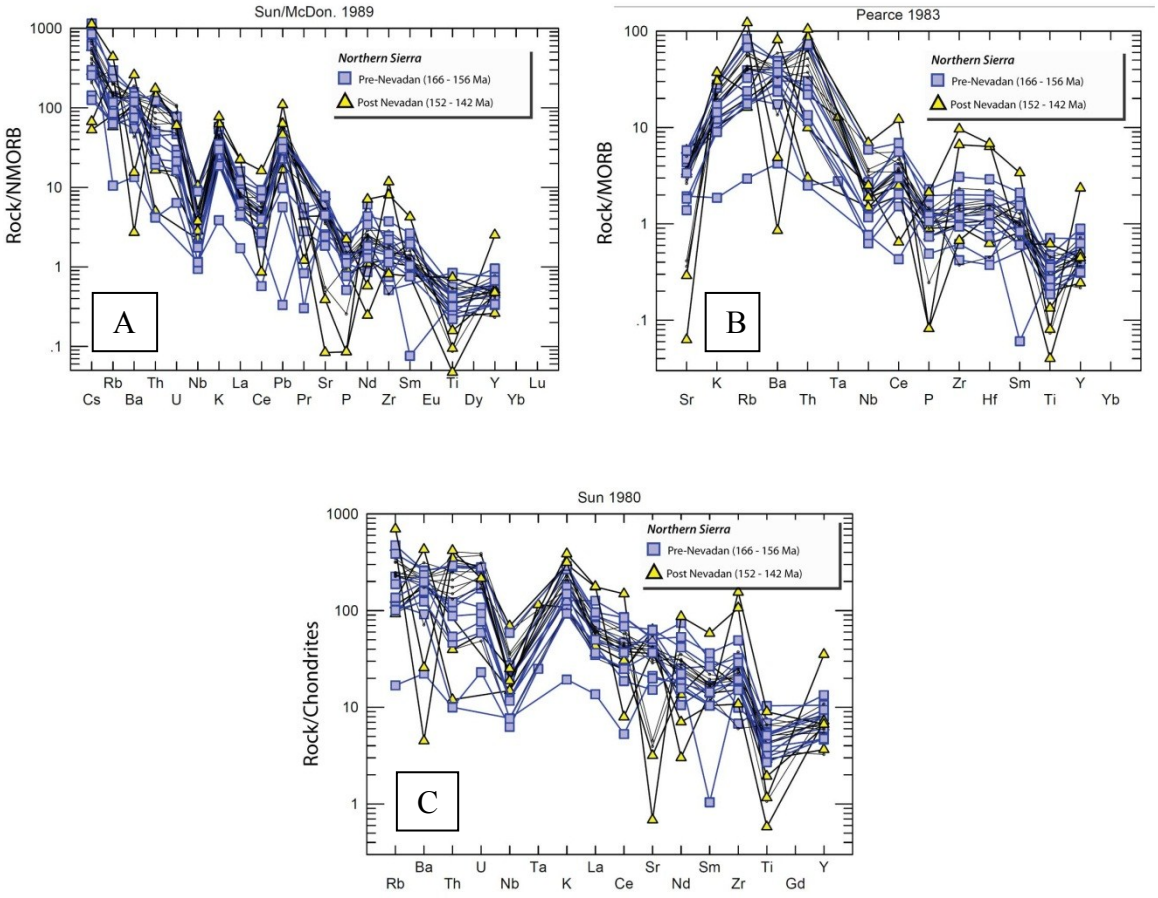

Figure 18 (A thru C). Spider diagrams representative of trace element abundance from the northern Sierra Nevada plutons. Northern Sierra samples are N-MORB normalized and yield Large Ion Lithophyle Element (LILE) enrichment and a depletion of high field strength elements (HFSE). (A) Normal-mid-ocean-ridge basalt (N-MORB) is from Sun and McDonald (1989). (B) Mid-ocean-ridge basalt (MORB) is from Pearce (1989). (C) Rock/chondrite is from Sun (1980). Additional northern Sierra data is from Cecil et al., 2012.

7. DISCUSSION

This thesis is a broad study of plutons in the northern Sierra Nevada, and one rock sample has been analyzed on each of seven plutons. The data observed in the petrographic analysis (Appendix A), U-Pb zircon geochronology (Appendix B), magma addition histogram (Figure 3 and 4), and geochemistry (Table 3) are discussed herein and are correlated with previous works in the northern Sierra, Klamath Mountains, and their history with the Nevadan orogeny. As such, rocks for this study, as well as data from Cecil (2012), are also correlated with the tectonic metamorphic terranes (Western, Central and Eastern) from which they have been emplaced using the two age brackets presented in figures 9 through 13 as pre-Nevadan (166 – 156 Ma) and post-Nevadan plutons (150 – 142 Ma). We take this approach in order to better emphasize the role orogeny played in the northern Sierra Nevada by comparing each of the two groups and make comprehensive interpretations of the tectonic history of the region. Therefore, the ages, geochemistry and petrology in this study are meant to explain whether the two-pulsed magmatic episodes not defined in Ducea (2001) were caused by crustal thickening during the time of the Nevadan orogeny.

7.1 U-Pb Zircon Geochronology

New data from 6 of 7 plutonic rock samples exhibit two pulses of high magma addition during the Middle Jurassic at ca. 165 – 160 Ma, and the Early Cretaceous at ca. 145 – 140 Ma (Figure 4). These two pulses were previously unrecognized and identified as a single pulse event. Ducea (2001) published an apparent intrusive flux curve depicting

2 episodes of magmatic fluxing events for the greater Sierra Nevada from 160 – 150 Ma and 121-85 Ma, which did not take into account plutons in the northern Sierra that are older, more dispersed, and not as well dated (Figure 2). Because of this lack of data, Ducea (2001) did not make apparent that between 170 and 140 Ma, the Jurassic to Early Cretaceous range may have undergone more than one flare-up event. By combining U-Pb age data from this study and previous studies, the single Jurassic peak depicted in Ducea (2001) had surprisingly exhibited two pulses of magma addition to the crust from 165 – 160 Ma and 145 – 140 Ma, highlighting a distinctive lulling period from 155 Ma to 150 Ma (Figure 4). These indicate that magmatism was introduced episodically to the crust and therefore underwent a loss in thermal development within the arc itself. This is not to say that magmatism had completely shut off during that time, as the evidence of syn-Nevadan dikes are expressed in the Klamath Mountains and areas of the northern Sierra respectively (Harper, 2006). Insomuch, the spatial and temporal trends of the two-peaked magmatic episodes hold moderate consistency with reported ages (Cecil et al, 2012; Patterson et al, 2011; Ducea, 2001) but does not explain the lull if the arc was relatively cooler during pre-Nevadan arc magmatism.

With respect to the plutons dated in this study, the youngest $^{206}Pb/^{238}U$ age reported is from Bald Rock pluton and yields an age of 133.4 ± 3.3 Ma (MSDW = 1.5). This age does not coincide with an earlier published age of 140 ± 2 Ma reported by Saleeby et al., 1989, yet it does indicate that it may be a pluton more related to post-Nevadan, Early Cretaceous magmatism that reside furthest north from 39°30'N to 40°N. Although Swedes Flat pluton ages from this study and published works differ slightly, they are within the window of 160 Ma and falls within the pre-Nevadan bracket.

Additionally, previous work had associated Cascade pluton as an early Cretaceous body and had derived an Ar/Ar hornblende age of 150 Ma (Fagan et al, 2001). It may be considered that because the Hartman Bar and Cascade pluton are mineralogically-similar, that they may also have a similarity in their spatial and temporal record described in Heitanen, 1976. With exception of Bald Rock pluton (133.4 ± 3.3 Ma), the range of ages correlate moderately-well within the array of two peak flux ages 142 Ma and 160 Ma (Figure 4). The distribution of ages reveals significant magmatic episodes in an active Jurassic arc not defined in previous works with peak episodes at ~160 and 142 Ma. In summarizing the correlations with the U-Pb data, plutons in the northern Sierra do not provide any indication of a patterned distribution of ages as would be seen from east to west in the Cretaceous batholith of the southern and Central Sierra Nevada. Pre-Nevadan plutons from 167-160 Ma were not limited to being emplaced in any one terrane much like post-Nevadan plutons.

7.2 Petrographic analysis

The northern Sierra Nevada is generally comprised of granodiorite, quartz diorite, diorite, and tonalitic plutons related to early subduction and the onset of episodic magmatism during the Middle Jurassic to Early Cretaceous. Pre-Nevadan plutons (Lake Spaulding, Swedes Flat, and Hartman Bar) were categorized into granodiorite and quartz diorite while post-Nevadan plutons (Bald rock, Cascade, and Lumpkin plutons) were categorized into diorite and tonalites. What was observed from this partition of rock types was their clear differentiation of mineralogical content. Pre-Nevadan plutons are clearly more hornblende-rich than plutons with higher silica (post-Nevadan) which present more

biotite-rich, I-type granitoids that plot slightly peraluminous, which will be further discussed in the geochemistry. Further analysis have shown that pre-Nevadan plutons within the Central belt contain high degrees of oscillatory zoning in large plagioclase laths, whereas the Western belt Swedes Flat pluton is more heavily altered by chloritization and resorbed rims on plagioclase. These features may indicate that post-Nevadan plutons are typical of rocks that would be generated by the convergence of a thicker continental crust along the older accreted terranes eastward versus the pre-Nevadan plutons that are suggested to be derived from a thinner crust typical of island arcs in the Western Belt.

Pre-Nevadan plutons in this study which include, Lake Spaulding (1301/1302), Swedes flat (1303), Hartman Bar (1307) all tend to portray higher degrees of fabrics present than their post-Nevadan counterparts, and that they were emplaced within the Paleozoic Central belt (Figure 1). Observations in thin section petrography revealed that the alignment of plagioclase laths, biotite and hornblende grains, including the presence of sutures and undulose extinction found in quartz, indicate that many pre-Nevadan plutons underwent magmatic foliation through plutonic gradational zoning more so than metamorphism. These observations do not suggest that metamorphism is not the only fabric-producing process encountered in these plutons. In fact, metamorphism is encountered in many parts of the plutonic suites, especially at edges where plutons meet fault boundaries. Yuba River pluton (pre-Nevadan), for example, contains highly-deformed rocks on its western margin adjacent to the Wolf Creek fault (Day and Bickford, 2004). Another consideration to understanding might be to apply the evidence of fabrics to the regional shape of the plutons. Regionally, the lobate pre-Nevadan

plutons lack a certain physical concentricity that is seen more prominently on their younger, post-Nevadan counterparts (Bald Rock, Merrimac, Granite Basin, Grizzly, and Bucks Lake plutons (Figure 1). With the exception of Cascade pluton, the lobe-shaped physical extent of Cascade pluton does not appear to have the same concentric shape as the rest of the post-Nevadan plutons depicted in Figure 1. Cascade pluton, however, could be considered to be a composite of more than one pluton. The shape of the pluton, or rather a portion of its body, coincides more with the other plutons that are pre-Nevadan in age within the Central belt and would, thus, require further investigation. All in all, these observations suggests that continued intrusion of magma during the Nevadan orogeny may have been affected by the docking and suturing of metamorphic belts from which these lobe-shaped plutons intruded. This however does not explain why pre-Nevadan plutons that reside in the Western belt do not contain prominent degrees of foliation, more than what is observed in Late Jurassic/Early Cretaceous plutonic rocks of the Central belt. It is possible that plutons like Swedes Flat (164.6 ± 0.43 Ma) do not contain fabrics in their mineralogy because, much like Cascade pluton (151.5 ± 5.9 Ma), it is also considered to have a composite make up (Beard and Day, 1986) and perhaps the island arc terrane was not fully affected due to the manner in which it was underthrusted onto the continent, causing crustal shortening on the Central and Eastern belts on the western edge of North America (Schweickert et al., 1984).

7.3 Whole Rock Major and Trace Element Geochemistry

Most rocks are predominantly calcic to slightly calc-alkaline. Post-Nevadan plutons, however, are more peraluminous, are higher in SiO_2, and span a greater calc-

alkaline range indicating their more evolved geochemistry than pre-Nevadan plutons. Although most pre-Nevadan rocks that plot in the metaluminous field are less silicic towards the west than in the east, they are also more hornblende-rich than plutons with higher silica (Bald Rock, Cascade and Lumpkin) which present more biotite-rich, I-type granitoids that plot slightly peraluminous. These indicate that the majority of pre-Nevadan plutons in the northern Sierra are products of fractional crystallization of mantle-derived magmas from an outboard island arc where magmas may have intruded thinner crust during tectonic accretion against the continent. This precursor to the voluminous and more mature post-Nevadan arc expands to a greater region than formerly realized. Whole-rock trace element geochemical features of pre-Nevadan plutons suggest that they are lesser-evolved products of subduction and show significant changes in geochemistry. Spider Diagrams (Figure 18) depict these petrogenetic similarities in most rocks in the northern Sierra. Light rare earth elements in steeper negative anomalies indicate the reflection of hornblende than garnet. Since there are no Eu anamolies to make a correlative observation, depth of melting may be consistent during the life of the arc. Enrichment of large ion lithopyhle elements (LILE) are also observed indicating metasomatism that occurred in plutonic rocks. The analysis of our data suggests that pre-Nevadan plutons underwent fractional crystallization of a more mafic magma due to a subducting oceanic slab brought upon by partial melting of the mantel wedge.

7.3.2 *Magma sources and Sr/Y variations*

Pre-Nevadan plutons in the northern Sierra show a bimodal variation of high and low Sr/Y values. Cecil (2012) reported that the majority of Jurassic and Cretaceous

plutonic rocks in transects made the northern Sierra have predominantly high Sr/Y values, an indication that the source of magmas had been produced at a depth sufficient to be garnet-bearing (Tulloch and Kimbrough, 2003). Rocks that contain Sr, Na, Al and low Y with high Sr/Y are a common characteristic to magmas that have been generated by the melting of the mafic slab during subduction (Drummond and Defant, 1990). An example of high Sr/Y have been studied in the Blue Mountains of Oregon which have investigated the link to high/low Sr/Y magmas related to a contractional event (Schwartz, 2011). They emphasize that there are a number of uncertainties concerning the significance of high Sr/Y magmatism during tectonic accretion of arc-related rocks and whether they are linked to other regions in western North American cordilleran. In that regard, high Sr/Y plutons (>40 ppm) that have been recorded in this study also appear restricted to the Central belt (ie. Cascade pluton (CP1305), Hartman Bar (HB1307); Table 2), including Yuba River (Cecil et al., 2012) which is bracketed as a pre-Nevadan pluton. One exception is Lumpkin pluton (LP1304), which does not express the same high Sr/Y values but yields a low Sr/Y value of 9.86, which suggests that it may be correlated with the rest of the pre-Nevadan low Sr/Y plutons of the Western belt despite its post-syn Nevadan age of 150.8 ± 4.7 Ma. Sampled plutons from previous works that exist in the Western belt (ie. Swedes Flat pluton, Pleasant Valley and San Juan Ridge, and Pilot Peak) have lower Sr/Y ratios (as low as 10) which indicates they may have been likely generated at a shallower regime. Their depletion of Yttrium suggests that the pressure of the magmatic source may have not been high enough to evoke fractional crystallization of garnet since garnet is typically sequestered at higher pressures and incorporates Yttrium. Where garnet becomes stable at the deep crust, it is rare to see high Sr/Y in

island arcs, however, during orogenic activity, crust is thickened, and magmatism that is produced by this thickening generally creates high Sr/Y (pers. comm, Schwartz, 2011). The low Sr/Y Middle Jurassic rocks that have intruded the Western belt indicates that the source of magma was not relatively deep as would magmas from the Central belt might be. Samples rich in hornblende (i.e. Swedes Flat) appear to have a correlation with low Sr/Y plutons also suggesting that their parental magmas may have originated from an island arc province.

The foliation that is present in the more easterly plutons (CP1305, HB1307, LS1301) are those that are in the high Sr/Y fields and may have developed coevally with Middle Jurassic deformation. These alterations are not present in the low Sr/Y rocks and may be a result of a deformational component to plutons and crustal thickening may have occurred to reflect higher Sr/Y ratios for the Central Belt Plutons where magma ascension encountered a thicker crust during the accretion of metamorphic terranes. Bald rock and Lumpkin pluton, for example appear to be unrelated [to each other] despite their low Sr/Y values; Lumpkin pluton has much lower SiO2 (~50 wt%) while Bald Rock is a more evolved pluton with ~70 wt%, thus, generating clear, dissimilar contrasts to their setting.

The relationship between Sr/Y in Nevadan collision indicates that low Sr/Y magmatism may have occurred from 167 – 157 Ma in the Western Belt, yet at 165 – 150 Ma, high Sr/Y magmas occurred in the Central belt which suggests that the chemistry in magmas changed from west to east depending on their location and not so much their temporal relationship (see Figure 17). Less felsic rocks have SiO2 contents between 49 – 62 wt% and have lower Sr/Y values. More felsic rocks contain SiO2 values between 65 -

66 wt% and have higher Sr/Y values from 57 – 95 wt% further constraining those differences.

7.4 Timing of plutons and influence of the Nevadan Orogeny

The northern Sierra underwent a period of compression by an island arc that had accreted onto western North America during the Jurassic. This event, in turn, had caused the introduction of magmatism, faulting and metamorphism – features that are also observed in the Klamath Mountains and attributed to the Nevadan orogeny (Hacker et al., 1995; Snoke and Barnes, 2006; Barnes et al., 2006; Hotz, 1971; Harper, 2006). Strictly in the northern Sierra, plutons underwent 2 high-peaked magma addition events in the Jurassic at 160 and 142 Ma (Figure 4). In determining the cause of renewed subduction after the first event following a lull in magmatism, specific investigations such as depth of magmatism on plutons investigated in this study are not addressed in this paper. Yet, correlations of the U-Pb ages and geochemistry help relate plutons and their relationship to the overall evolution of the northern Sierra and the distinctions made of both events. We emphasize the prominent, episodic flare-up events have a part to play with the Nevadan orogeny, a heavily investigated, controversial deformational event which may have played an important role in the change of episodicity and has been suggested to have begun in the northern Sierra (Schweickert, 1984). This study does not investigate the timing of the Nevadan orogeny. Rather, it uses previous works as a marker to associate events in the northern Sierra with the Klamath Mountains and compares the similarities with the two regions. How extensive the Nevadan Orogeny originated in California was, and how far south it affected the northern Sierra as a whole is uncertain,

but Schweickert (1984) places the Nevadan orogenic age in the northern Sierra at ~155 ± 3 Ma and is followed by later studies that believe there was a greater time interval (Hacker et al, 1995). Our histogram portrays a magmatic lull that exists between 155 – 150 Ma and may suggest a coinciding relationship to the lull and the Nevadan orogeny. Using this perspective, the dated plutons that were divided pre-Nevadan (Middle Jurassic (166 – 156 Ma), and post-Nevadan (early Cretaceous 145-140 Ma) based on U-Pb data were used to compare and contrast the geochemical data. Because this study does not incorporate REE to gain a perspective on crustal thickness at the time of magma generation or depth of melting, we used previous studies of the timing and extent of Nevadan features and Sr/Y in this study to make a well-researched assumption of the impact the orogeny may have had on magmatism in the northern Sierra Nevada versus crustal thickness. In that regard, it must be noted that Jurassic plutons that exist eastward such as Haypress creek and Emigrant Gap dated in previous studies were considered to be products of post Nevadan deformation, however, their Jurassic age and deformation history suggests that the Nevadan orogeny was not as widespread in the eastern belt (Girty et al, 1995), and this observation may include areas of Lake Spaulding.

These plots suggest that, while improving the single-peaked emplacement rate depicted in a previous flux curve at 160-150 Ma (Ducea, 2001), magmatism was less melt-fertile prior to the Nevadan orogeny in the mid-to-Late Cretaceous (ca. 100 – 85 Ma) and that the subduction process was not steady-state. In summarizing the events that occurred off the coast of western North America during the Jurassic, the formation of island arc convergence was created via an east-dipping subduction zone (Dilek and Moores, 1989; Godfrey and Dilek, 2000) (Figure 19) similar to what is depicted in the

Model 2 scenario in figure 5. Before the accretion and compression of the island arc, the first magmatic flare up event took place 166 – 156 Ma. Plutons that intruded the thicker Paleozoic and Mesozoic oceanic altered crust and continental crust were higher in Sr/Y than plutons of around the same age that were generated in the outboard island arc. From 155 – 150 Ma, during the Nevadan orogeny, the western coast of North America underwent a period of compression, faulting, and slowed magmatism. The Island arc and eastern ophiolitic components met with the continental crust and caused the crust to thicken and fold. From 150 – 142 Ma (Late Jurassic-Early Cretaceous), post orogenic magmatism resumed. The prior inhibition of the ascending magma through a thicker crust caused melts to become more silicic and higher in Sr/Y within the Central belt with the exception of Bald Rock pluton, a late Jurassic component of the Western belt. Lastly, from 121 – 90 Ma, the widely-known voluminous magmatism in the Cretaceous generated much of the granitic plutons seen today in the Sierra Nevada. We conclude that crustal thickening associated with the Nevadan Orogeny led to a change in geochemistry, as seen in plutons that lie in the Central belt, and was likely responsible for the lull between the two episodes of magmatic flux during the Jurassic. While Yuba Rivers pluton (162.2 ± 2.2 Ma; Cecil et al, 2012) in the Central Belt has a proximal time frame to Swedes Flat pluton in the Western Belt (164.6 ± 3.5 Ma; this study), they vary greatly in Sr/Y (Table 2). One possible reason for this difference could potentially be that plutons that intruded the Central Belt underwent coeval magmatism in areas of thicker crust while the Western Belt was actively being accreted onto the continent. Another possibility is that the components of the Central belt (i.e. metamorphic rocks, metasediments remnant to an accretionary wedge) may have been incorporated and/or

assimilated into the melt, thus, altering the geochemistry of these particular plutons. Samples collected for this study do not show the presence of garnet, yet, it is possible that the fractionation of garnet occurred in plutons within the Central belt that contain high Sr/Y with exception to the smaller Lumpkin pluton which exhibits low Sr/Y as well as plutons within the Western belt.

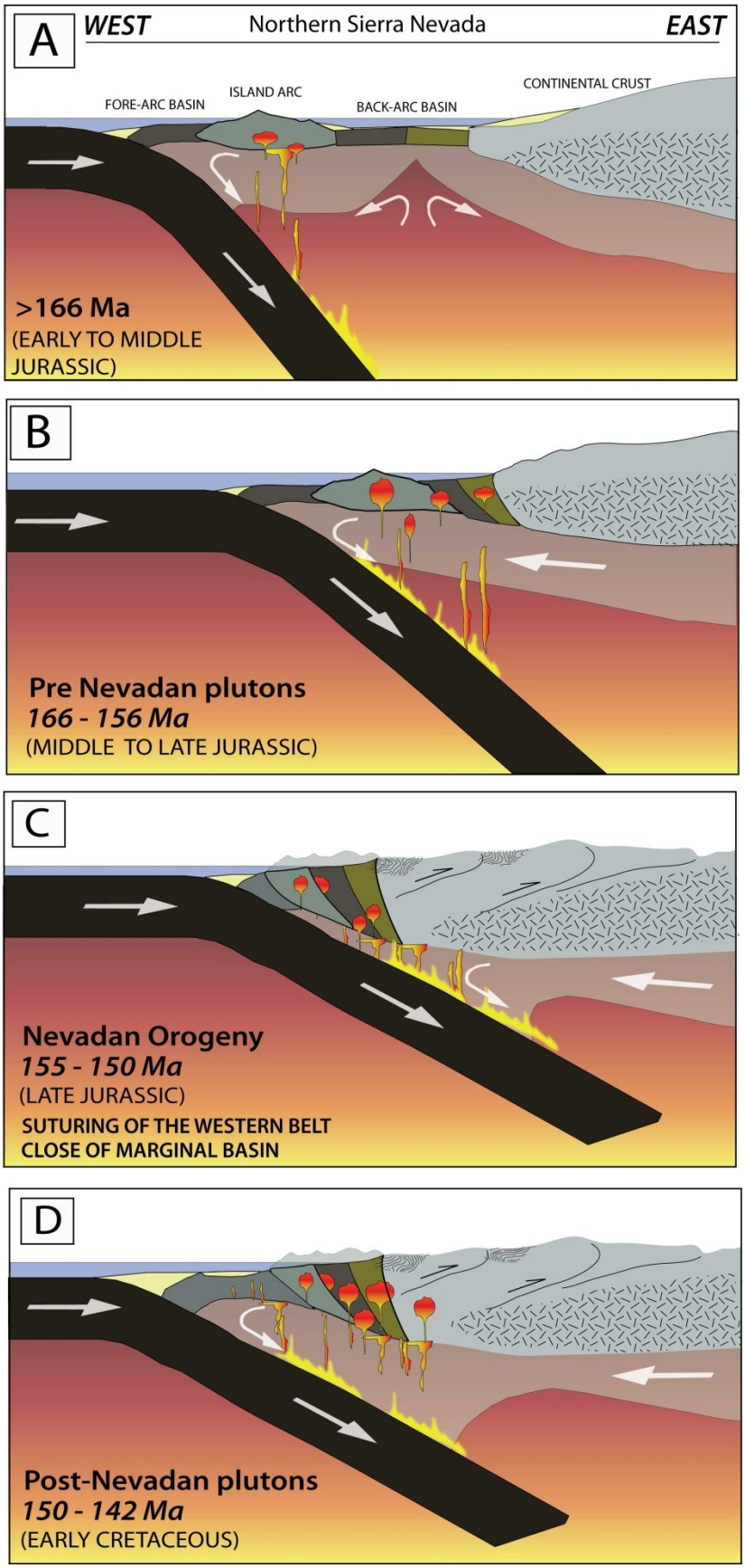
A
WEST
Northern Sierra Nevada
EAST
FORE-ARC BASIN
ISLAND ARC
BACK-ARC BASIN
CONTINENTAL CRUST
>166 Ma
(EARLY TO MIDDLE JURASSIC)
B
Pre Nevadan plutons
166 - 156 Ma
(MIDDLE TO LATE JURASSIC)
C
Nevadan Orogeny
155 - 150 Ma
(LATE JURASSIC)
SUTURING OF THE WESTERN BELT
CLOSE OF MARGINAL BASIN
D
Post-Nevadan plutons
150 - 142 Ma
(EARLY CRETACEOUS)

Figure 19. A proposed schematic depiction of the tectonic development of plutons in the northern Sierra Nevada (A thru D) from west to east. White arrows represent direction of oceanic slab motion. (A) Early to Middle Jurassic island arc subduction with fore-arc and back-arc basins. (B) pre-Nevadan plutons are introduced to the arc while Paleozoic-Mesozoic altered oceanic crust accrete onto the continental crust from 166 – 156 Ma. Magmatism ascends through thinner crust. (C) From 155 – 150 Ma, Island arc terrane is sutured onto the metamorphic terranes as the marginal basin closes. Nevadan Orogeny begins and magmatism is essentially slowed by lithospheric thickening of crust. (D) From 150 – 142 Ma (Late Jurassic-to-Early Cretaceous), magmatism resumes in a series of post Nevadan magmatic flux events into thicker crust. After Lackey et al., 2012; Godfrey et al., 1997; Dilek and Moores, 1989; Godfrey and Dilek, 2000. Depictions are not to scale.

8. CONCLUSION

U-Pb geochronological analysis, geochemical and petrographic data are presented here for 7 plutonic rock samples from the northern Sierra Nevada. Ages determined herein, coupled with previous work, have illuminated that plutons in the northern Sierra are more complex than previously estimated. The data examined in this study offer a new indication of two smaller episodes of Middle Jurassic (165 – 160 Ma) and Early Cretaceous (145 – 140 Ma) magmatism that was not qualitatively acquired before. While older estimates have determined that a single event of increased magma production occurred during the Late Jurassic, this study suggests that there were, in fact, two significant episodes that were likely caused by the initiation of magmatism through subduction and the compression of an island arc province on western North America, causing a thickening period during the Nevadan orogeny. This crustal thickening was likely responsible for the magmatic lull seen at 155 – 150 Ma. These clear distinctions are made through whole-rock and trace element geochemistry, petrography, and U-Pb zircon ages and suggests these rocks in the northern Sierra are subductive components that were added to the magmatic budget at two different intervals. Likewise, plutons show up as the remnant of a typical Andean arc setting, also seen through the mineralogy of granitoids. However, island arc and continental arc settings both seem to play a role with the development of plutons in the northern Sierra. Making these determinations could only be done by assigning U-Pb ages through LA-ICPMS analysis. Differentiating these plutons proves to be difficult in that their spatial references cannot be exactly used to determine their origin of tectonic setting, thus their temporal interpretation can place them into two groups, or 2 different magmatic pulses of pre and post Nevadan time.

Using Sr/Y has identified that plutons that exist in the Central belt tend to have higher Sr/Y than most other plutons in the vicinity of the northern Sierra. The current data presented in this paper offers a refined introspection into the early development of the Sierra Nevada batholith, yet it does not provide a full representation of a complete magma addition histogram due, in part, by the total of 7 plutons chosen in this study. The lack of information that we have for plutons in the furthest northern Sierra (Grizzly, Buck's Lake, Concow, Granite Basin, and Merrimac) pose gray areas and problematic constraints to the overall petrogenesis and relationship to the Nevadan orogeny. A further geochronologic investigation into plutons that reside north of 39°30'N that make up the edge of the northern Sierra would be useful in order to fill in gaps of the histogram and geochemistry so that a more robust representation of the Jurassic flare-ups are represented. Additionally, a further geochemical rare earth element isotopic analysis would provide a further understanding of the depth of melting which could not be achieved at this time. This study alone offers a beginning insight to the evolution of plutonism in the Sierra Nevada batholith and the growth on continental crust as a whole.

REFERENCES

Ague, J.J., 1997, Thermodynamic calculation of emplacement pressures for batholithic rocks, California: Implications for the aluminum-in-hornblende barometer: Geology, v. 25, p. 563-566.

Ague, J.J., and Brimhall, G.H., 1988, Regional variations in bulk chemistry, mineralogy, and the compositions of mafic and accessory minerals in the batholiths of California, Geological Society of America Bulletin, v. 100, p. 891-910.

Argus, D.F., and Gordon, R.G., 1991, Current Sierra Nevada-North America motion from very long baseline interferometry: Implications for the kinematics of the western United States: Geology, v. 19, p. 1085-1088.

Armstrong, R.L., 1988, Mesozoic and early Cenozoic magmatic evolution of the Canadian Cordillera, *in* Clark, S.P., Burchfield, B.C., Suppe, J., eds., Processes in continental lithospheric deformation: Geological Society of America Special Paper 218, p. 55-91.

Bateman, P.C., 1992, Plutonism in the Central Part of the Sierra Nevada Batholith, California: U.S Geological Survey Professional Paper 1483, p. 186.

Barnes, C.G., Snoke, A.W., Harper, G.D., Frost, C.D., McFadden, R.R., Bushey, J.C., Barnes, M.A.W., 2006. Arc plutonism following regional thrusting; petrology and geochemistry of syn- and post-Nevadan plutons in the Siskiyou Mountains, Klamath Mountains province, California. In: Snoke, A.W., Barnes, C.G. (Eds.), Geological studies in the Klamath Mountains Province, California and Oregon: a volume in honor of William P. Irwin: Geological Society of America, 410, pp. 357–376.

Barth, A.P., Walker, J.D., Wooden, J.L., Riggs, N.R., Schweickert, R.A., 2011, Birth of the Sierra Nevada magmatic arc: Early Mesozoic plutonism and volcanism in the east-central Sierra Nevada of California, Geosphere, v. 7, p. 877-897.

Barton, M.D., Battles, D.A., Bebout, G.E., Capo, R.C., Christensen, J.N., Davis, S.R., Hanson, R.B., Michelsen, C.J., and Trim, H.E., 1988, Mesozoic contact metamorphism in the western United States, *in* Ernst, W.G., ed., Metamorphism and crustal evolution of the western United States: Volume 7: Englewood Cliffs, New Jersey, Prentice Hall, p. 110–178.

Barstow, J.A., Nilsen, T.H., 1990, Review of the Great Valley sequence, eastern Diablo Range and northern San Joaquin Valley, central California, Department of the Interior U.S. Geological Survey, Open-File Report 90-226, p. 1-25.

Beard, J.S., Day, H.W., 1987, The Smartville intrusive complex, Sierra Nevada, California: The core of a rifted volcanic arc, Geological Society of America Bulletin, v. 99, p. 779-791.

Beard, J.S., Day, H.W., 1986, Origin of gabbro pegmatite in the Smartville intrusive complex, northern Sierra Nevada, California, American Mineralogist, Vol. 71, p. 1085-1099.

Cecil, M.R., Rotberg, G., Ducea, M.N., Saleeby. J.B., Gehrels, G.E., 2012, Magmatic

growth and batholithic root development in the northern Sierra Nevada, California, Geosphere, June, v. 8, no.3.

Cecil, M.R., Ducea, M.N., Reiners, P., Gehrels, G., Mulch, A., Allen, C., Campbell, I., 2010, Provenance of Eocene river sediments from the central northern Sierra Nevada and implications for paleotopography, Tectonics, Vol. 29, p. 1-13.

Chang, Z., Vervoort, J.D., McClelland, W.C., Knaack, C., 2006, U-Pb dating of zircon by LA-ICP-MS, American Geophysical Union, v. 7, p. 1-14.

Chen, J.H., Moore, J.G., 1982, Uranium-lead isotopic ages from the Sierra Nevada batholith: California Journal of Geophysical Research, v. 87, p. 4761-4784.

Coleman, D.S., Gray, W., Glazner, A.F., 2004, Rethinking the emplacement and evolution of zoned plutons: Geochronologic evidence for incremental assembly of the Tuolumne Intrusive Suite, California: Geology, v. 32, p. 433-436.

Day, H.W., Bickford, M.E., 2004, Tectonic setting of the Jurassic Smartville and Slate Creek complexes, northern Sierra Nevada, California, GSA Bulletin, v. 116; no. 11/12; p, 1515-1528.

Day, H.W., Moores, E.M., Tuminas, A.C., 1985, Structure and tectonics of the northern Sierra Nevada, Geological Society of America Bulletin, v. 96, p. 436-450.

DeCelles, P.G., Ducea, M.N., Kapp, P., and Zandt, H.G., 2009, Cyclicity in Cordilleran orogenic systems: Nature Geoscience, v. 2, p. 251–257, doi: 10.1038/ngeo469.

Dickson, W.R., 2008, Accretionary Mesozoic-Cenozoic expansion of the Cordilleran continental margin in California and adjacent Oregon, Geosphere, v.4, p. 329-353.

Dickinson, W.R., 1981, Plate tectonics and the continental margin of California, *in* Ernst, W.G., ed., The geotectonic development of California: Englewood Cliffs, New Jersey, Prentice-Hall, p. 1-28.

Dickinson, W., and Snyder, W.S., 1978, Plate tectonics of the Laramide orogeny, *in* Mathews, V., III, ed., Laramide folding associated with basement block faulting in the western United States, Geological Society of America Memoir 151, p. 335–366.

Dilek, Y., Moores, E.M., 1989, Island-arc evolution and fracture-zone tectonics in the Mesozoic Sierra Nevada, California, and implications for transform offset of the Sierra/Klamath convergent margins, International Basement Tectonics Association, v. 8, p. 179-196.

Drummond, M.S., Defant, M.J., 1990. A model for trondhjemite-tonalite-dacite genesis and crustal growth via slab melting: Archean to modern comparisons. Journal of Geophysical Research 95, 21,503–21,521.

Ducea, M.N., Paterson, S.R., DeCelles, P.G., 2015, High-Volume Magmatic Events in Subduction Systems, Elements, Vol. 11, pp. 99-104.

Ducea, M.N., Barton, M.D., 2007, Igniting flare-up events in Cordilleran arcs, The Geological

Society of America, v. 35, p. 1047-1050.

Ducea, M.N., 2001, The California Arc: Thick Granitic Batholiths, eclogitic Residues, Lithospheric-Scale Thrusting, and magmatic Flare-Ups, Geological Society of America Today, November, p. 4-10.

Ducea, M.N., Otamendi, J.E., Bergantz, G., Stair, K.M., Valencia, V.A., Gehrels, G.E., 2010, Timing constraints on building an intermediate plutonic arc crustal section: U-Pb zircon geochronology of the Sierra Valle Fertil-La Huerta, Famatinian arc, Argentina, Tectonics, Vol. 29, p. 1-22.

Edleman, S.H., Day, H.W., Bickford, M.E., 1989, Implications of U-Pb zircon ages for the tectonic settings of Smartville and Slate Creek complexes, northern Sierra Nevada, California, Geology, v. 17, p. 1032-1035.

Ernst, W.G., Snow, C.A., Scherer, H.H., 2008, Contrasting early and late Mesozoic petrotectonic evolution of northern California, GSA Bulletin, v. 120, p. 179-194.

Evernden, J.F., Kistler, R.W., 1970, Chronology of Emplacement of Mesozoic Batholithic Complexes in California and Western Nevada, U.S. Geological Survey Professional Paper 623, p. 42.

Fagan, T.J., Day, H.W., Hacker, B.R., 2001, Timing of arc construction and metamorphism in the Slate Creek Complex, northern Sierra Nevada, California, GSA Bulletin, v.113, p. 1105-1118.

Frost, B.R., Barnes, C.G., Collins, W.J., Arculus, R.J., Ellis, D.J., Frost, C.D., 2001, A Geochemical Classification of Granitic Rocks, Journal of Petrology, V. 42, p. 2033 - 2048.

Gehrels, G., Rusmore, M., Woodsworth, G., Crawford, M., Andronicos, C., Hollister, L., Patchett, J., Ducea, M., Butler, R., Klepeis, K., Davidson, C., Friedman, R., Haggart, J., Mahoney, B., Crawford, W., Pearson, D., Girardi, J., 2009, U-Th-Pb geochronology of the Coast Mountains batholith in north-coastal British Columbia: Constraints on age and tectonic evolution, GSA Bulletin, September/October, no. 9/10, p. 1341-1361.

Gehrels, G., Valencia, V.A., Ruiz, J., 2008, Enhanced precision, accuracy, efficiency, and spatial resolution of U-Pb ages by laser ablation-multicollector-inductively coupled plasma-mass spectrometry, Geochemistry Geophysics Geophysics Geosystems, v. 9, p. 1-13.

Girardi, J.D., Patchett, P.J., Ducea, M.N., Gehrels, G.E., Cecil, M.R., Rushmore, M.E., Woodsworth, G.J., Pearson, D.M., Manthei, C., Wetmore, P., 2012, Elemental and Isotopic evidence for granitoid genesis from deep-seated sources in the Coast Mountains Batholith, British Columbia, Journal of Petrology, vol. 53, N. 7, P. 1505-1536.

Girty, G.H., Hanson, R.E., Girty, M.S., Schweiskert, R.A., Harwood, D.S., Yoshinobu, A.S., Bryan, K.A., Skinner, J.E., Hill, C.A., 1995, Timing of emplacement of the Haypress Creek and Emigrant Gap plutons: Implications for the timing and controls of Jurassic orogenesis, northern Sierra Nevada, California, Geological Society of America Special Paper, p. 191 – 201.

Godfrey, NJ., Dilek, Y., 2000, Mesozoic assimilation of oceanic crust and island arc into the North American continental margin in California and Nevada: Insights from geophysical data, Geological Society of America Special Paper 349, p. 365-382.

Godfrey, N.J., Beaudoin, B.C., Klemperer, S.L., 1997, Ophiolitic basement to the Great Valley forearc basin, California, from seismic and gravity data: Implications for crustal growth at the North American continental margin, GSA Bulletin, v. 108, p. 1536-1562.

Hacker, B.R., Donato, M.M., Barnes, C.G., McWilliams, M.O., Ernst, W.G., 1995, Timescales of orogeny: Jurassic construction of the Klamath Mountains, Tectonics, vol. 14, no. 3, p. 677-703.

Hacker, B.R., 1993, Evolution of the northern Sierra Nevada metamorphic belt: Petrological, structural, and Ar/Ar constraints, Geological Society of America Bulletin, v. 105, p. 637-656.

Hacker, B.R., Peacock, S.M., 1990 Comparison of the Central Metamorphic Belt and Trinity terrane of the Klamath Mountains with the Feather River terrane of the Sierra Nevada, Geological Society of America, Special Paper 225, p. 75-92.

Harper, G.D., 2006, Structure of syn-Nevadan dikes and their relationship to deformation of the Galice Formation, western Klamath terrane, northwestern California, Geological Society of America, Special Paper 410, p. 121 – 140.

Harper, G.D., Saleeby, J.B., Heizler, M., 1994. Formation and emplacement of the Josephine Ophiolite and the Nevadan Orogeny in the Klamath Mountains, California–Oregon; U/Pb zircon and 40Ar/39Ar geochronology. Journal of Geophysical Research 99, p. 4293–4321.

Hietanen, A., 1977, Paleozoic-Mesozoic Boundary in the Berry Creek quadrangle, northwestern Sierra Nevada, California, Geological Survey Professional Paper 1027, p. 1 – 30.

Hietanen, A., 1976, Metamorphism and Plutonism around the Middle and South Forks of the Feather River, California, Geological Survey professional Paper 920, p. 1 – 37.

Hotz, P.E., 1971, Plutonic rocks of the Klamath Mountains, California and Oregon, Geological Survey Professional paper 684-B, United States Government Printing Office, p. 1-24.

Kay, S.M., Godoy, E., Kurtz, A., 2005, Episodic arc migration, crustal thickening, subduction erosion, and magmatism in the south-central Andes, GSA Bulletin; v. 117, no. ½, P. 67-88.

Kistler, R.W., 1990, Two different lithosphere types in the Sierra Nevada, California, *in* Anderson, L., ed., The Nature and Origin of Cordilleran Magmatism: Geological Society of America Memoir 174, p. 271-281.

Kistler, R.W., Peterman, Z.E., 1978, Reconstruction of crustal blocks of California on the basis of

initial strontium isotopic compositions of Mesozoic granitic rocks: U.S. Geological Survey Professional Paper 1071, p. 17.

Kistler, R.W., Peterman, Z.E., 1973, Variations in Sr, Rb, K, Na, and initial Sr^{87}/Sr^{86} in Mesozoic granitic rocks and intruded wall rocks in central California: Geological Society of America Bulletin, v. 84, p. 3489-3512.

Lackey, J.D., Cecil, M.R., Windham, C.J., Frazer, R.E., Bindman, I. N., Gehrels, G.E., 2012, Fine Gold Suite: The roles of basement terranes and magma source development in the Early Cretaceous Sierra Nevada batholith, April, v. 8: no. 2, p. 1-22.

Lackey, J.S., Valey, J.W., Saleeby, J.B., 2005, Suprecrustal input to magmas in the deep crust of Sierra Nevada batholith: Evidence from high-$\delta^{18}O$ zircon, Earth and Planetary Sciences, v. 235, p. 315-330.

Larsen, L.H., Poldervaart, A., 1961, Petrologic Study of Bald Rock Batholith, near Bidwell Bar, California, Geological Society of America Bulletin, v. 72, p. 69-92.

Ludwig, K.R., 2008, Isoplot 4.15, A Geochronological toolkit for Microsoft Excel, Berkeley Geochronology Center, Special Publication No. 4, p. 1-76.

MacDonald, J.H., Harper, D.H., Zhu, B., Petrology, Geochemistry, and provenance of the Galice Formation, Klamath Mountains, Oregon, and California, 2006, Geological Society of America, Special Paper 410, p. 77-101.

Nadin, E.S., Saleeby, J.B., 2008, Disruption of regional primary structure of the Sierra Nevada batholith by the Kern Canyon fault system, California, Geological Society of America, v. 438, p.1-26.

Paterson, S.R., Ducea, M., 2015, Arc Magmatic Tempos: Gathering the Evidence, Elements, Vol. 11, pp. 91-98.

Paterson, S.R., Okaya, D., Memeti, V., Economos, R., Miller, R.B., 2011, Magma addition and flux calculations of incrementally constructed magma chambers in continental margin arcs: combined field, geochronologic, and thermal modeling studies, Geosphere, v.7; no.6, p. 1439-1468.

Saleeby, J., Ducea, M.N., Busby, C., 2008, Chronology of pluton emplacement and regional deformation in the southern Sierra Nevada batholith, California, Geological Society of America Special Paper, p. 1-32.

Saleeby, J., Farley, K.A., Kistler, R.W., Fleck, R., 2007, Thermal evolution and exhumation of deep-level batholithic exposures, southernmost Sierra Nevada, California, Geological Society of America, v. 419. P. 39-66.

Saleeby, J.B., 1990, Progress in tectonic and petrogenetic studies in an exposed cross section of young (~100 Ma) continental crust, southern Sierra Nevada, California, *in* Salisbury, M.H., and Fountain, D.M., eds., Exposed crustal sections of the continental crust: Norwell, Massachusetts, Kluwer Academic, p. 137–158.

Saleeby, J., Hannah, J.L., Varga, R.V., 1987, Isotopic age constraints on middle Paleozoic deformation in the northern Sierra Nevada, California, Geology, v. 15, p. 757-760

Saleeby, J., 1982, Polygenic Ophiolite Belt of the California Sierra Nevada: Geochronological and Tectonostratigraphic Development, Journal of Geophysical Research, v. 87, p. 1803-1824.

Sambridge, M.S., Compston, W., 1994, Mixture modeling of multi-component data sets with application to ion-probe zircon ages, Earth and Planetary Science letters 128, p. 373-390.

Saucedo, G.J., Wagner, D.L., 1992, Geologic map of the Chico quadrangle, California, California Division of Mines and Geology, regional Geologic Map Series, Map 7A, scale 1:250,000.

Schwartz, J.J., Johnson, K., Mueller, P., Valley, J., Strickland, A., Wooden, J.L., 2014, Time scales and processes of Cordilleran batholith construction and high-Sr/Y magmatic pulses: Evidence from the Bald Mountain batholith, northeastern Oregon, Geosphere, V. 10, p. 1456-1481.

Schwartz, J.J., Johnson, K., Miranda, E.A., Wooden, J.L., 2011, The generation of High Sr/Y plutons following Late Jurassic arc-arc collision, Blue Mountains province, NE Oregon, Lithos 126, p. 22-41.

Schweickert, R.A., Bogen, N.L., Girty, G.H., Hanson, R.E., Merguerian, C., 1984, Timing and structural expression of the Nevadan orogeny, Sierra Nevada, California, Geological Society of America, v. 95, p. 967-979.

Snoke, A.W., Barnes, C.G., 2006, The development of tectonic concepts for the Klamath Mountains province, California and Oregon, Geological Society of America special paper 410, p. 1-29.

Tobisch, O.T., Paterson, S.R., Longiaru, S., Bhattacharyya, T., 1987, Extent of the Nevadan orogeny, central Sierra Nevada, California, Geology, v.15, p. 132-135.

Tulloch, A.J., Kimbrough, D.L., 2003, Paired plutonic belts in convergent margins and the development of high Sr/Y magmatism: Peninsular Ranges batholith of Baja-California and Median batholith of New Zealand, Geological Society of America, Special Paper 374, p. 275-295.

Unruh, J.R., 1991, The uplift of the Sierra Nevada and implications for late Cenozoic epeirogeny in the western Cordillera, Geological Society of America Bulletin, v. 103, p. 1395-1404.

Wright, J.E., Fahan, M.R., 1988, An expanded view of Jurassic orogenesis in the western United States Cordillera: Middle Jurassic (pre-Nevadan) regional metamorphism and thrust faulting within an active arc environment, Klamath Mountains, California, Geological Society of America Bulletin, v. 100, p. 859-876.

Zak, J., Paterson, S.R., Memeti, V., 2007, Four magmatic fabrics in the Tuolumne batholith, central Sierra Nevada, California (USA): Implications for interpreting fabric patterns in plutons and evolution of magma chambers in the upper crust, GSA Bulletin, v. 119, p. 184-201.

APPENDIX A:

PETROGRAPHIC ANALYSIS

SAMPLE: **LS-1301**

Location of sample: Lake Spaulding
W121°38'7.296", N39°19'31.584"

Rock Name: Quartz Monzodiorite

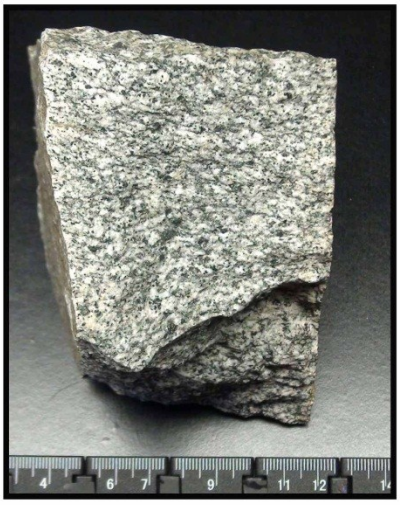

Megascopic description: Rock sample (LS-1301) exhibits an intermediate, phaneritic texture with visible phenocrysts that include a suite of course, equigranular felsic minerals that range from 1 mm to 4 mm in size, to a division of medium inequigranular mafic grains 3 - 5 mm. Visible grains include hornblende, plagioclase, biotite and accessory epidote, along with enclaves 2-4 cm. Mineral grains present a weakly-oriented fabric that is more noticeable with mafic grains. An uncut, surface-exposed portion of the rock exhibits weathering and oxidation. Enclaves appear to be predominated with mafic minerals of hornblende and perhaps biotite with ~10% plagioclase seen through a hand lens.

THIN SECTION: **LS-1301**

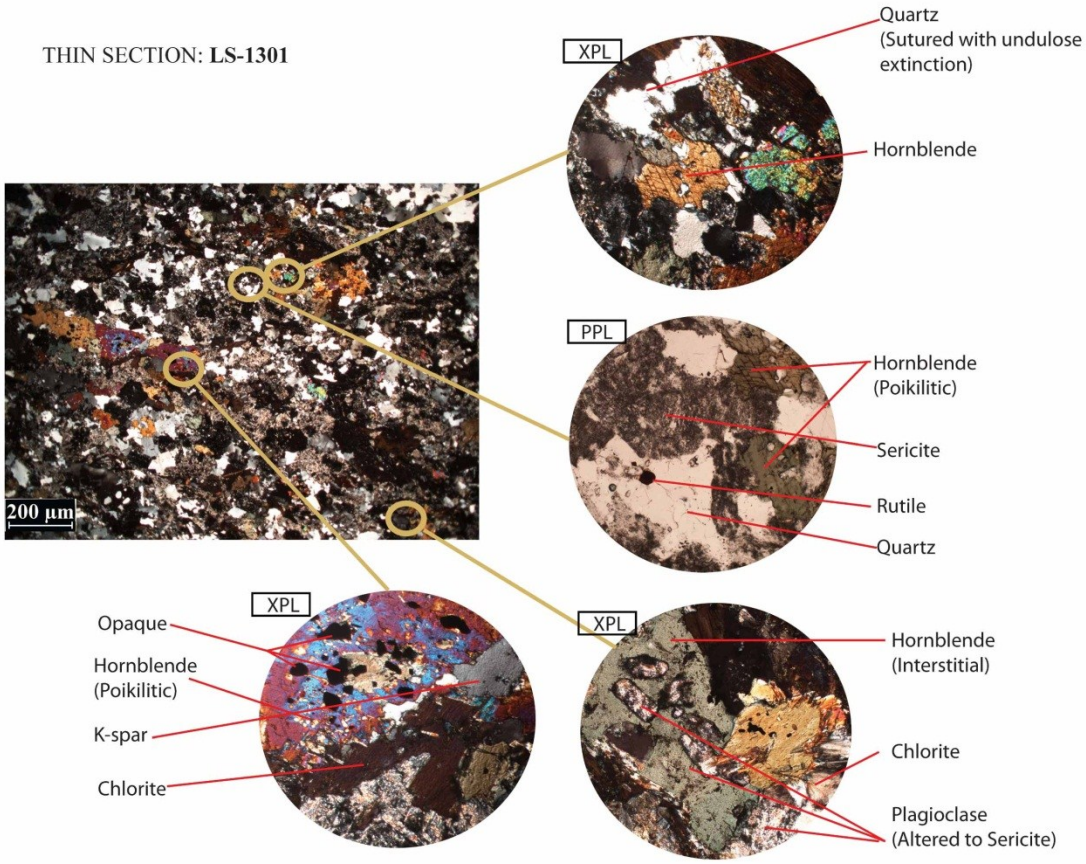

Microscopic description: Thin section reveals a subophitic texture with a division of inequigranular-to-equigranular, hypidiomorphic grains. Heavily-included and corroded plagioclase laths depict alteration to sericite within the entirety of most grains. Rare merymikites have vermicular wormy structures of quartz replacement with association to plagioclase and possibly k-spar. Quartz grains present very strong undulose extinction and are subhedral to anhedral. Grain boundaries around quartz contain sutured, lobate edges. Resorbed and poikiloblastic hornblende grains have incorporated magnetite replacement as well as chlorite. Chloritization associated with hornblende have also worked into quartz grains as "hair-like" inclusions.

Thin Section: **LS-1301B (with enclave)**

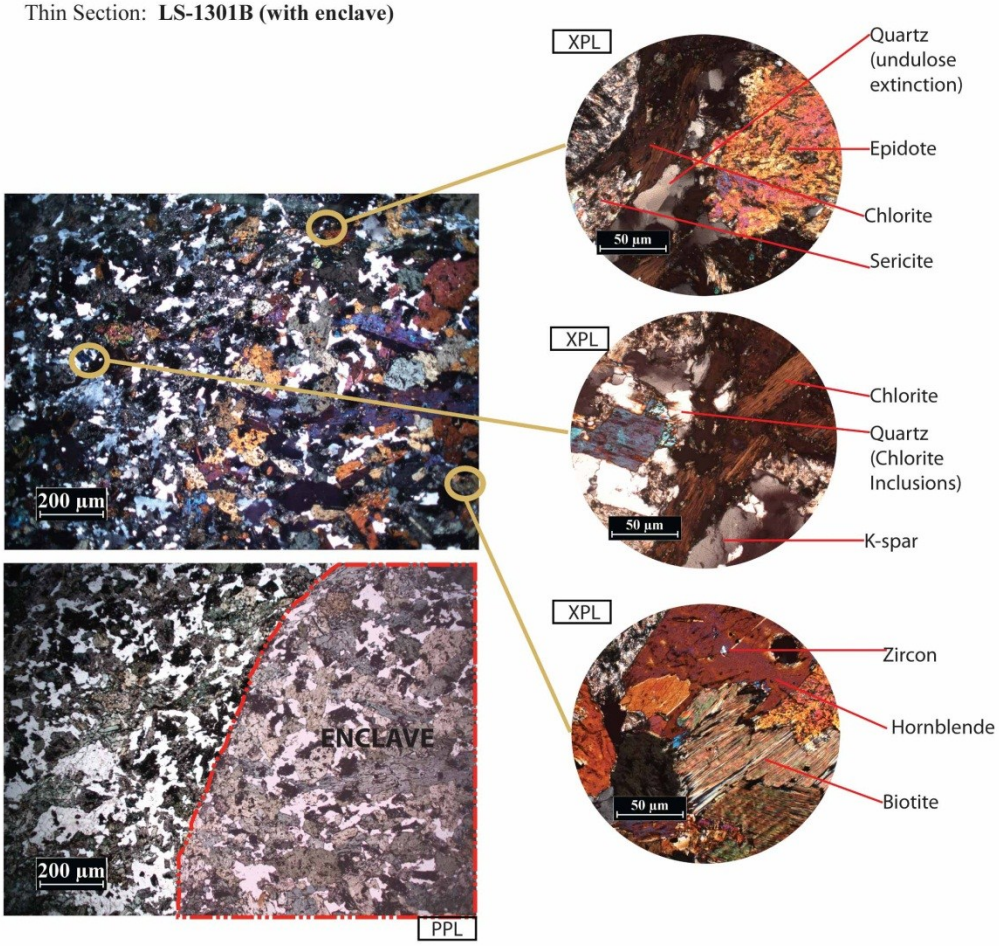

Microscopic description: Thin section (LS-1301B) reveals a cross section of an enclave with inequigranular, allotriomorphic grains. Hornblende grains are more elongate and euhedral-to-subhedral than in the host rock and appear to portray simple twinning in their resorbed structure. The presence of biotite is much more profound with chloritization associated with hornblende grains and the pressence of chlorite fibers are seen included in the pressence of quartz. Lath-shaped grains that are depicted in the enclave are relict plagioclase crystals that have been completly altered into sericite.

Primary Minerals

Essential:
Plagioclase - 37%
K-Spar - 12%
Quartz - 15%

Varietal:
Hornblende - 25%
Biotite -1%
Chlorite - 5%

Accessory:
Rutile - 1%
Zircon - 1%
Epidote - 1%
Opaque - 2%

An Content: 67%

Petrographic name:

Hornblende Biotite Quartz Monzodiorite

Enclave

Primary Minerals

Essential:
Plagioclase - 20%
K-Spar - 1%
Quartz - 5%

Varietal:
Hornblende - 60%
Biotite -10%

Accessory:
Opaque - 2.0%

SAMPLE: **LS-1302 (with enclave)**

Location of sample: Lake Spaulding
W121°37'55.344", N39°19'23.556"

Rock Name: Granodiorite

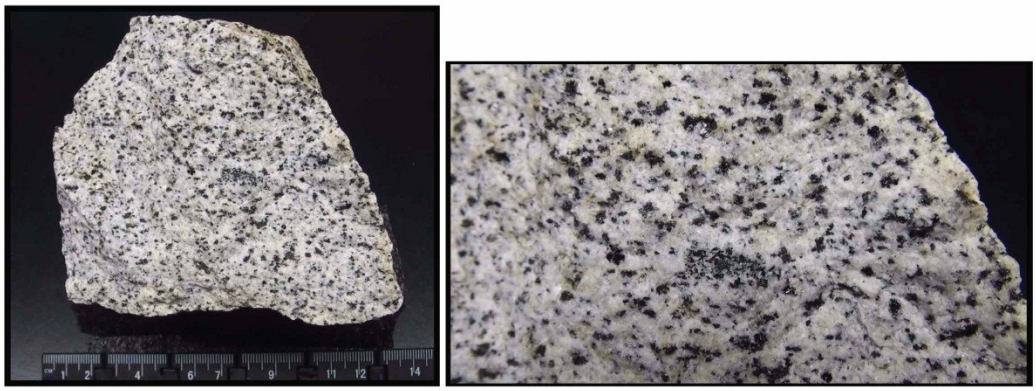

Megascopic description: Rock sample (LS-1302) exhibits an course-grained felsic, phaneritic texture with visible phenocrysts that include a suite of fine equigranular felsic minerals that range from 2 mm to 3 mm in size. Mafic grains are euhedral and range from 1 to 5 mm in size. Visible grains include plagioclase, quartz, bitotite and hornblende with a lack of k-spar grains. The presence of enclaves in hand sample portrays sharp contatcs as well as a significant difference between mafic and felsic grains and are sub-angular-to-sub-rounded. While there appears to be no definite fabric, rock sample contains patches of oxidation and weathering.

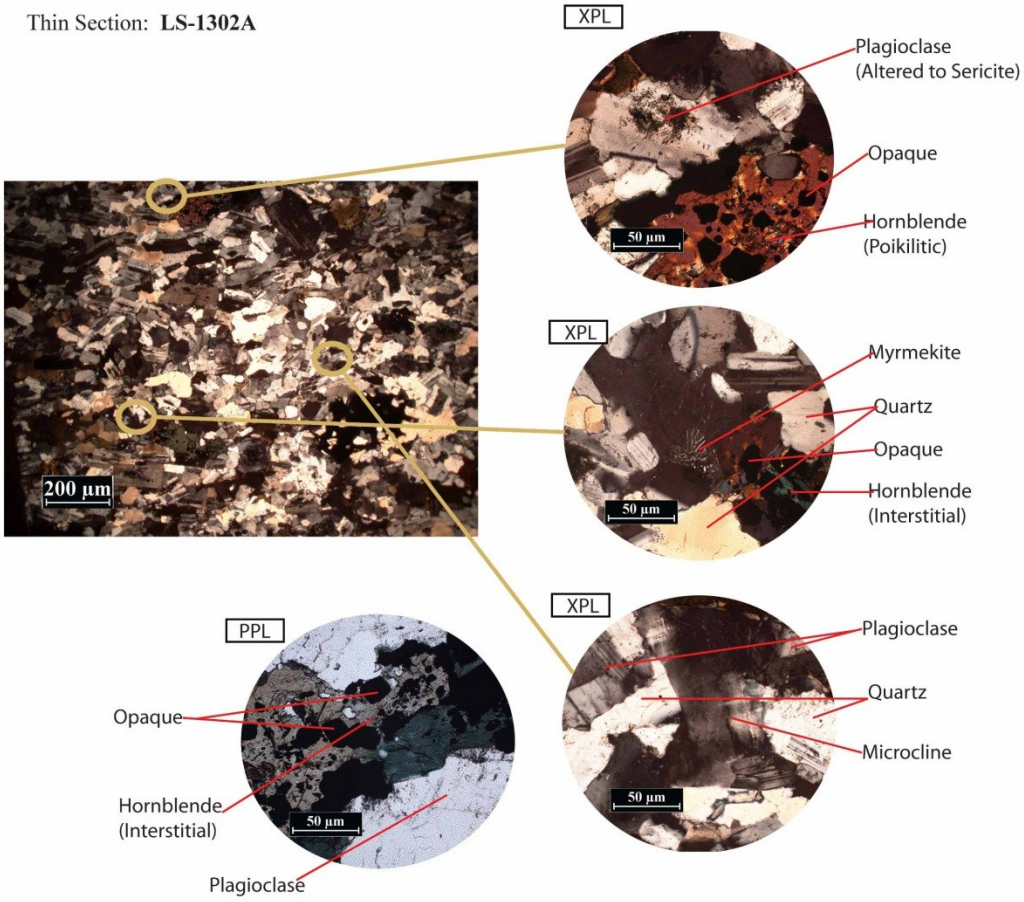

Microscopic description: Thin section (LS-1302) reveals a course-grained, inequigranular, hypidiomorphic texture that shows definite crystal alignment with the abundance of tabular plagioclase laths oriented in the same direction as quartz grains. Very strong undulose extinction exists in an abundance of quartz grains as they are seen adjacent to plagioclase and quartz- most likely a secondary texture intermingling with K-spar. The presence of magnetite can be found in association with resorbed and anhedral hornblende grains. Poikilitic hornblende contains possible epidote crystals as it can be found interstitially with plagioclase.

Thin Section **LS-1302B (enclave)**

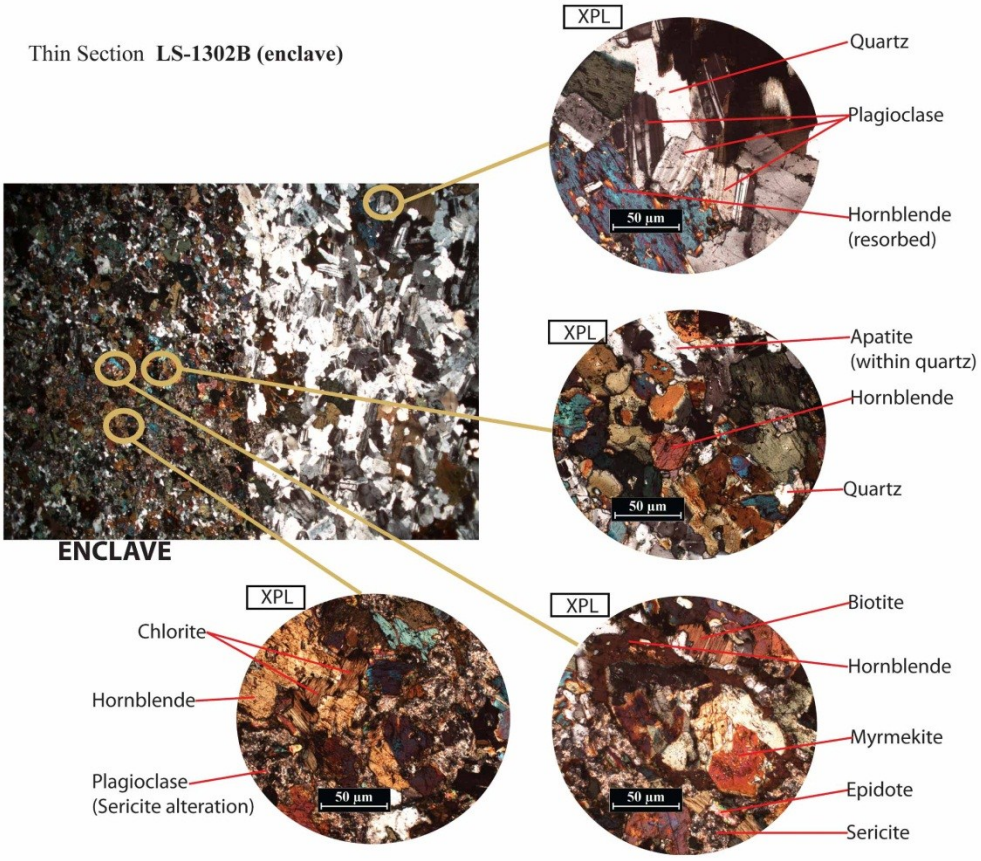

Microscopic description: Thin section (LS_1302B) reveals the division of phenocrysts with minerals that are associated with a mafic enclave. Enclave contains subhedral-to-anhedral grains of predominant hornblende, moderate chlorite, moderate plagioclase, and trace epidote. The trend of resorption tends to be associated with bitotie and hornblende grains into sieve textures. Chloritization is due to the alteration of hornblende while rare myrmekite intergrowth textures show the interaction of hornblende and quartz. Plagioclase within the encalve itself shows heavy sericitization with exception to the host rock where the alignment of euhedral plagioclase laths predominate.

Primary Minerals

Essential:
Plagioclase - 40%
K-Spar - 10%
Quartz - 25%

Varietal:
Hornblende - 10%
Biotite -10%

Accessory:
Zircon - .5%
Opaque - 4%

An Content: 74%

Petrographic name:

Biotite Hornblende Granodiorite

Enclave

Primary Minerals

Essential:
Plagioclase - 10%
Quartz - 5%

Varietal:
Hornblende - 10%
Biotite -4%
Chlorite - 2%

Accessory:
Opaque - 1.0%

Thin Section: **SF-1303**

Location of sample: Swedes Flat Pluton
W121°23'33", N39°24'25"

Rock Name: Quartz Diorite

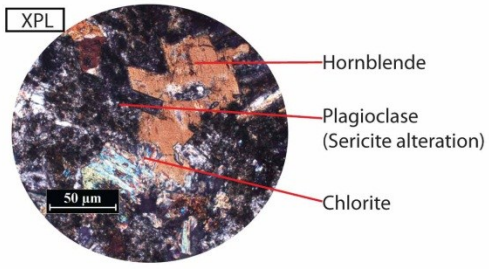

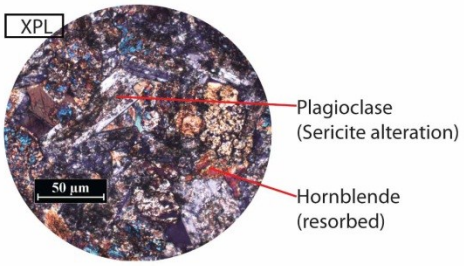

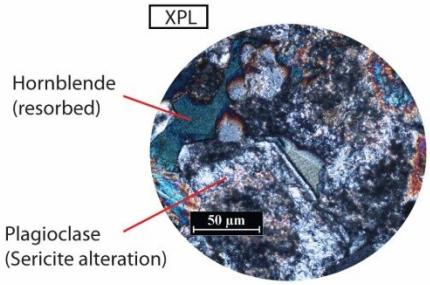

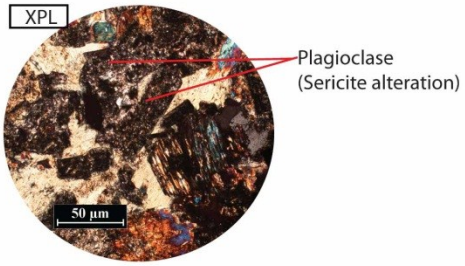

Microscopic description: Thin section (SF-1303) reveals a serite porphyritic, inequgranular, hypidiomorphic texture. Thin section contains predomiant plagioclase, moderate quartz, moderate green-to-brownish hornblende with trace k-spar. Plagioclase laths are heavily-altered to other minerals such as sericite and present ophitic growths over quartz. Chloritization is associated with the alteration of hornblende where many crystal are partially resorbed. Opaque minerals are mostly pyrite and magnetite.

Megascopic description: Rock sample (SF-1303) exhibits a fine-grained, intermediate, phaneritic texture with visible phenocrysts that include predominant greenish-tinged plagioclase, moderate quartz and hornblende, and trace pyrite. Quartz and plagioclase are equigranular from .5 mm to 2 mm in size along with inequigranular mafic minerals. Rock sample contains an outer rind with remnant lichen and oxidation.

Primary Minerals

Essential:
Plagioclase - 65%
K-Spar - 5%
Quartz - 15%

Varietal:
Hornblende - 10%

Accessory:
Zircon - .5%
Rutile - .5%
Epidote - .5%
Opaque - 4%

An Content: 70%

Petrographic name:

Hornblende Quartz Diorite

Thin Section: **LP-1304**

Location of sample: Lumpkin Pluton
W121°13'9", N39°36'38"

Rock Name: Diorite

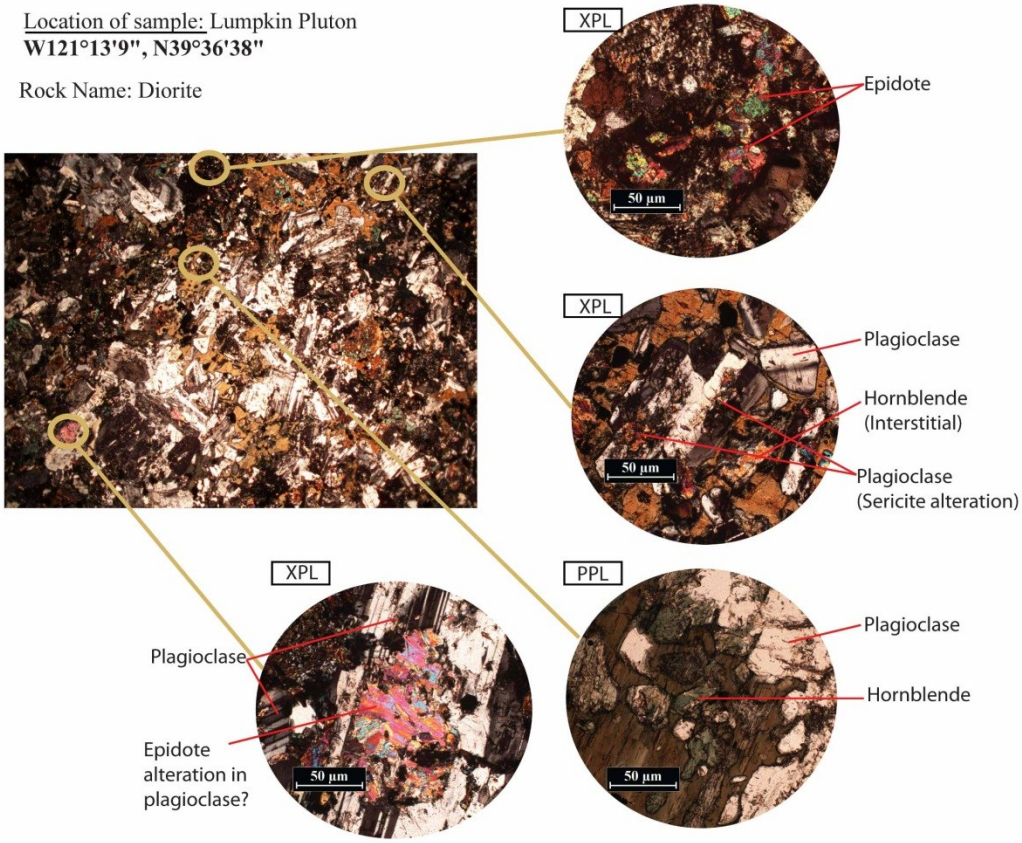

Microscopic description: Thin section reveals a hypidiomorhic, seriate porphyritic texture with inequigranular grains. Plagioclase crystals present a fabric of oriented laths and are euhedral-to-subhedral with ~15% alteration into sericite. Sparse normal ocsillatory zoning can be identified in plagioclase and relict polysynthetic twinning is visible with many altered grains. Mineral replacement is presented in both sassuritization (epidote replacement) and seritization (sericite replacement) and crystals tend to have interstitial overgrowths over hornblende. Resorbed and embayed hornblende crystals are anhedral and contain chloritization at most rims.

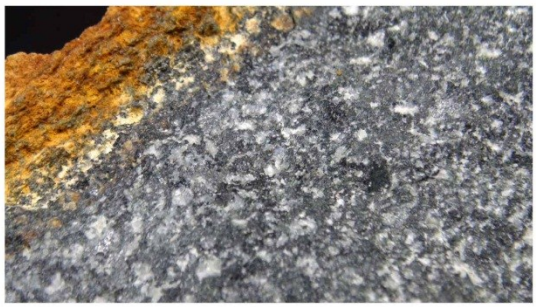

Megascopic description: Rock sample (LP-1304) exhibits an intermediate, phaneritic texture with visible equigranular grains that range from 1 mm to 4 mm in size. Visible phenocrysts include predomant hornblende and plagioclase with trace amounts of pyrite. Mafic minerals tend to be more finer-grained than felsic grains. A strongly-oxidized, rusty outer rind with a thicknes of 2-3 cm exists at the exposed egdes of rock yet does not penetrate the inner mineral textures.

Primary Minerals

Essential:
Plagioclase - 50%
K-Spar - 5%
Quartz - 5%

Varietal:
Hornblende - 30%

Accessory:
Epidote - 2%
Rutile - 1%
Opaque - 3%

An Content: 67%

Petrographic name:

Hornblende Diorite

Thin Section: **CP-1305**

Location of sample: Cascade Pluton
W121°8'33", N39°37'31"

Rock Name: Tonalite

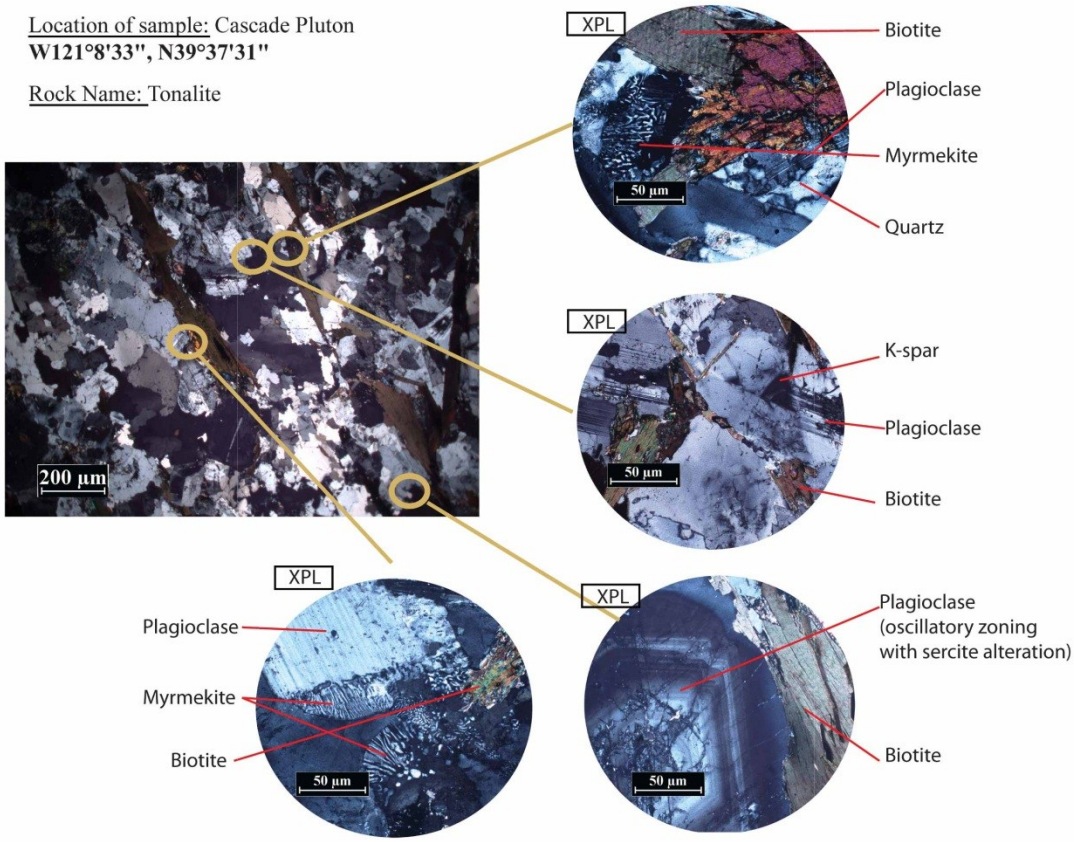

Microscopic description: Thin section reveals a subophitic texture with a division of inequigranular-to-equigranular, hypidiomorphic grains. Heavily-included and corroded plagioclase laths depict alteration to sericite within the entirety of most grains. Rare Merymikites have vermicular wormy structures of quartz replacement with association to plagioclase and possibly K-spar. Quartz grains present very strong undulose extinction and are subhedral to anhedral. Grain boundaries around quartz contain sutured, lobate edges. Resorbed and poikiloblastic Hornblende grains have incorporated magnetite replacement as well as chlorite. Chloritization associated with hornblende have also worked into quartz grains as "hair-like" inclusions.

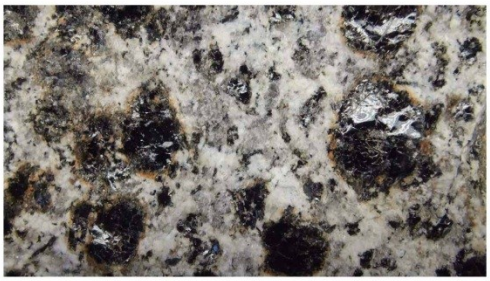

Megascopic description: Rock sample (CP-1305) exhibits a felsic, phaneritic texture with visible grains that include a suite of course-grained, inequigranular felsic minerals that range from 2 mm to 5 mm in size, to a division of course-grained equigranular mafics grains. Visible phenocrysts include abundant quartz, abundant plagioclase, predominant biotite and moderate hornblende with accessory epidote. A strong mineral fabric is seen through the orientation and alignemnt of large biotite crystals alongside the flattening of quartz grains. Euhedral biotite crystals range from 3 mm to 10 mm in size and contain an oxidation reaction rim to each grain. An thin oxidized rind exists on protions of the sample that has been exposed to the surface.

Primary Minerals

Essential:
- Plagioclase - 45%
- K-Spar - 5%
- Quartz - 30%

Varietal:
- Hornblende - 5%
- Biotite - 10%

Accessory:
- Zircon - .5%
- Rutile - 1%
- Opaque - 3%

An Content: 70%

Petrographic name:

Biotite Hornblende Tonalite

Thin Section: **HB-1307**

Location of sample: Hartman Bar Pluton
W121°9'59", N39°44'28"

Rock Name: Tonalite

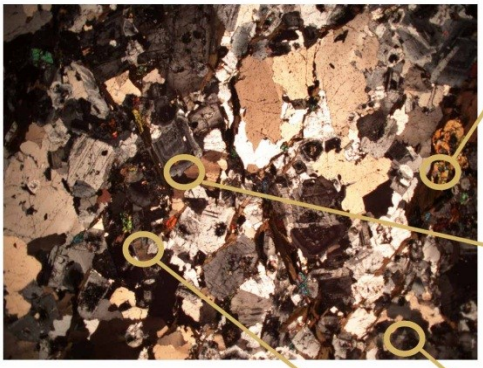

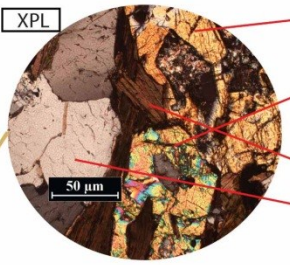

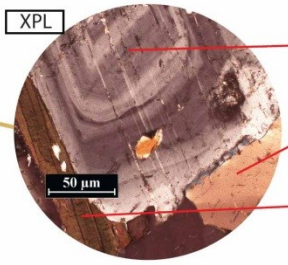

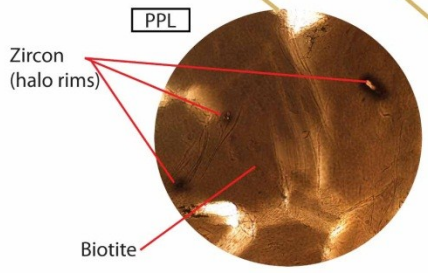

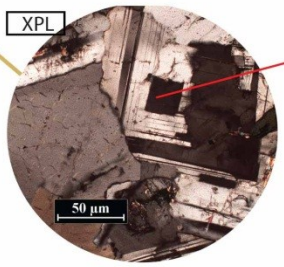

Microscopic description: Thin section reveals a seriate porphyritic texture with a division of inequigranular-to-equigranular, hypidiomorphic grains. Phenocrysts include predominant plagioclase, moderate quartz, moderate biotite, trace CPX and trace K-spar with accessory euhedral epidote, zircon and rutile. Plagioclase crystals are lath-shaped and present normal-to-patchy oscillatory zoning and resorption within their stucture. Alteration of plagioclase into sericite are seen at their cores and along the axis of twinning. Crystals of brownish biotite presents an aligned fabric in thin sction, and many grains contain zircons with halo rims. Rare myrmekite is associated with perthitic k-spar and plagioclase. Anhedral quartz crystals appear sutured and are heavily fractured.

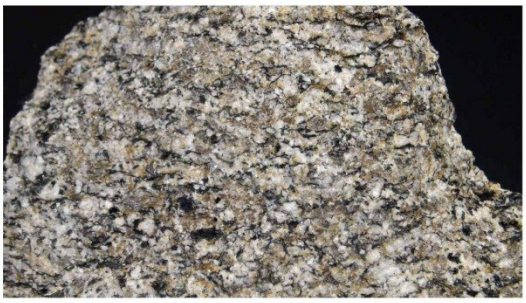

Megascopic description: Rock sample (HB-1307) exhibits an intermediate, phaneritic texture with equigranular-to-inequigranular felsic grains and inequigranular mafic grains. Sample presents a weakly-foliated fabric with visible phenocrysts that include abundant plagiocalse, abundant quartz, moderate biotite and trace CPX and hornblende. Felsic grains appear to be flattend along fabric and range from 2 mm to 6 mm in size. Mafic grains appear to range from 3 mm to 8 mm. Quartz has a grayish-to weakly brown appearance and exhibits more equigranular structures than other felsic minerals.

Primary Minerals

Essential:
- Plagioclase - 35%
- K-Spar - 5%
- Quartz - 25%

Varietal:
- Biotite - 20%
- CPX - 4%
- Hornblende - 5%

Accessory:
- Epidote - 3%
- Zircon - .5%
- Rutile - 1%
- Opaque - 1%

An Content: 67%

Petrographic name:

Biotite Hornblende Tonalite

Thin Section: **BR-1308**

Location of sample: Bald Rock Pluton
W121°20'16", N39°34'1"

Rock Name: Granodiorite

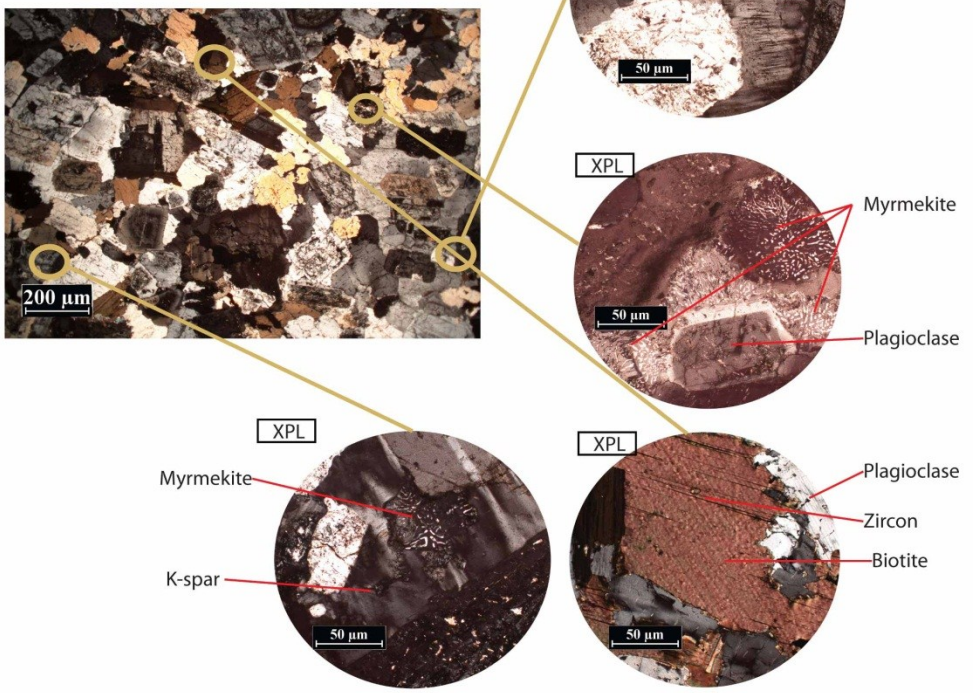

Microscopic description: Thin section reveals a course-grained, hypidiomorphic texture with subhedral grains. Predominant plagioclase crystals are subhedral and present normal oscillatory zoning with mild alteration at their cores and along zoning rings. Moderate myrmekite textures are associated with the intergrowth of many of these plagioclase crystals and they are most likely due to the pressence of perthitic k-spar.

Megascopic description: Rock sample (BR-1308) exhibits a course-grained, felsic, phaneritic texture with visible phenocrysts that include quartz, k-spar, plagioclase, biotite and hornblende. Equigranular felsic grains range from 2 mm to 7 mm in size along with inequigranular mafic grains that range from 3 mm to 5 mm. Rock sample exhibits sligth weathering and oxidation and no apparent fabric is seen.

Primary Minerals

Essential:
- Plagioclase - 40%
- K-Spar - 12%
- Quartz - 30%

Varietal:
- Biotite - 10%
- Hornblende - 6%

Accessory:
- Epidote - 3%
- Zircon - .5%
- Rutile - 1%
- Opaque - 1%

An Content: 67%

Petrographic name:

Biotite Hornblende Granodiorite

APPENDIX B:

CATHODOLUMINESCENCE IMAGES

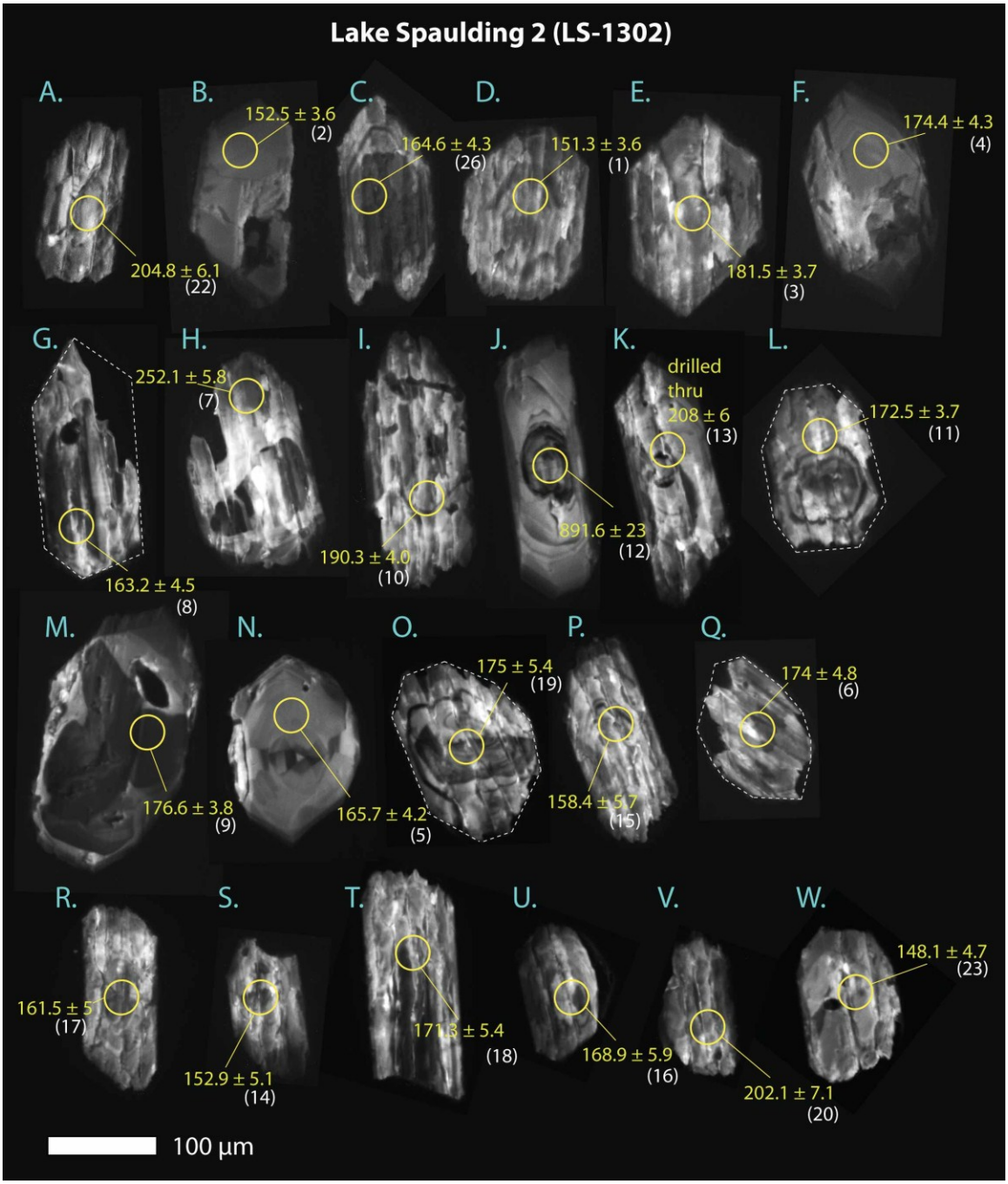

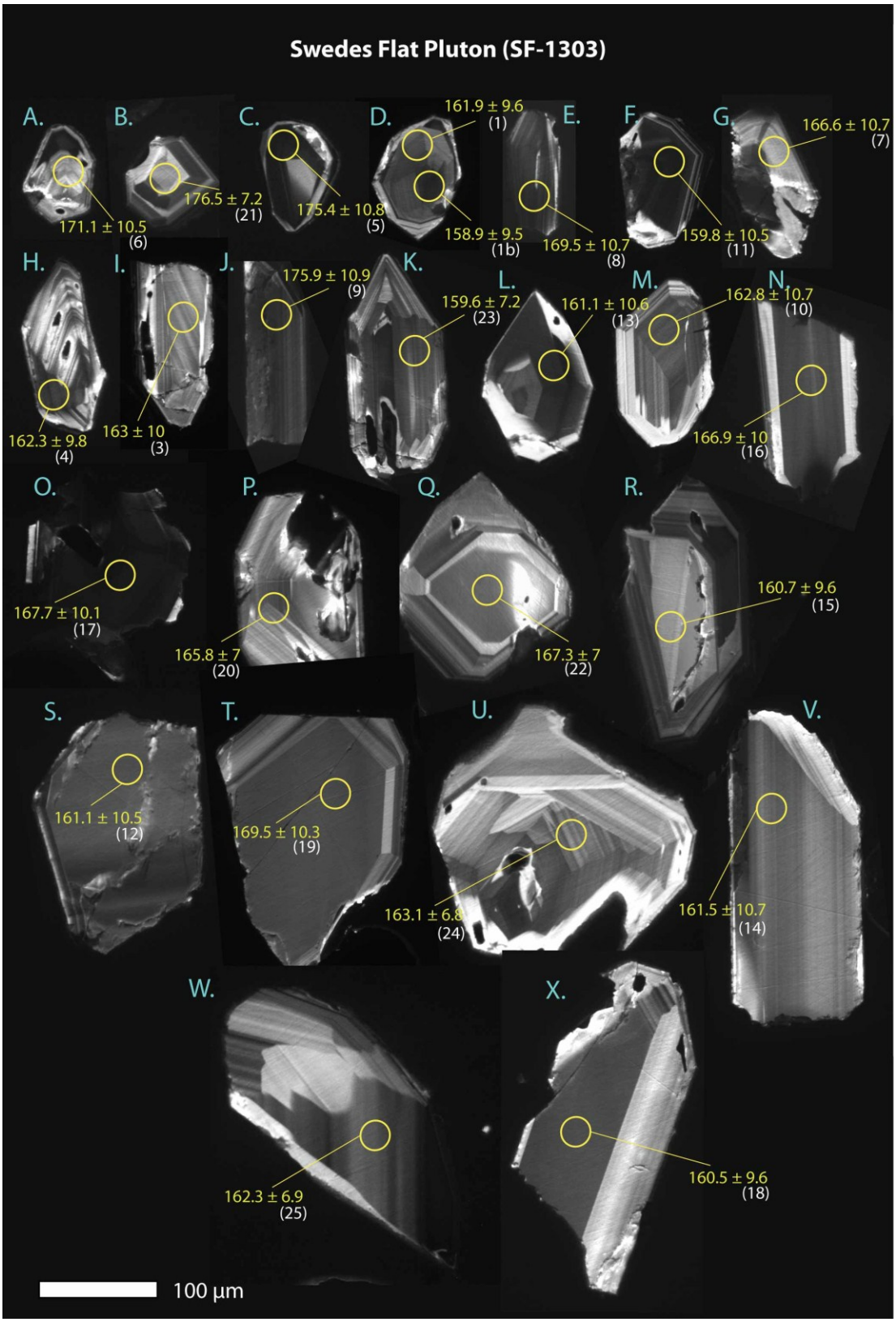
Swedes Flat Pluton (SF-1303)
A.
171.1 ± 10.5
(6)
B.
176.5 ± 7.2
(21)
C.
175.4 ± 10.8
(5)
D.
161.9 ± 9.6
(1)
158.9 ± 9.5
(1b)
E.
169.5 ± 10.7
(8)
F.
159.8 ± 10.5
(11)
G.
166.6 ± 10.7
(7)
H.
162.3 ± 9.8
(4)
I.
163 ± 10
(3)
J.
175.9 ± 10.9
(9)
K.
159.6 ± 7.2
(23)
L.
161.1 ± 10.6
(13)
M.
162.8 ± 10.7
(10)
N.
166.9 ± 10
(16)
O.
167.7 ± 10.1
(17)
P.
165.8 ± 7
(20)
Q.
167.3 ± 7
(22)
R.
160.7 ± 9.6
(15)
S.
161.1 ± 10.5
(12)
T.
169.5 ± 10.3
(19)
U.
163.1 ± 6.8
(24)
V.
161.5 ± 10.7
(14)
W.
162.3 ± 6.9
(25)
X.
160.5 ± 9.6
(18)
100 µm

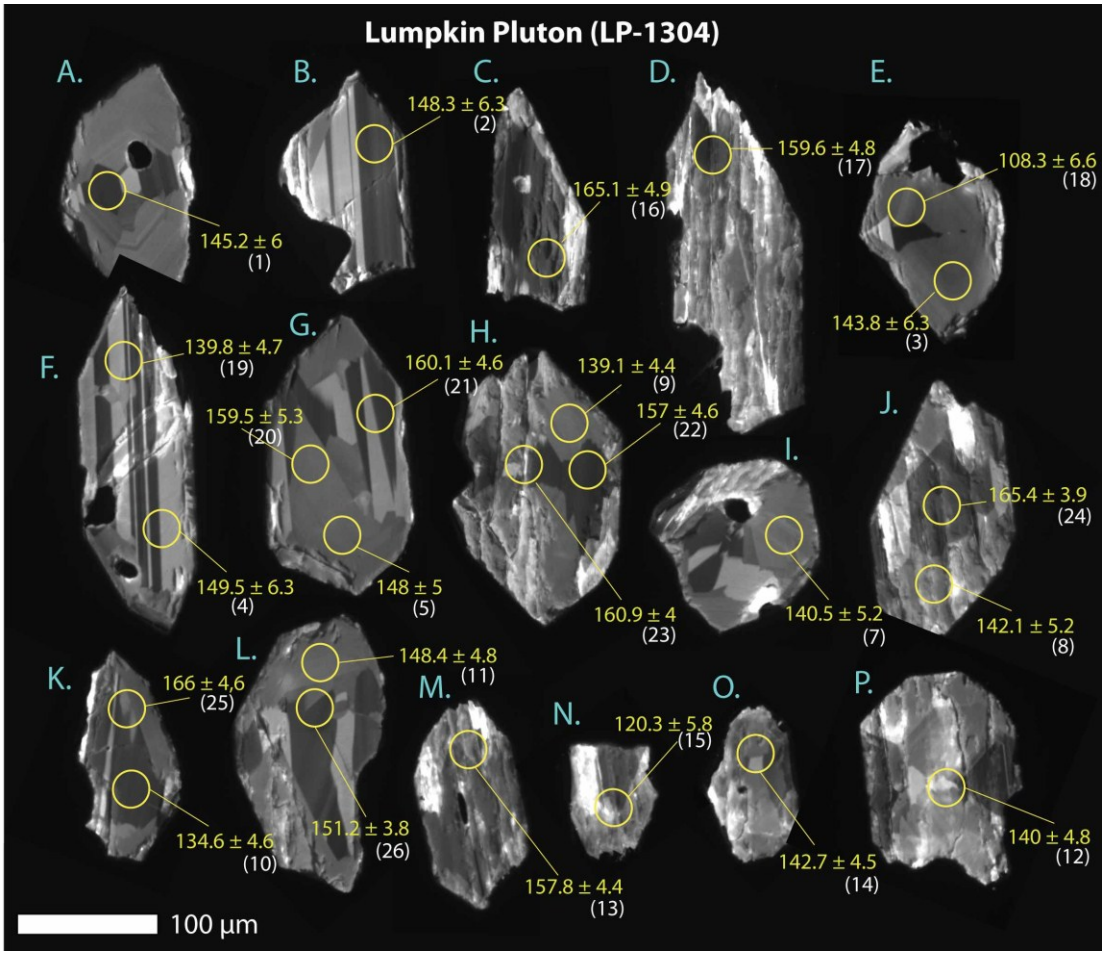
Lumpkin Pluton (LP-1304)
A.
B.
C.
D.
E.
145.2 ± 6
(1)
148.3 ± 6.3
(2)
165.1 ± 4.9
(16)
159.6 ± 4.8
(17)
108.3 ± 6.6
(18)
143.8 ± 6.3
(3)
F.
G.
H.
139.8 ± 4.7
(19)
159.5 ± 5.3
(20)
160.1 ± 4.6
(21)
139.1 ± 4.4
(9)
157 ± 4.6
(22)
149.5 ± 6.3
(4)
148 ± 5
(5)
160.9 ± 4
(23)
I.
J.
140.5 ± 5.2
(7)
165.4 ± 3.9
(24)
142.1 ± 5.2
(8)
K.
L.
M.
N.
O.
P.
166 ± 4.6
(25)
148.4 ± 4.8
(11)
120.3 ± 5.8
(15)
134.6 ± 4.6
(10)
151.2 ± 3.8
(26)
157.8 ± 4.4
(13)
142.7 ± 4.5
(14)
140 ± 4.8
(12)
100 µm

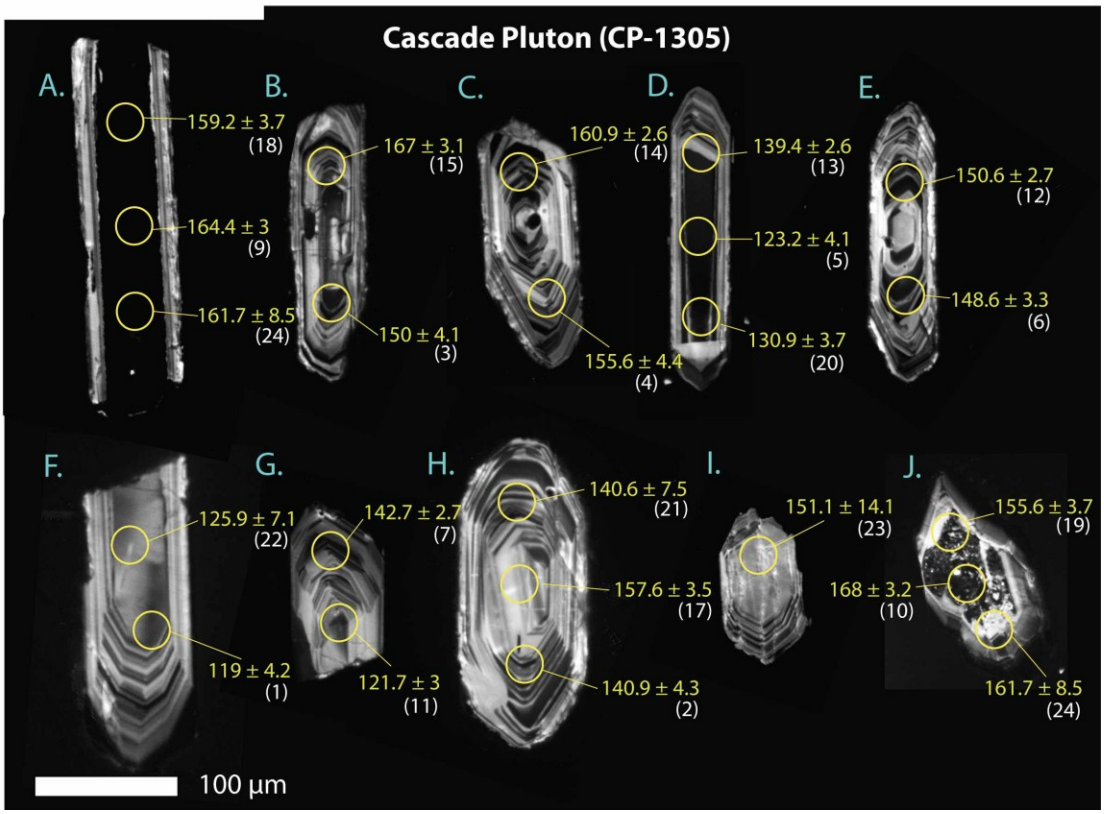
Cascade Pluton (CP-1305)
A.
159.2 ± 3.7
(18)
164.4 ± 3
(9)
161.7 ± 8.5
(24)
B.
167 ± 3.1
(15)
150 ± 4.1
(3)
C.
160.9 ± 2.6
(14)
155.6 ± 4.4
(4)
D.
139.4 ± 2.6
(13)
123.2 ± 4.1
(5)
130.9 ± 3.7
(20)
E.
150.6 ± 2.7
(12)
148.6 ± 3.3
(6)
F.
125.9 ± 7.1
(22)
119 ± 4.2
(1)
G.
142.7 ± 2.7
(7)
121.7 ± 3
(11)
H.
140.6 ± 7.5
(21)
157.6 ± 3.5
(17)
140.9 ± 4.3
(2)
I.
151.1 ± 14.1
(23)
J.
155.6 ± 3.7
(19)
168 ± 3.2
(10)
161.7 ± 8.5
(24)
100 µm

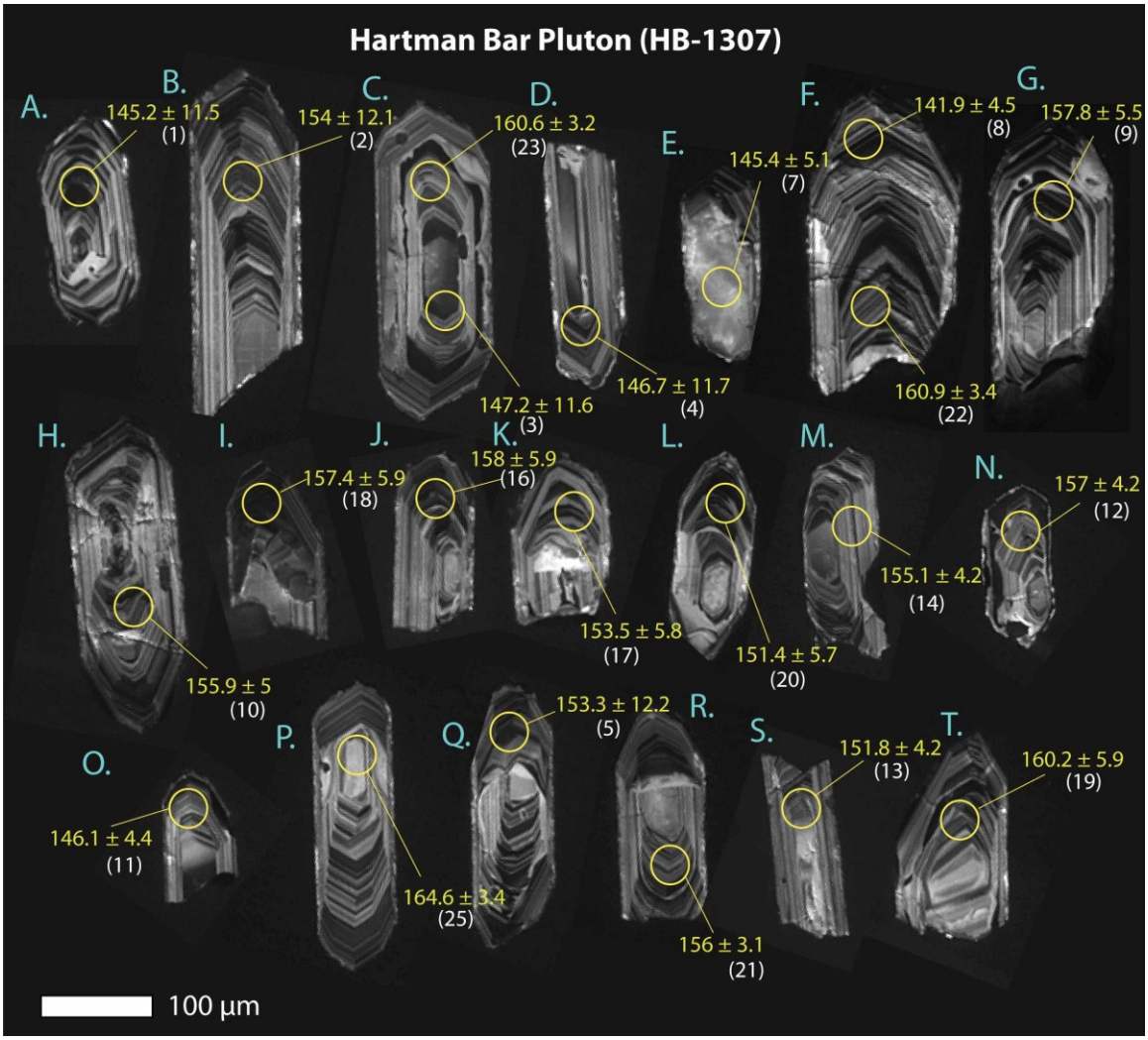
Hartman Bar Pluton (HB-1307)
A.
B.
145.2 ± 11.5
(1)
C.
154 ± 12.1
(2)
D.
160.6 ± 3.2
(23)
E.
145.4 ± 5.1
(7)
F.
141.9 ± 4.5
(8)
G.
157.8 ± 5.5
(9)
147.2 ± 11.6
(3)
146.7 ± 11.7
(4)
160.9 ± 3.4
(22)
H.
I.
J.
K.
L.
M.
N.
157.4 ± 5.9
(18)
158 ± 5.9
(16)
157 ± 4.2
(12)
155.1 ± 4.2
(14)
153.5 ± 5.8
(17)
151.4 ± 5.7
(20)
155.9 ± 5
(10)
O.
P.
Q.
R.
S.
T.
153.3 ± 12.2
(5)
151.8 ± 4.2
(13)
160.2 ± 5.9
(19)
146.1 ± 4.4
(11)
164.6 ± 3.4
(25)
156 ± 3.1
(21)
100 µm

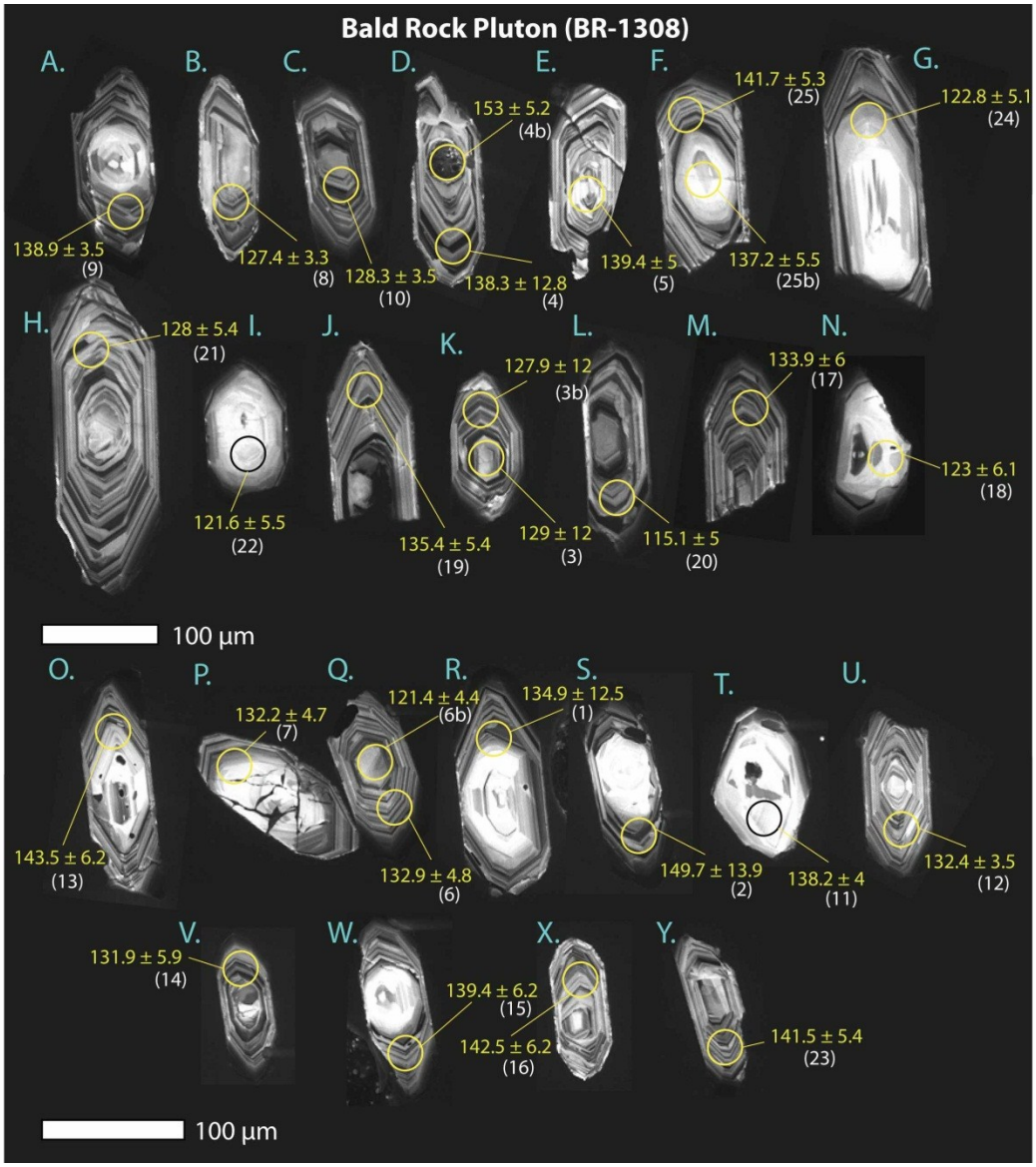
Bald Rock Pluton (BR-1308)
A.
B.
C.
D.
E.
F.
G.
138.9 ± 3.5
(9)
127.4 ± 3.3
(8)
128.3 ± 3.5
(10)
153 ± 5.2
(4b)
138.3 ± 12.8
(4)
139.4 ± 5
(5)
141.7 ± 5.3
(25)
137.2 ± 5.5
(25b)
122.8 ± 5.1
(24)
H.
I.
J.
K.
L.
M.
N.
128 ± 5.4
(21)
121.6 ± 5.5
(22)
135.4 ± 5.4
(19)
127.9 ± 12
(3b)
129 ± 12
(3)
115.1 ± 5
(20)
133.9 ± 6
(17)
123 ± 6.1
(18)
100 µm
O.
P.
Q.
R.
S.
T.
U.
143.5 ± 6.2
(13)
132.2 ± 4.7
(7)
121.4 ± 4.4
(6b)
132.9 ± 4.8
(6)
134.9 ± 12.5
(1)
149.7 ± 13.9
(2)
138.2 ± 4
(11)
132.4 ± 3.5
(12)
V.
W.
X.
Y.
131.9 ± 5.9
(14)
139.4 ± 6.2
(15)
142.5 ± 6.2
(16)
141.5 ± 5.4
(23)
100 µm